Sol-Gel Mesoporous Silica Aerogels and Bio Hybrids for Functional Applications

THESIS SUBMITTED TO

COCHIN UNIVERSITY OF SCIENCE AND TECHNOLOGY
IN PARTIAL FULFILMENT OF THE REQUIREMENTS
FOR THE DEGREE OF

**DOCTOR OF PHILOSOPHY
IN CHEMISTRY**

UNDER THE FACULTY OF SCIENCE

BY

SMITHA SASIDHARAN

Under the Supervision of
Dr. K.G.K. Warrier

Materials and Minerals Division
NATIONAL INSTITUTE FOR INTERDISCIPLINARY SCIENCE AND TECHNOLOGY
(Formerly Regional Research Laboratory)
Council of Scientific and Industrial Research
Thiruvananthapuram, Kerala, India – 695 019

JULY 2009

Dedicated to my beloved family

DECLARATION

I hereby declare that the work embodied in the thesis entitled **"Sol-Gel Mesoporous Silica Aerogels and Bio Hybrids for Functional Applications"** is the result of the investigations carried out by me at Materials and Minerals Division, National Institute for Interdisciplinary Science and Technology (formerly RRL-T), CSIR, Thiruvananthapuram, under the supervision of **Dr. K. G. K. Warrier** and the same has not been submitted elsewhere for any other degree.

Smitha Sasidharan

Thiruvananthapuram

July 2009

National Institute for Interdisciplinary Science and Technology
(formerly Regional Research Laboratory)
An ISO 9001 Certified Organisation
Council of Scientific and Industrial Research

Dr. K. G. K. Warrier Ph.D., F.IICer
Deputy Director
Head, Materials & Minerals Division
Ceramic Technology

Industrial Estate P.O., Thiruvananthapuram - 695 019, INDIA
Phone : +91- 471- 2490674, 2515280 (O)Fax : +91- 471- 2491712
E-mail:warrier@niist.res.in Website : www.nist.res.in, http//kgkwarrier.tripod.com

CERTIFICATE

This is to certify that the work embodied in the thesis entitled **"Sol-Gel Mesoporous Silica Aerogels and Bio Hybrids for Functional Applications"** has been carried out by **Mrs. Smitha Sasidharan** under my supervision at Materials and Minerals Division, National Institute for Interdisciplinary Science and Technology (formerly RRL), CSIR, Thiruvananthapuram, in partial fulfilment of the requirements for the award of the Degree of Doctor of Philosophy in Chemistry, under the Faculty of Science, Cochin University of Science and Technology, Thiruvananthapuram and the same has not been submitted elsewhere for any other degree.

K. G. K. Warrier

Thiruvananthapuram
July 2009

iii

Acknowledgements

Dr. Aravind P. R., Mr. Jayasankar M. and Mr. B. B. Anilkumar which made my days at NIIST a memorable one. I would also like to thank Mrs. Priya M. and Dr. Nila Devi for their loving companionship.

I would like to express my sincere thanks to former project students Mr. Akhilesh, Mrs. Shanila and Mrs. Shiji for their assistance in some of the experiments reported in the thesis.

I wish to thank my present colleagues Mr. Anas. S, Ms. Athira N. Raj, Ms. Sumaletha N., Mr. Vinod, Mr. Sanoop P. K., Mr. Sankar Sasidharan, Mrs. Smitha V. S., Mrs. Manjumol K. A., Ms. Jaimy K. B., Mr. Mirash A. J., Mr. Divish K., Ms. Sreeremya T. S. and Ms. Saritha S. In different ways, their support has been crucial for the completion of the thesis, and their humour and friendship have made working at NIIST very enjoyable. The support and companionship with colleagues at other divisions especially Fine Ceramics Division helped shaping this dissertation as well.

At this juncture I remember with gratitude my parents, brother and sister for their whole hearted support to achieve this goal in my life. Words fall short in expressing my thanks to Mr. Ajith, my beloved husband, who was always a source of constant support and stimulation. Without his love, care and inspiration this PhD thesis would never be realized. At this moment I would also like to remember Adwaith, my dearest son who missed my presence and affection during the final stages of my thesis.

Above all I bow before 'The Almighty' for his immense blessings.

Thiruvananthapuram   Smitha Sasidharan
24-7-09

CONTENTS

PREFACE

Silica aerogels are a fascinating class of nano porous materials derived by sol-gel technique and have shown great potential for a range of applications. They possess unique properties such as ultra low density, high porosity, large inner surface area, small index of refraction, low sound velocity, low thermal conductivity and low dielectric constant. Hydrolysis and polycondensation of a multifunctional silicon alkoxide followed by supercritical drying is the well known method to prepare silica aerogels. The supercritically dried silica aerogels possess very low strength and are fragile, while they are quite transparent.

Ambient pressure drying has evolved as an alternate technique for the synthesis of silica aerogels. The basic concept of this technique is to improve the strength and stiffness of the gel network and avoid shrinkage or cracking during drying. Earlier work reported on subcritical route has emphasis on the solvent exchange and the pore wall strengthening. Tailoring of porosity of aerogels is very much required for different end applications. The porosity as well as pore size is decided based on the gel precursor. On the other hand, the properties of precursor are greatly dependent on experimental parameters. Information on synthesis conditions to tailor the porosity features as well as further surface modification of silica aerogels is rather recent development and seldom found in published

literature. The present work, therefore has emphasis on the influence of the experimental parameters which control the porous structure, morphology and surface functionalization using biopolymers. The thesis is presented in four chapters; each consists of introduction, experimental section, results and discussion, and conclusion.

A general introduction to nano porous materials, followed by brief coverage of inorganic-organic hybrids, subcritical drying technique and silica-biopolymer hybrids is the highlight of the first chapter. An updated literature review on silica aerogel, subcritical drying technique, silica-gelatin and silica-chitosan hybrids, and definition of the present research problem are provided in this chapter.

Second chapter deals with the synthesis and characterization of silica aerogels and microspheres through sol-gel subcritical technique. Effect of hydrolysis temperature, gelation pH, aging pH and aging solvent on the porosity characteristics of subcritically dried silica aerogels was investigated. By changing the hydrolysis-condensation conditions average pore size in the range 6.2-18 nm and total pore volume in the range 0.99-2.04 cc/g were achieved. Aging pH was also varied to tailor the porosity; average pore size in the range 5.8-13.5 nm and total pore volume in the range 0.88-1.45 cc/g are obtained by changing the pH from 3 to 11. This chapter also describes synthesis of silica aerogels using different organic

templates/DCCAs such as Polyethyleneoxide, Cetyltrimethyalammoniumbromide, Hexamethylenetetramine, Polyethyleneglycol (PEO, CTAB, HMTA, PEG). The effect of varying concentration of organic additives on the porosity features of resultant aerogels is presented. Average pore size in the range 5-20 nm, total pore volume in the range 0.8- 4.5 cc/g and surface area in the range 400-910 m^2/g were tailored by varying the concentration of organic additives. The dielectric constant of pure silica aerogel was found to be 2.29 at 13 MHz. Si-PEG aerogels showed a lower average pore size in the range 4.2 nm-5.1 nm compared to other additives. Low molecular weight of polymer (PEG, MW ~ 285) resulted in lower average pore size, total pore volume and surface area whereas high molecular weight of the polymer (PEO, MW ~80,000,00) resulted in a larger average pore size, total pore volume and surface area. Third section of chapter II describes synthesis of silica microspheres through a sol–emulsion–gel process. Mesoporous silica microspheres were synthesized through sol–emulsion–gel process using Span 80 as the surfactant in silica sol/n-hexane water in oil emulsion system. Surfactant concentration and aging time for the silica sol to obtain uniform spheres were optimized to 1.4 volume percentage and 8 hours respectively. Various parameters related to the synthesis of microspheres, including concentration of surfactant and viscosities of sol were studied. Thermal stability, porosity, and morphological features of the microspheres were also investigated. Surface modification of the microspheres was done with

trimethylchlorosilane to obtain hydrophobic silica microspheres. Hydrophobic microspheres with a contact angle of ~90° could be synthesized.

Inorganic-organic hybrid materials possess well defined pore structure, highly accessible functional groups and controlled surface reactivity. Sol–gel process was used to synthesize silica-gelatin hybrids and functionalization, and this forms the basis of chapter III. Gelatin is immobilized in the mesoporous silica gel network through hydrolysis of tetraethoxysilane in presence of gelatin solution at controlled pH conditions. Silica–gelatin hybrid was also synthesized starting from colloidal silica and the hybrid was further functionalized by using methyltrimethoxysilane (MTMS) and vinyltrimethoxysilane (VTMS) as an intermediate precursor so as to introduce hydrophobicity and improve the mechanical properties. The process involved an in situ hydrolysis-condensation reaction of MTMS/VTMS in the reaction medium to obtain silica-gelatin-MTMS (SGM) and silica-gelatin-VTMS (SGV) hybrids which are novel materials. The hybrid precursor sol was coated on glass and leather substrates. The chemical interactions, gelation characteristics, thermal decomposition, porosity features, optical transmittance and thickness of silica-gelatin hybrid coatings were analysed. Silica and gelatin interact through hydrogen bonding of C=O and N-H groups of gelatin to the silanol hydrogen. Optical transmittance of coatings on glass substrates was nearly 100%. This is expected to useful in optical applications and

also for transparent biocompatible coatings. Thermal analysis data showed that the physically adsorbed water is replaced by gelatin molecule and the decomposition of gelatin took place at ~320 °C. Oxidation of organic group responsible for the hydrophobicity took place at ~200 ^{o}C and ~530 ^{o}C in the case of SGV and SGM hybrids respectively. Hence SGM hybrids possess a greater thermal stability compared to SGV hybrids in terms of hydrophobicity. By varying the concentration of MTMS/VTMS, the hydrophobic property was tailored. The optimum concentration for the effective surface modification of silica–gelatin hybrid is found to be 50wt%. SEM micrograph indicated uniform distribution of silica–gelatin hybrid over the substrate. A maximum contact angle of 125° was achieved for SGV hybrids while retaining the porosity of leather.

Chapter IV describes the synthesis of silica-chitosan hybrids and its functionalization for antiwetting coatings. Functionalization of hybrid was carried out with MTMS and VTMS, and the hybrid precursor sol was coated on glass substrates, which resulted in water-repellant surfaces without affecting the transparency of substrates. The process involved an in situ hydrolysis–condensation reaction of MTMS/VTMS in the reaction medium to obtain silica–chitosan–MTMS (SCM) and silica–chitosan–VTMS (SCV) hybrids which are novel materials. The chemical interactions, gelation characteristics, thermal decomposition, porosity features, optical transmittance and thickness of silica-

chitosan hybrids and coatings were analysed. Coatings of silica-chitosan hybrid developed on glass surface had thickness of 130 nm and were found to be >90% transparent as evidenced by optical transmittance measurements. FTIR spectra was used to study the interaction of silica and chitosan and was found that the linkage is through hydrogen bonding of C=O groups of chitosan and the silanol hydrogen. Thermal degradation of chitosan took place at ~ 350 °C. Oxidation of organic groups responsible for the hydrophobicity took place at ~180°C and ~470 °C in the case of SCV and SCM hybrids respectively. In terms of hydrophobicity, SCM hybrids showed a higher thermal stability compared to SCV hybrids. By varying the concentration of MTMS and VTMS, the hydrophobic properties were tailored. A maximum contact angle of 95° (modifier to precursor ratio = 9) was obtained for transparent hydrophobic silica–chitosan coatings on glass substrates. An optimum molar ratio of 2.5 of functionalizing agent to precursor was required for the effective functionalization in terms of hydrophobicity in the case of glass substrates. Water repellant textile was attempted as a possible application of coatings of these novel ternary hybrids on cotton fabrics. The contact angle of the hydrophobic textiles was found to be as high as ~130° even with 2.5 moles VTMS in the coating solution.

The thesis covers a systematic investigation on the synthesis of silica aerogels and microspheres with tailored porosity at ambient conditions by varying

the experimental parameters as well as using organic templates. Organically modified silica-gelatin and silica-chitosan hybrids were developed for the first time using alkylalkoxysilanes such as MTMS and VTMS. Development of novel silica-biopolymer antiwetting coatings on different substrates such as glass, leather and textile is also demonstrated in the thesis.

Acronyms

BET	Brunauer Emmett Teller
BJH	Barrett–Joiner–Halenda
CMC	Critical micellar concentration
CTAB	Cetyltrimethylammoniumbromide
DCCA	Drying control chemical additives
DTA	Differential thermal analysis
FTIR	Fourier Transform Infrared Spectroscopy
HMDZ	Hexamethyldisilazane
HMTA	Hexamethylenetetramine
IPA	Isopropyl alcohol
IUPAC	International Union of Pure and Applied Chemistry
MCM	Mobil Crystalline Material
MTMS	Methyltrimethoxysilane
PEG	Polyethyleneglycol
PEO	Polyethylene oxide
RLMC	Reaction limited Monomer cluster aggregation
SANS	Small Angle Neutron Scatterning
SAXS	Small Angle X-ray Diffraction
SCM	Silica-Chitosan-MTMS Hybrid
SCV	Silica-Chitosan-VTMS Hybrid
SEI	Secondary electron image
SEM	Scanning Electron Microscopy
SGM	Silica-Gelatin-MTMS Hybrid
SGV	Silica-Gelatin-VTMS Hybrid
Span 80	Sorbitanmonooleate
TEOS	Tetraethoxysilane
TGA	Thermo gravimetric analysis
TMCS	Trimethylchlorosilane
TMOS	Tetramethyl orthosilicate
VTMS	Vinyltrimethoxysilane

Chapter I

An Introduction to Nano Porous Materials, Inorganic-Organic Hybrids, Sol-Gel Process and the Present Work

1.1 Introduction to Nanomaterials

Nanomaterials are materials with morphological features smaller than 100 nm in at least one dimension. Materials reduced to the nano scale can show very different properties compared to what they exhibit on a macro scale, enabling unique applications. For instance, opaque substances become transparent (copper); inert materials become catalysts (platinum, gold); stable materials turn combustible (aluminum); solids turn into liquids at room temperature (gold) and insulators become conductors (silicon). Unique aspect of nanotechnology is the vastly increased ratio of surface area to volume, which opens new quantum mechanical effects. Nanoparticles can comprise a range of different morphologies including nano tubes, nano wires, nano fibres, nano dots and a range of spherical or aggregated dendritic forms. Interest in the unique properties associated with materials having structures on a nanometer scale is increasing at an exponential rate.[1] These materials have found application in a wide range of industries including electronics, pharmaceuticals, chemical-mechanical polishing, catalysis, and it is likely that the next few years will see a dramatic increase in the industrial generation and use of nanoparticles.[2-3] Using a variety of synthesis methods, it is

1

possible to produce nanostructured materials in the form of thin films, coatings, powders and as bulk materials.

1.2 Nanoporous Materials

A solid material that contains cavities, channels or interstices can be regarded as porous. Porous materials are of great interest in various applications, ranging from catalysis, adsorption, sensing, energy storage and electronics owing to their high surface area, tunable pore size, adjustable framework and surface properties.[3] The specific surface area can reach values of up to several thousand square meters per gram, depending on the material.[4] The behaviour and performance of such materials can be determined by many characteristics such as surface area, porosity and pore size distribution. Physical properties such as density, thermal conductivity and strength are dependent on the pore structure of the solid. Porosity influences the chemical reactivity of solid and the physical interaction of solids with gases and liquids. High surface area porous materials are of great importance especially as catalyst, catalyst supports, thermal insulators, sensors, filters, electrodes and burner materials.[3,5] The science and technology of porous materials has progressed steadily and is expanding in many new directions with respect to processing methods and applications. Many synthetic pathways have been reported for the synthesis of porous materials, either with a disordered pore system or ordered with various structures, which can meet the demands of the

target application.[4] Porous ceramic materials are synthesized by various methods such as polymer sponge method, foam method, leaching, sintering of particles having a range of sizes, emulsion templating, gel casting, injection moulding, sol-gel process and heat treatment of a ceramic precursor containing carbon rich compound.

Classification of Pores

Based on the accessibility of an external fluid, pores can be classified in to closed pores and open pores. Closed pores are totally isolated from their neighbours and surface of the particle. They influence macroscopic properties such as bulk density, mechanical strength and thermal conductivity, but are inactive in processes such as fluid flow and adsorption of gases. Pores which have a continuous channel of communications with external surface of the body are called open pores. In Fig. 1.1 region 'a' represents the closed pores, and regions such as b, c, d, e and f represent open pores.

Fig. 1.1. Classification of pores

3

In the figure 'b' and 'f' (one end) are described as blind or saccate pores. Based on the pore size, IUPAC classified porous materials in to microporous, mesoporous and macrporous as given in the Fig. 1.2.
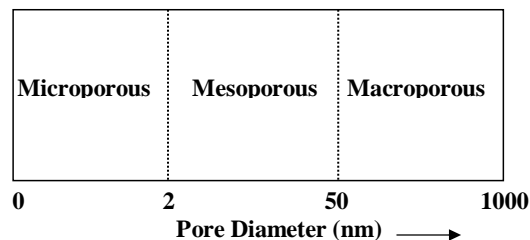
Fig. 1.2. IUPAC classification of pores

1.3 Sol-Gel Synthesis of Inorganic Oxides

Sol-gel process is a colloidal route used to synthesize nanomaterials with an intermediate stage including a sol and /or a gel state. Sol is a stable suspension of colloidal particles in a liquid medium and the dimension of the particles in the solid phase is between 1 and 100 nm. Gel is a porous three dimensionally interconnected solid network that expands in a stable fashion through out the liquid medium.

The chemical reactant, which contains the cation 'M' present in the final inorganic sol or gel, is called chemical precursor,[6] whose chemical transformations are complex and involve a competition at the molecular level between the reaction responsible for the formation of open structures and the one leading to dense solid.

4

The same reactions are responsible for the controlled dispersion of dense colloidal particles in a sol or their agglomeration into a gel. Metal salts and alkoxides are the two main groups of precursors. The general formula of metallic salt is M_mX_n where 'M' is the metal: 'X' is an anionic group. $M(OR)_n$ is the general formula of alkoxides. Sol-gel precursors undergo chemical reactions both with water and other species present in the solution. In sol-gel processing, very small colloidal particles are first formed in solution by hydrolysis of organic compounds of metals to the hydrous oxides. These particles are only 3–4 nm in size. These very small particles link together in chains and then 3–D networks that fill the liquid phase as a gel.[6] These sol can be casted in any desired shape, with dimensions enlarged to allow for shrinkage during drying and sintering. The precursor sol can be either deposited on a substrate to form a film (e.g. by dip-coating or spin-coating), cast into a suitable container with the desired shape (e.g. to obtain monolithic ceramics, glasses, fibers, membranes, aerogels), or used to synthesize powders (e.g. microspheres, nanospheres). Fig. 1.3 represents sol-gel process and its various products. Advantages of sol-gel process are increased homogeneity, high purity, low processing temperature and high surface area of the gels or powders obtained. The inherent usefulness of this approach is largely due to the ease at which sol-gel derived materials can be prepared, modified, and processed. The mild reaction conditions afford an opportunity to incorporate various molecules such as proteins,

5

enzymes, dyes, organic, and organometallic reagents into glass composites[7]. Sol-gel derived materials have diverse applications in optics, electronics, energy, space, biosensors, medicine (controlled drug release) and separation (chromatography) technology. Thin films and coatings find application in optics, electronics, protective coatings and porous thin films. Porous gels and membranes find application in filtration, separation, catalysis and chromatography. Furthermore, the average pore size, pore size distribution, surface area, refractive index and polarity of the resultant matrix can also be controlled and tailored via manipulations in the sol-gel processing conditions.
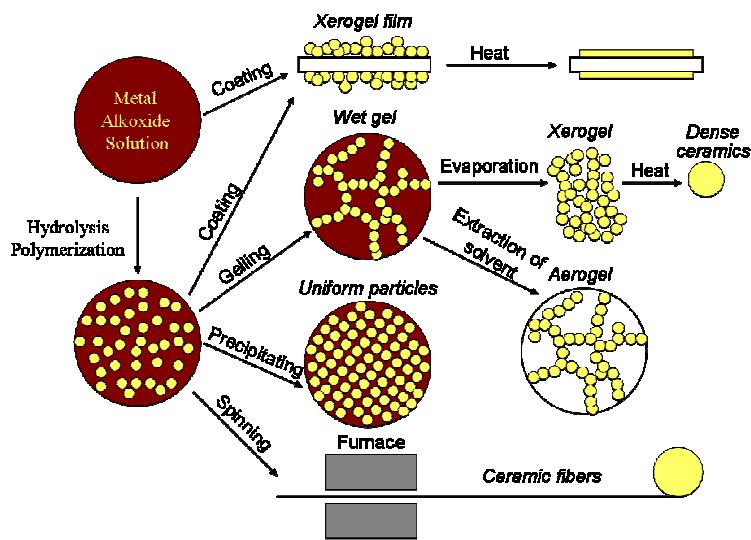
Fig. 1.3. Sol-gel process and its various products

6

1.4 Sol-Gel Process as Applied to Silica

Silica gels are most often synthesized by hydrolyzing monomeric, tetrafunctional alkoxide precursors employing a mineral acid or base as a catalyst. Most common tetraalkoxysilanes used in the sol-gel process are tetraethoxysilane [TEOS, $(SiOC_2H_5)_4$] and tetramethoxysilane [TMOS, $Si(OCH_3)_4$]. Following reactions are used to describe the sol-gel process of silica.

$$\equiv Si-OR + H_2O \underset{\text{Esterification}}{\overset{\text{Hydrolysis}}{\rightleftharpoons}} \equiv Si-OH + ROH$$

$$\equiv Si-OR + HO-Si\equiv \underset{\text{Alcoholysis}}{\overset{\substack{\text{Alcohol}\\\text{condensation}}}{\rightleftharpoons}} \equiv Si-O-Si\equiv + ROH$$

$$\equiv Si-OH + HO-Si\equiv \underset{\text{Hydrolysis}}{\overset{\substack{\text{Water}\\\text{condensation}}}{\rightleftharpoons}} \equiv Si-O-Si\equiv + H_2O$$
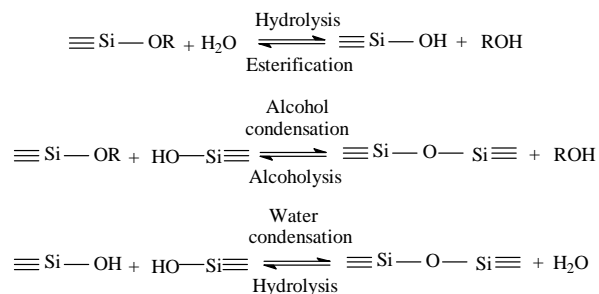
The hydrolysis reaction replaces alkoxide groups with hydroxyl groups. Subsequent condensation reactions involving the silanol groups produce siloxane bonds and the by-products, alcohol or water. Under most conditions, condensation commences before hydrolysis is complete. Since water and alkoxysilanes are immiscible, a mutual solvent such as alcohol is normally used as a homogenizing agent. In order to reduce the reactivity of the alkoxide precursor, organic functional groups can be introduced in to the siloxane network. This type of alkoxide precursors are known as organoalkoxysilanes. Examples for this type of precursors are methyltrimethoxysilane, trimethylethoxysilane etc. Organically

7

modified silicates represent hybrid systems in which several precursor types are combined. Schmidt and coworkers developed silicate products with unique properties by combining tetraalkoxysilanes with alkyl substituted and organofunctional alkoxysilanes.[8]

$$Si(OR)_4 + R_2Si(OR)_2 + YR'Si(OC_2H_5)_3$$
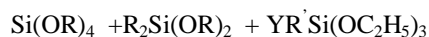
R is an alkyl group, R is an alkylene and Y is an organo-functional group such as – $(CH_2)_3NH_2$, $(CH_2)_3NHCO-O-NH_2$ etc. Unlimited number of chemical and structural modifications is possible in such hybrid systems.[9]

The surface and structural characteristics of the silica gels are affected by various parameters that control the rate of hydrolysis and condensation and these can be summarized into three categories:[10]

a) Compositions: Type of starting materials, quantity of water, catalysts and solvents.

b) Reactions (up to gel formation): Rate of mixing, reaction temperature and gelation schemes.

c) Process variables (after gel formation): Type of dehydration, drying temperature and heating.

Mukherjee et al. reported that the molar ratio of H_2O to alkoxides and pH values played a significant role in determining reaction rates.[11] Sakka et al. found that the same parameters influence the morphology and composition.[12] It has been

reported that the changes in pH values during the sol preparation stage would significantly affect the appearance of sample, porosity, density, viscosity, gelation time, and activation energy.[13-14] The variations of surface area, pore volume, and pore size distribution were discussed in their studies. Investigations on the effect of different types of catalysts such as HF, HCl, HNO_3, H_2SO_4, HOAc and NH_4OH during the sol-gel process, which lead to different physical gel structures due to different reaction mechanisms were also studied.[15,16] Furthermore, Ro et al. found that acidic catalysts were related to the formation of slit-shaped microstructures and cylindrical micropores were obtained by the use of basic catalysts.[17] Many studies have been carried out on the effect of gelation temperature on the sol-gel process of silica.[18-19] Increase in the gelation temperature could make the gelation process shorter. Yasumori et al. reported an increase of 50% in surface area of silica gel by increasing the dehydration temperature.[20] Lee et al. claimed that increase of drying temperature would cause the pore diameter to become bigger, with a wider distribution.[21] Acid catalyzed hydrolysis with low H_2O:TEOS ratio produces weakly branched polymeric sols, where as base catalyzed hydrolysis with large H_2O:TEOS ratio produces highly condensed particulate sols. Intermediate conditions produce structures intermediate to these extremes.[16]

Hayashi et al. studied the effect of solvents on the properties such as bulk density, specific surface area, pore size distribution and pore volume of the dried

gel.[22] Depending upon the pH either protonated or deprotonated silanols are involved in the condensation mechanism. Protic solvents hydrogen bond to nucleophilic deprotonated silanols and aprotic solvents hydrogen bond to electrophilic protonated silanols. Hence protic solvents retard base-catalyzed condensation and promote acid catalyzed condensation where as aprotic solvents have the reverse effect. Shukla et al. have studied the effect of ethanol on the morphology, oxide content and density of the TEOS derived gels.[23] Steric factors exert great effect on the hydrolytic stability of alkoxysilanes. Hydrolysis rate is lowered the most by branched-alkoxy hydroxyl or bridging oxygen substitution. The condensation rate of triorganosilanols decreases with increase in the length or branching of the chain of the alkyl radical, or if aromatic groups are present. In the case of tetra functional alkoxides, substituents that increase steric crowding in the transition state will retard condensation. Although inductive effects are important, in the acid catalyzed condensation of dialkyl silanols, steric effects predominate over inductive effects.[6]

1.5 Aging of Gels

Aging is the process of keeping the gels in various solutions for a period of time in order to increase the strength of the gel network so that cracking of gels during drying can be prevented. The chemical reactions that cause gelation continue long after gel point strengthening, stiffening and producing shrinkage of

the network.[24-25] The composition, structure and properties of gel change during aging. The changes that occur during aging are categorized into three.

1) Polymerization: Increase in connectivity of the gel network by condensation reactions. Schematic representation of polymerization of silica is provided as Fig. 1.4.[6]

2) Coarsening: Process of dissolution and reprecipitation driven by differences in solubility between surfaces with different radii of curvature.

3) Syneresis: Shrinkage of the gel and the resulting expulsion of liquid from the pores.

1.6 Drying of Gels

The microstructure of a xerogel is the consequence of gelation, aging and drying. During drying the gel can initially shrink to accommodate loss of pore fluid maintaining the liquid-vapour interface at the exterior surface of the gel. At the final stage of drying liquid-vapour menisci recede into the gel interior.[24] The magnitude of the capillary pressure, Pc, exerted on the network depends on the surface tension of the liquid, γ, the constant angle θ, and the pore size, r:

$$Pc = 2 \gamma \cos\theta/r$$

If the pore size is very small, the capillary pressure will be large. The original gel network collapses due to this pressure.[26] Aging may be used to reduce the extent of collapse of the gel structure during drying.

11
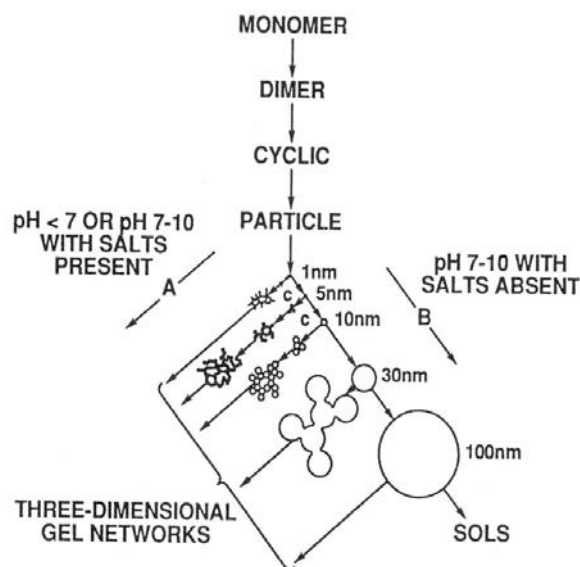
Fig. 1.4. Schematic representation of polymerization of silica

1.7 Aerogels

Aerogels are a fascinating class of nanoporous materials derived by sol-gel technique which possess sophisticated potentialities for a range of applications.[27] They possess unique properties such as high porosity, large inner surface area, low density, small index of refraction, low sound velocity, low thermal conductivity and low dielectric constant.[27] Aerogels are quite transparent since they scatter light weakly because of the extremely small particle and pore sizes. Important structural properties of aerogels are provided in Table 1.1.

Table 1.1. Properties of silica aerogel

Property	Range
Bulk density (g/cc)	0.003-0.500
Skeletal density (g/cc)	1.700-2.100
Porosity (%)	80-99.8
Mean pore diameter(nm)	20-150
Inner surface area (m^2/g)	100-1600
Refractive index	1.007-1.24
Thermal conductivity (in air 300)(w/(mk)	0.017-0.021
Modulus of elasticity (mpa)	0.002-100
Sound velocity c_l (m/s)	<20-800
Dielectric constant	1-2 (18-40 GHz)

Aerogels find applications as pesticides, in cosmic dust capture, waste water treatment, moulds for casting aluminium metal, aerocapacitors, absorbing media for dessication, heat storage device for automobiles, encapsulation media, hydrogen fuel storage material, ideal dielectric for ultra fast integrated circuits, thermal insulators, fillers, particle detectors, catalysts, gas sensors, light guides, capacitors.[28-37] Many reviews on aerogel were also published with more focused on the applications of aerogels.[38-42] Synthesis of aerogel starts with the controlled

13

conversion of a sol into a gel. The growth of clusters or polymer chains from a chemical solution occurs initially and these primary entities cross-link leading to the formation of a coherent network-still embedded in a liquid. The structure of aerogel is characterized by well accessible, cylindrical branched mesopores.[6] Nitrogen adsorption studies, mercury porosimetry, microscopic techniques and scattering techniques (SAXS and SANS) are used to explore the structure of aerogels. Schematic diagram of aerogel structure is presented as Fig. 1.5. When a silica aerogel monolith breaks under force only secondary particle lose contact with one another while primary particle remains undisturbed. So the mesoporous space between these particles would be maintained. The silica aerogels exhibit microstructures consisting of loosely interconnected silica particles which form an open network.
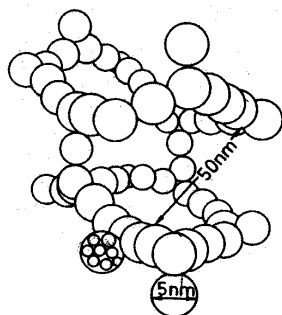
Fig. 1.5. Structure of aerogel

The first aerogels were made by S. S. Kistler in 1931 from a water glass based recipe.[43] Later Teichner et al. improved this sol-gel process.[44] They

14

hydrolysed TMOS by adding controlled amount of water in a methanol medium. Silica form a coherent network embedded in alcohol. This alcogel was then successfully dried under hypercritical conditions (T_C=239°c, P_C=81 bar). Using a two step sol-gel process and CO_2 drying, a group at Lawrence Livermore National Laboratory (LLNL) prepared ultra low density aerogels with densities as low as 3 Kg/m^3. The potential of the material was only widely recognized in the 1970's when the aerospace industry was looking at the possibility of developing extremely light thermal insulator. Further developments resulted in using aerogel as insulator in pathfinder mission to mars, for insulating the sensitive electronics from harsh temperature of mars. Conventional method of synthesis of aerogel is by a sol-gel process followed by supercritical drying of the wet gel in an autoclave. A schematic diagram which shows the process of synthesis of aerogel is provided as Fig. 1.6.[27] During initial stages of drying, the capillary forces caused by the evaporation of solvents from pores in the gel, create an overall drying stress and local differential stresses owing to non uniform pore size distribution.[45] Silica aerogels are ultra pure gels derived by hydrolysis-condensation reaction of silica alkoxide or salts.
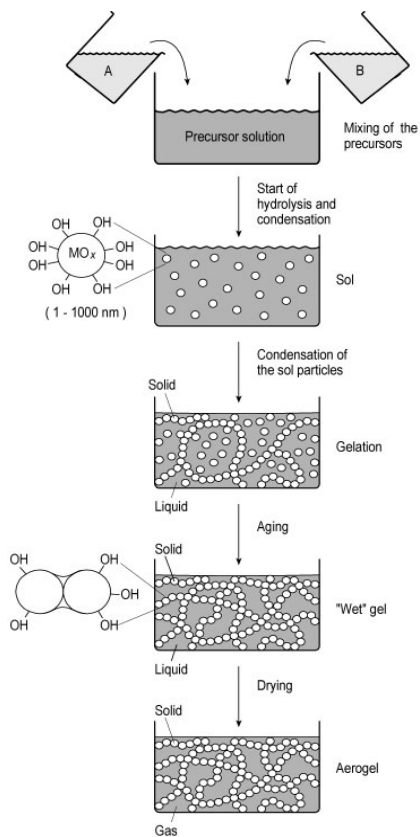
Fig. 1.6. General scheme for the synthesis of aerogels by sol-gel processing

1.7.1 Supercritical Drying

Supercritical drying involves the process of drying a wet gel in an autoclave above the critical temperature and pressure of its solvent. At the critical point of drying there is no longer any distinction between the liquid and vapour phases, and there is no liquid-vapour interface or capillary pressure.[45] The resulting gels called

aerogels have about 99% porosity, extremely low densities and a high inner surface area. A schematic representation of supercritical drying is provided in Fig.1.7. At the critical point [T_c, p_c] the density of the liquid and the gas are equal. Supercritical drying can be performed along path A or B. However this technique is expensive and hazardous, and results in fragile aerogels having low strength. Table 1.2 provides supercritical constants of some solvents.
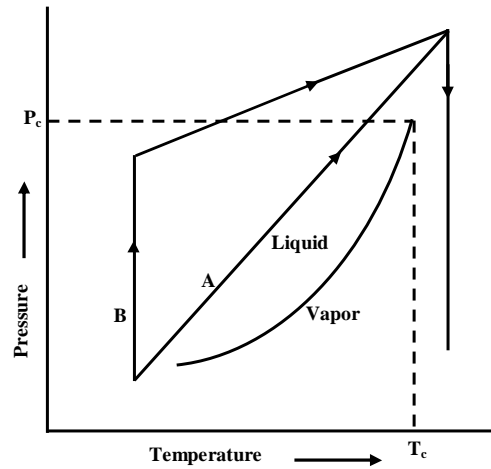
Fig. 1.7. Schematic representation of supercritical drying

1.7.2 Subcritical Drying

Subcritical drying technique, a less expensive method for the synthesis of aerogel, which involves controlled solvent exchange, aging and surface modification is evolving as a promising technique for the synthesis of aerogel at ambient temperature and pressure.

17

Table 1.2. Supercritical constants of some solvents

Solvent	Tc (^{o}C)	Pc (MPa)
Methanol	240	7.9
Ethanol	243	6.3
Acetone	235	4.7
Isopropanol	235	4.7
H_2O	374	22.1
CO_2	31	7.3

Ambient pressure methods for silica aerogels include surface modification, network strengthening and use of DCCAs. The basic concept of this technique is to improve the strength and stiffness of the gel network and avoid shrinkage or crack during drying.[46] The extent of shrinkage during drying is governed by the capillary pressure exerted by the pore fluid and the modulus of the solid matrix. Solvent exchange with a low surface tension liquid can reduce the capillary pressure.[47] Haereid et al. reported that aging of silica gel in a silane solution increase the strength and stiffness of the gel network.[48] Their study showed that an increase in aging time and pH improve the mechanical strength of the gel network due to dissolution-reprecipitation reactions of silica monomers.[48] Einarsrud et al. investigated the structural development of silica gels agend in TEOS.[49] They found that primary particles and cluster size increases when silica is precipitated from the aging solution. Effect of aging time, temperature and concentration of

aging solution on the porosity characteristics of subcritically dried silica aerogels were reported.[50-51] The investigation showed that best concentration of TEOS in the aging solution and time of aging were 80 % and 48 h respectively. As the temperature of aging increased the bulk density decreased whereas the surface area and pore volume increased. Haereid et al. investigated the effect of aging alcogels in water and found a maximum in both modulus and modulus of rupture. This was independent of the aging temperature, but the aging time required to reach the maximum decreased with increasing temperature.[52] Surface modification with various silylating agents avoid condensation reactions during drying.[53] Deshpande et al. developed a new method for synthesis of aerogel, in which the wet gel is washed with an aprotic solvent, reacted with trimethylchlorosilane (TMCS) and then dried at ambient pressure.[53] This treatment minimizes shrinkage of the gel by a reduction in the surface tension of the solvent and the contact angle between the solvent and the surface of the silica network. Since neighbouring surface organic groups are chemically inert and detach with little activation energy, the gel is able to re-expand (spring back effect). Rao et al. prepared two step processed ambient pressure dried silica aerogel with improved properties in terms of density, volume shrinkage, thermal conductivity, hydrophobicity and optical transmission, at ambient pressure, with TEOS precursor and hexamethyldisilazane (HMDS) as silylating agent.[54] The best quality silica

19

aerogels was obtained with the molar ratio of TEOS:HMDS at 1:0.36. They have also studied the effect of silylating agents on properties of silica aerogels prepared by ambient drying and reported that by using the TMOS precursor, TMCS resulted the best quality silica aerogels in terms of monolithicity, visual transparency and lowest density.[55] Schwertfeger et al. developed a one-step process in which solvent exhange and surface modification were performed simultaneously using a HMDS/TMCS solution.[56] Kim[57] and Lee[58] used a one step solvent exchange/surface modification process using IPA/TMCS/n-Hexane solution. Use of organic additives termed drying control chemical additives (DCCA) to alkoxide solutions is another approach to obtain monolithic aerogel at ambient conditions.[59] DCCA controls the rate of hydrolysis and condensation reactions, pore size distributions, vapour pressure of pore liquid and hence the drying stresses. If a uniform scale of structure obtains during gelation, it will result in uniform growth of the network during aging. This will improve the strength of the gel and its ability to resist drying stresses.[60-61] Polyethyleneglycol (PEG) has been used by many researchers as a porogen.[62-63] They claimed that high concentrations of PEG weaken the solid matrix, whereas small concentrations of PEG strengthen the matrix. Reetz et al. used additives such as polyvinylalcohol and PEG as biocatalyst supports, and found that the lipase activity was significantly enhanced in the presence of these additives.[64] Rao et al. used glycerol as an additive and achieved

20

a narrow and uniform distribution of pores.[65] Even though many approaches have been attempted on subcritical drying lot of experimental parameters are still to be optimized for the commercialization of the process.

1.8 Inorganic-Organic Hybrids

Inorganic and organic components mixed at the nanometric scale in virtually any ratio are called inorganic-organic hybrid. The combination of organic and inorganic molecules in different formulations can give rise to a number of hydrid materials whose properties can be tailored, even to mimic nature. Inorganic-organic hybrid materials possess well defined pore structure, highly accessible functional groups and controlled surface reactivity.[66] Inorganic-organic hybrid materials are subject of intense research in the field of contemporary material chemistry as these materials exhibit excellent electrical, magnetic and optical properties. Sol–gel process is very attractive and versatile to prepare inorganic or hybrid films with tunable thickness. Moreover, mild synthetic conditions provided by sol–gel chemistry are advantageous for the incorporation of organic components into the inorganic network, allowing the preparation of a variety of hybrid architectures. [66] Two approaches are widely practiced for the incorporation,

1. Mixing of an organic polymer with a metal alkoxide such as tetraethoxysilane.

2. Introduction of organosilyl group into the organic polymer prior to the sol-gel reaction with metal alkoxide such as tetraethoxysilane.

Usually inorganic-organic hybrids prepared by a sol-gel process show unique mechanical properties such as high ductility, low elastic modulus and high mechanical strength.[67] Typical advantages of organic polymers are flexibility, low density, toughness and formability where as ceramics have excellent mechanical and optical properties such as hardness, modulus, strength, transparency and high refractive index. If these materials can be combined effectively, a new class of high performance, highly functional inorganic-organic hybrid materials can be prepared.[68] Inorganic-organic hybrids find applications in optoelectronics for protective optical coating, high refractive index films, contact lenses, thin film transistors, light emitting diodes, solar cell, optical waveguide materials and photochromic materials, adsorption, catalysis and high energy fields.[66,69] Biocomposites are excellent inorganic-organic hybrid materials produced by natural biomineralisation. Bones, teeth and shells are typical biocomposites, which consists of an organic polymer matrix reinforced by an inorganic deposit. In bio-composites, the inorganic phase is regularly and highly organized in a matrix.[68]

1.9 Silica-Biopolymer Hybrids

The combination of biopolymers with siloxanes under mild chemical conditions has been used for the preparation of silica-biopolymer hybrids in the

form of films for membranes or coatings, or as precursors for the preparation of porous materials.[70] The biopolymer–silica hybrid materials have recently drawn attention owing to their promising properties and compatibility with living matter.[71,76] These hybrid materials find application in the field of biocompatible materials, bone substituents, cements for bone repair and reconstruction, enzyme and cell immobilization, catalysis and sensors.[77,80] The presence of functional groups such as amino, amide or carboxyl in some polymers can allow compatibility of the polymeric phase with inorganic matrix at a submicroscopic level through hydrogen bonding with silanol groups. Biocomposite layers of silica and various bone-relevant proteins such as collagen, gelatin and chitosan can be obtained from coating solution containing silica sols mixed with proteins in water/dioxane.[73] The interest in these biopolymers as organic additives in composites of inorganic nano-hybrids is mainly because of its biodegradable, bioadhesive and multifunctional properties.[71] Silica–gelatin biohybrids find application in bone tissue engineering, biocatalysis and controlled drug delivery systems. [77-78] A number of research articles and reviews are available in literature on the promising properties of silica-chitosan composites.[81-83] Silica-chitosan composites are also known to act as immobilization matrix for several molecules and complexes.[83-87] Fuentes et al. synthesized oriented silica-chitosan hybrid films using 3-aminopropyltrimethoxysilane precursor by a sol-gel process.[88] Use of

23

organically modified silane precursors for the silica component in the hybrids are rare but can impart enhanced properties to the hybrid.

1.9   Gelatin

Gelatin is a protein, which is obtained by breaking the single helix structure of collagen into single stranded molecules. The amino acid composition of gelatin is given in Fig. 1.8. Since it is biodegradable and biocompatible, it is a suitable compound for medical applications. Gelatin is cheap and possesses bioadhesive property. Therefore gelatin-linked inorganic hybrids have applications in biotechnology. In this context, silicate species can be considered as potentially interesting cross-linking agents since they were shown to interact through both electrostatic interactions and hydrogen bonding with some polyaminoacids and proteins.
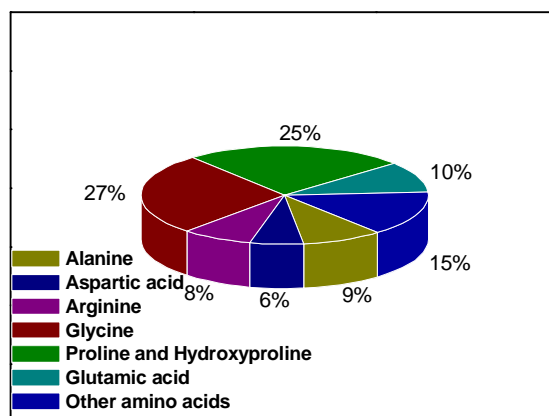
Fig. 1.8. Composition of gelatin

24

Silica/gelatin composites have been employed for enzyme and cell immobilization. Porous gelatin-siloxane hybrids are finding application as biodegradable scaffolds that act as biocompatible material for bone repair or generation.[72] Physical measurements of the rheological, swelling and thermal properties of the gels and chemical analysis of the number of junctions introduced by chemical cross-linking were used to elucidate the structure of the chemical gelatin networks. The basic structural unit of gelatin is provided in Fig. 1.9.
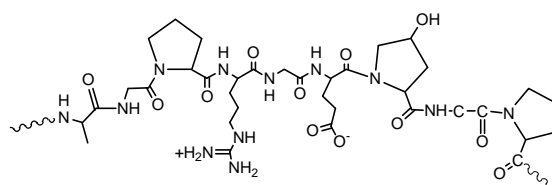
Fig. 1.9. A basic structural unit of gelatin molecule

1.10 Chitosan

Chitosan is a copolymer of linked $\beta(1\rightarrow 4)$, 2-amino2-deoxy-D-glucose and 2-acetamidodeoxy-D-glucan which is mainly used in medical, pharmaceutical, cosmetics and food industries.[89] Chitosan is also used as a flocculent, thickener, film, gas selective membranes, and wound healing promoting agent.[90] Fig. 1.10 shows the structure of chitosan. The presence of amino and hydroxyl functional groups allow these molecules to self assemble into various supramolecular structures and enable them to be used in the synthesis of novel monophasic inorganic materials.

25

R= H or COCH$_3$
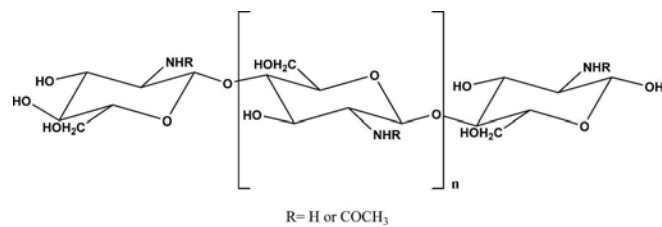
Fig. 1.10. Structure of chitosan

A number of research articles and reviews are available in literature on silica-chitosan composites which indicate the promising properties of the hybrid.[81-85] High sorption capacities, stability of metal anions on chitosan and physical and chemical versatility of the biopolymer enable chitosan when incorporated with Pt or Pd to be used in heterogeneous catalysis.[86,87] Functionalization of these hybrids with organically modified silanes is reported to enhance the properties of these hybrids.[88]

26

Definition of the Present Research Problem

Aerogels are unique among solid materials because of their extremely low densities, large open pores, and a high inner surface area. Hydrolysis and polycondensation of a multifunctional silicon alkoxide is the well known method for the synthesis of silica aerogels. The initially formed gels have a sponge like solid network filled with liquid. Special drying techniques must be applied to exchange the pore liquid with air while maintaining the fragile solid network. Supercritical drying is the most common technique. However the supercritical drying process involves heating and evacuation of highly flammable solvents at high temperature and pressures. In addition supercritically dried aerogels possess very low strength and are fragile. Ambient pressure drying which involves controlled solvent exchange, aging and surface modification is evolving as a promising technique for the synthesis of silica aerogels.

Major problems during the synthesis of aerogels at ambient pressure primarily arise from the large capillary pressure that occurs during drying (a result of the small pore sizes) and low stiffness (a result of the low-density). Tailoring of porosity of aerogels is very much required for different end applications. However information on synthesis conditions to tailor the porosity feature as well as surface modification of silica aerogels is seldom found in the literature. Therefore present work has been designed based on the following:

1) Influence of experimental parameters such as hydrolysis temperature, gelation pH, aging pH and aging solvent on the porosity characteristics is to be investigated in detail. Silica aerogels will be synthesized using organic additives such as PEO, CTAB, PEG and HMTA to control porosity. Effect of concentration of organic templates on the porosity characteristics will be studied.

2) Synthesis of mesoporous materials having regular geometries has been of considerable interest in recent years owing to their great potential in catalysis, adsorption, separation, sensing, medical use, ecology, and nanotechnology.   Hence hydrophobic silica microspheres will be synthesized through a sol–emulsion–gel process. Effect of surfactant concentration, aging time, and viscosity of the silica sol on microsphere formation will be investigated.

3) Synthesis of hydrophobic silica-biopolymer hybrid is an area of great interest since it finds application as water repellant coatings in different substrates. Sol-gel process will be used as an effective technique for the synthesis of silica-biopolymer hybrids using gelatin and chitosan as biopolymers. Functionalization of the hybrid will be done using alkylalkoxysilanes such as vinyltrimethoxysilane and methyltrimethoxysilane. These hybrids will be applied as coatings on

different substrates such as glass, leather and textiles. The coatings will be tested for its transparency, uniformity and hydrophobicity.

The thesis has been designed on the above objectives. The results obtained have been discussed and correlations have been derived between the experimental parameters and the properties.

Chapter II

Mesoporous Silica Aerogels and Microspheres through Sol-Gel Subcritical Technique

2.1 Synthesis of Silica Aerogels by Varying Experimental Parameters

2.1.1 Introduction

Silica aerogels are sol–gel derived materials which possess unique properties such as large inner surface area, low density, small index of refraction, low sound velocity, low thermal conductivity and low dielectric constant. Hydrolysis and polycondensation of a multifunctional silicon alkoxide followed by supercritical drying is the well known method to prepare silica aerogels.[91] However the supercritical drying process involves the heating and evacuation of highly flammable solvents such as alcohols, which are hazardous at high temperature and high pressures and are also not very ecofriendly. In 1984, in Sweden, the failure in a pilot plant for the production of aerogel tiles released 1000 litres of methanol and a big explosion destroyed the whole building.[92] Problems arise from the combination of high temperatures and high pressure as well as the flammability of the solvents. In addition, the supercritical drying results in aerogels which are fragile having very low strength making it difficult for easy handling.[93]

Ambient pressure drying has evolved as a promising technique for the synthesis of silica aerogels. Main methods adopted for ambient pressure drying include network strengthening and solvent exchange/surface modification of wet gels.[46,55,56] The increase in stiffness and large pore size bring down the capillary pressure during drying, resulting in low density xerogels. Smith et al. synthesized mesoporous aerogel like materials at ambient pressures by introducing hydrophobic groups in the gel net work.[94] In this method also gel shrinks during drying. However gel undergoes reversible expansion at critical point and retains wet gel structure due to 'spring back effect'. Schertfeger et al. prepared hydrophobic water glass based aerogels without solvent exchange and supercritical drying.[56] Aging the precursor gel in silane solution is another approach to obtain high strength.[49,48,95,96,97] Earlier reports indicate that the mechanical properties of the wet gel are improved by aging in mother liquor at different temperatures.[98-99] During the aging step, the strength and stiffness of the wet gel increase due to an increased degree of condensation reactions, siloxane cross linking within the gel network, dissolution and reprecipitation of silica and attachment of unreacted oligomers from the gelation process or monomers added from the aging solution.[52] Titulaer et al. found that the pore structure development on aging spherical silica gel bodies is influenced by temperature, pH and the silica to water ratio which affects the rate of silica transport.[100] Chou et al. studied the

effect of aging solvent on silica gels.[101] They related surface area to the polarity parameter of the aging solvent. Hdach et al. investigated the influence of aging and pH on the modulus of aerogels.[102] Davis et al. reported that aging at higher pH yield lower surface area, larger pore volume and a narrow pore size distribution.[103] Haereid et al. has shown that by aging TEOS-based alcogels in solutions of TEOS/ethanol the strength and stiffness can be favourably increased and thereby reduce the shrinkage during drying at ambient pressure. Low-density silica xerogels ($\rho = 0.24$ g/cm^3) are obtained by changing aging parameters such as time and temperature.[46,48,95]

Numerous studies are available in literature on the effect of processing parameters on the properties of resultant silica aerogels.[104] Lee et al. studied the effect of pH on the physicochemical properties of silica aerogels prepared by an ambient pressure drying.[105] Rao et al. investigated the effect of precursors, methylation agents and solvents on the properties of resultant silica aerogels.[55] They prepared low density aerogels (0.14–0.3 g/cm^3) using TMOS and sodium silicate based recipes and TMCS or HMDS as surface modifiers. Using the TMOS precursor, TMCS; and for sodium silicate precursor, HMDS resulted in the best quality silica aerogels in terms of monolithicity, visual transparency and lowest density. Kumar et al. reported the synthesis of high surface area silica by solvent exchange in alkoxy derived silica aerogel under subcritical conditions.[106] They

found that solvents of low vapour pressure and high molecular weight favour the formation of gels with high pore volume. Takahashi reported that the solvent exchange influences the pore structure of silica aerogels.[96] However synthesis of silica aerogel at ambient conditions and its commercialization still remain a great challenge. Since various processing parameters have great influence on the structural and porosity features of the resultant aerogel, the experimental parameters has to be investigated in detail. The present study deals with the synthesis of silica aerogel at subcritical temperature and pressure by varying the synthesis conditions. This chapter includes the effect of hydrolysis temperature, gelation pH, aging pH, aging solvent and surface modification on the porosity characteristics of subcritically dried silica aerogels.

2.1.2 Experimental

2.1.2.1 Materials and Methods

Tetraethoxysilane (Fluka Chemicals) was used as the precursor for the synthesis of silica aerogel under acidic conditions. TEOS was mixed with isopropanol (SD Fine Chemicals) and kept for stirring. Acidified water (0.001 M Hydrochloric acid (SD Fine Chemicals) was added to this mixture very slowly. TEOS:isopropanol:water molar ratio was maintained as 1:4:16.[106] The stirring was continued until a homogeneous mixture was obtained. This sol was then transferred to cylindrical moulds for gelation. After gelation, the gels were

transferred to a 1:1 mixture of isopropanol and water for 24 h. The solvent exchange was done using isopropanol. The gels were washed 5 times with isopropanol within 24 h. For aging, the gel was kept in 80% silane solution in isopropanol for different time intervals. The final step of solvent exchange of these gels was carried out with isopropanol. The gels were taken out and dried at 50 °C for one day and 70 °C for two days. Fig. 2.1.1 shows a process scheme for the synthesis of silica aerogel by subcritical drying method. For the present study hydrolysis temperature, gelation pH, aging solvent composition (isopropanol:water ratio) and aging pH (silane:isopropanol) was varied. Hydrophobic silica aerogel was synthesized by surface modification with trimethylchlorosilane.

2.1.2.2 Characterization of Aerogels

Bulk density of the rod shaped gels was calculated using mass by volume ratio. It is the density of the material including pores and interparticle voids.

$$Volume, V = \pi d^2 h/4$$

where 'd' is the diameter and 'h' is the length of the gel.

Specific surface area and adsorption isotherm of the calcined aerogels were obtained using a BET surface area analyzer (Micromeritics, Gemini Model 2360). The samples were preheated in a flow of nitrogen for 3 h at 200 ^{o}C to remove all the volatiles and chemically adsorbed water from the surface.

TEOS+Isopropanol+H_2O
(1:4:16)

| Hydrolysis

Silica precursor sol

| Gelation

Silica gel rods

Aging
Isopropanol:H_2O

| 50 °C

Solvent exchange → Surface modification
(Isopropanol)   (TMCS)

| 5 times, 50 °C

Aging
Silane:Isopropanol

| 50 °C

Solvent exchange
(Isopropanol)

| 5 times, 50 °C

Drying
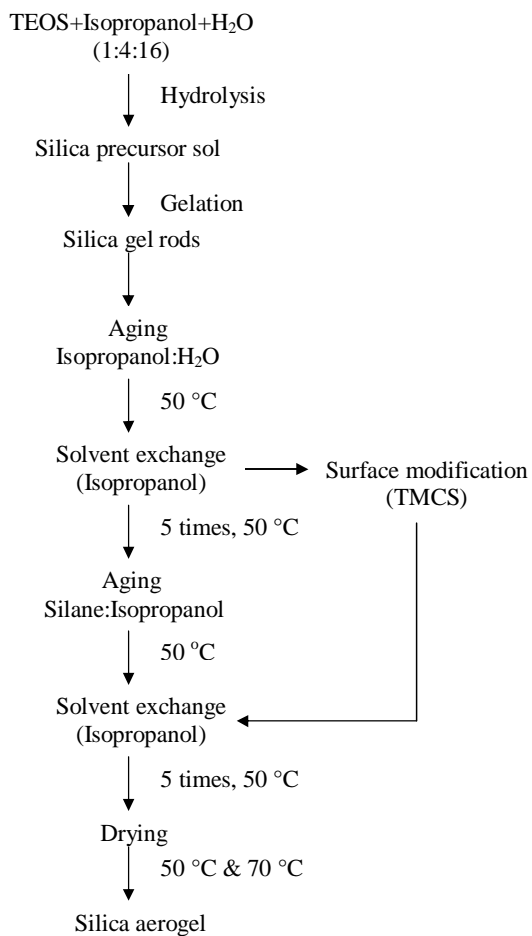| 50 °C & 70 °C

Silica aerogel

Fig. 2.1.1. Flow chart used for the synthesis of silica aerogels

Structural characteristics of the aerogels were investigated by a Fourier Transform Infrared Spectrophotometer (Nicolet, Magna 560) in the range 4,000-400 cm^{-1} by the KBr pellet method. Thermal decomposition curves of the dried

aerogels were obtained using a Differential Thermal Analyzer (Schimadzu, DTA 50) in air at a heating rate of 10 ^{o}Cmin^{-1}. Contact angles were measured using a Tensiometer (Data Physics, DCTAT11). The increase in square of sample weight, when in contact with water was calculated using the same instrument. Porous morphology of the aerogels was observed by Scanning Electron Microscopy (JEOL, JSM 5600LV) in the secondary electron image (SEI) mode.

2.1.3. Results and Discussion

2.1.3.1 Effect of Hydrolysis-Condensation Conditions

The density measurements and BET surface area measurements are given in Table 2.1.1. Density decreased with the increase in hydrolysis temperature. The decrease in density is due to the increased porosity of the aerogels synthesized at a higher hydrolysis temperature. Surface area analysis also reveals that the aerogels possess high porosity. Surface area, average pore size and total pore volume of silica aerogels synthesized at 60 ^{o}C increased to 648 m^2/g, 8.8 nm and 1.44 cc/g from 635 m^2/g, 6.2 nm and 0.99 cc/g respectively.

According to Iler, polymerization of silica occurs in three stages, 1) polymerization of monomers into particles 2) growth of particles 3) linking of these particles into chains and three dimensional networks. Growth of particles (Ostwald ripening) depend on the dissolution-reprecipitation of silica.[26] Dissolution of silica is directly proportional to the temperature.[6] As the

36

temperature is increased, small silica particles dissolve and reprecipitate on larger silica particles. Hence in the present study at higher hydrolysis temperature large number of silica particles are dissolved and reprecipitated. This will improve the strength of the gel network which in turn reduces the shrinkage during drying. Hence we could get a higher pore size and pore volume at higher hydrolysis temperature. Solubility of amorphous silica is largely dependent on the pH of the solution also. Hence gelation of silica aerogels in an NH_3 atmosphere enhances the dissolution-reprecipitation reactions. Necks between particles grow resulting in an increase in the average pore size of the gel. A comparatively large pore size of 18 nm and a higher pore volume of 2.04 cc/g is obtained. Dissolution-reprecipitation reactions of small silica particles are responsible for the increase in mesoporosity. As can be seen from Table 2.1.1, the mesopore volume largely contributes to the total pore volume of the aerogels.

Fig. 2.1.2 shows adsorption isotherms of silica aerogels synthesized at different hydrolysis-condensation conditions. All the isotherms show a type IV behaviour which is the characteristics of a mesoporous material.[107] In the case of silica aerogels synthesized under NH_3 atmosphere volume adsorption is lower at lower relative pressures and it shows a sudden increase at above 0.8. This is due to the increased mesopore volume. Micropores contribute more to the volume adsorption at lower relative pressures whereas mesopores are responsible for the

volume adsorption at higher relative pressures. As the temperature and pH are increased ostwald ripening occurs at a greater extent and the mesopore volume increases.

Table 2.1.1. BET surface area analysis and density measurements of silica aerogels synthesized by varying hydrolysis-condensation conditions

Sample details	Density (g/cc)	Surface area (m²/g)	Average pore size (nm)	Total pore volume (cc/g)	Mesopore volume (cc/g)	Micropore volume (cc/g)
Hydrolysis (30 °C)	0.54	635	6.2	0.99	0.96	0.03
Hydrolysis (60 °C)	0.42	648	8.8	1.44	1.42	0.01
Gelation (NH$_3$ atm.)	--	452	18	2.04	2.01	0.03

BJH pore size distribution of silica aerogels synthesized at different hydrolysis-condensation conditions are provided in Fig. 2.1.3. As the hydrolysis temperature is increased smaller pores decreased and larger pores increased in volume. With the increase in gelation pH (NH$_3$ atm.) a similar trend is observed but to a greater extent. This supports our earlier observation that dissolution-reprecipitation contributes to the increase in the porosity of silica aerogels synthesized at a higher temperature and pH. Larger particles and pores are formed

at the expense of smaller particles and pores. Hence a decrease in smaller pores and increase in larger pores.
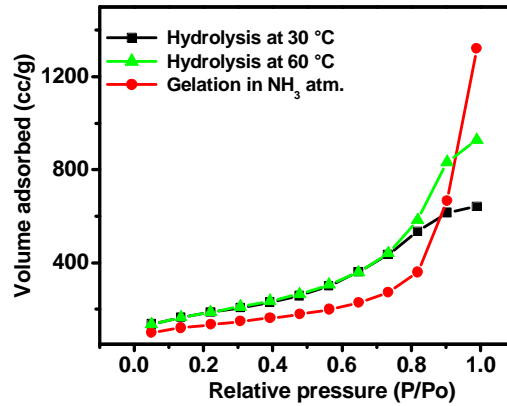

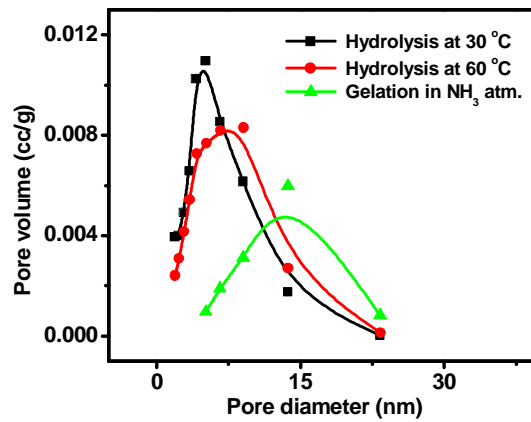**Fig. 2.1.2.** Adsorption isotherms of silica aerogels synthesized by varying hydrolysis-condensation conditions

Fig. 2.1.3. BJH pore size distribution of silica aerogels synthesized by varying hydrolysis-condensation conditions

39

2.1.3.2 Effect of Aging Solvent

Table 2.1.2 gives the surface area results of silica aerogel synthesized using different solvent composition in aging step. Average pore size, total pore volume and surface area decreases as water content is increased in the aging solvent. Silica aerogels aged in isopropanol has a surface area 641 m^2/g, pore volume 1.27 cc/g and pore size of 7.9 nm where as water aged sample has a surface area 621 m^2/g, pore volume 0.62 cc/g and pore size of 3.9 nm.

Table 2.1.2. BET surface area characteristics of silica aerogel aged in different solvent composition

Aging solvent	Surface area (m^2/g)	Average pore size (nm)	Total pore volume (cc/g)	Mesopore volume (cc/g)	Micropore volume (cc/g)
Isopropanol (IPA)	641	7.9	1.27	1.24	0.03
IPA:Water (1:1)	635	6.2	0.99	0.96	0.03
IPA:Water (1:3)	630	4.9	0.89	0.85	0.04
Water	621	3.9	0.62	0.58	0.04

The decrease in porosity is due to the shrinkage during drying. In the present case this can be attributed to the difference in surface tension of the solvent compositions. Capillary pressure, P_c exerted on the pore walls is directly

proportional to the surface tension of the pore liquid. A high surface tension liquid will generate a high capillary pressure and a greater shrinkage during drying.[56] Surface tension of isopropanal and water are 23 mN/m and 72.8 mN/m respectively at 20 ^{o}C. Mixture of these solvents has surface tension in between these values. When a high surface tension liquid such as water is used capillary pressure exerted in the pores will be maximum and greater shrinkage occurs for the dried gel structure. Hence the reduction in porosity is observed. In the case of isopropanol aged samples surface tension is minimum at the pore walls and lesser shrinkage to the gel structure during drying. Hence a greater porosity is observed.

Adsorption isotherms of silica aerogels aged in different solvent composition is provided in Fig. 2.1.4. All the isotherms show type IV behaviour (mesoporous materials). At above a relative pressure of 0.6 water aged samples showed a decrease in volume adsorption. Volume adsorption at higher relative pressure are mainly due to the mesopores. Mesopore voume is decreased in the case of water aged samples. Hence the reduction in volume adsorption. Fig. 2.1.5. shows the BJH pore size distribution of silica aerogels aged in various isopropanol:water ratios. Water aged samples have a narrow pore size distribution and majority of the pores lie below 10 nm. Aging in other solvents resulted in a broader distribution. The pore size distribution of 1:3, 1:1 and isopropanol aged samples shift to the higher pore size region. This shift in pore size distribution can

be again attributed to the surface tension of the aging solvent. Low surface tension liquid will exert less capillary pressure and shrinkage during drying. Hence a greater mesopore volume is achieved with isopropanol.
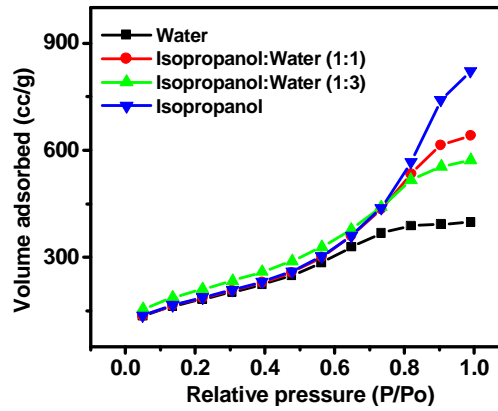

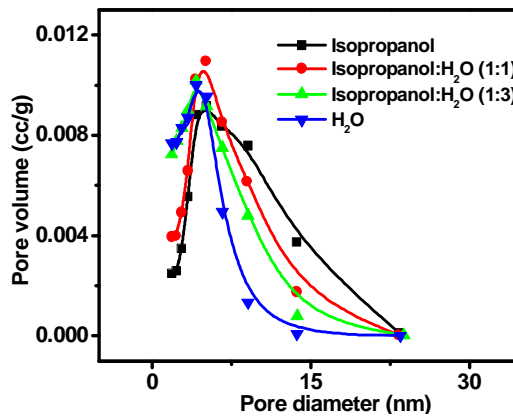**Fig. 2.1.4.** Adsorption isotherms of silica aerogels aged in different solvent composition

Fig. 2.1.5. BJH pore size distribution of silica aerogels aged in different solvent compositions

42

2.1.3.3 Effect of Aging pH

Table 2.1.3 provides BET surface area results of silica aerogels synthesized by changing the pH of aging solution. Surface area decreased from 607 m^2/g to 431 m^2/g where as pore volume and pore size increased from 0.88 cc/g and 5.8 nm to 1.45 cc/g and 13.5 nm respectively when the aging pH was changed from 3 to 11. Solubility of amorphous silica is proportional to pH.[96] At lower pH, dissolution is minimum and as the pH increases solubility of silica increases. The dissolution-reprecipitation reactions increases the pore size and pore volume. In the case of silica aerogels gelled in NH_3 atmosphere (Table 2.1.1), a similar trend is observed. The present results show that even after long time of gelation, aging can influence the final gel structure. The high surface area at an aging pH of 3 can be attributed to small pore size of the aerogel.[107]

Adsorption isotherms of silica aerogels synthesized by aging in different pH are provided in Fig. 2.1.6. All the isotherms show a type IV behaviour which is the characteristic of mesoporous material. For silica aerogels aged at pH ~ 11 volume adsorption is less at lower relative pressures and it is high at higher relative pressures. This shows the high mesoporosity of the samples aged at high pH which is due to the ostwald ripening of silica (Fig. 1.4).

43

Table 2.1.3. BET surface area characteristics of silica aerogel aged
in silanes of different pH

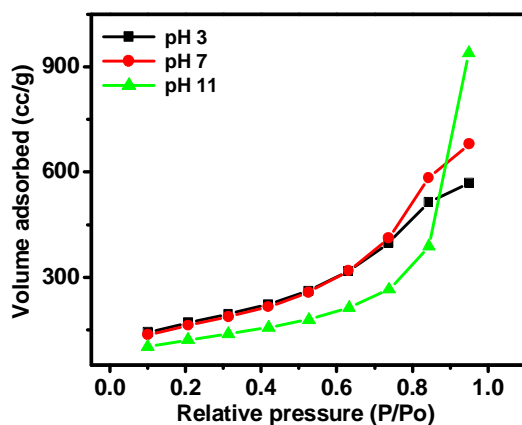| Aging pH	Surface area (m^2/g)	Average pore size (nm)	Total pore volume (cc/g)	Mesopore volume (cc/g)	Micropore volume (cc/g)
3	607	5.8	0.88	0.86	0.020
7	583	7.2	1.05	1.04	0.007
11	431	13.5	1.45	1.44	0.010

Fig. 2.1.6. Adsorption isotherms of silica aerogels aged in silanes of different pH

Fig. 2.1.7 shows the BJH adsorption isotherms of silica aerogels synthesized after aging at different pH. As the pH increases pore size distribution

44

becomes broad and shifts to the right. Aging at a pH of 11 resulted in larger pores and contribution from the small pores are very less.   Dissolution and reprecipitation of silica occur at a greater extent at high aging pH and hence the increase in mesporosity.
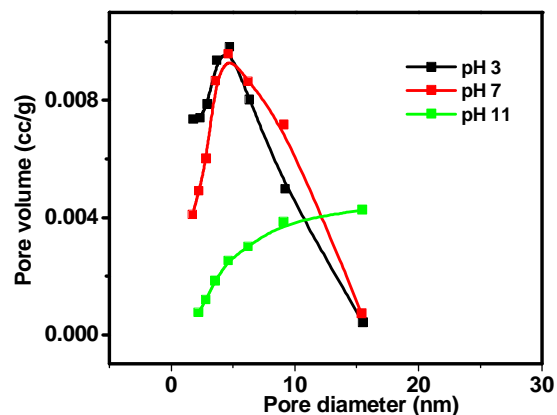

Fig. 2.1.7. BJH pore size distribution of silica aerogels in silanes of different pH

2.1.3.4 Effect of Surface Modification

Long term use of pure silica aerogel is not recommended because of the hydrophilicity of the surface hydroxyl groups of the silica.[108] The hydroxyl groups absorb moisture and minimize the inherent properties of silica aerogel. Besides, surface modification of the hydroxyl groups will reduce the condensation during the drying and reduces collapse of the gel structure. Functionalization of these hydroxyls with organic moieties is an interesting area of research. Many research articles and reviews are available in the literature on these aspects.[108-112] In the

45

present study the effect of surface modification with trimethylchlorosilane in the present synthetic conditions was investigated. Fig. 2.1.8 gives the FTIR spectra of silica aerogels with and without surface modification. Both the graphs show the peak of Si-O-Si asymmetric stretching vibration at 1100 cm^{-1}. The intensity of broad peak corresponding to OH stretching (~3500 cm^{-1}) decreases in the case of hydrophobic silica aerogel. There are additional absorption bands for modified silica aerogels at 2900 and 1450 cm^{-1} related to C-H bonds and at 840 cm^{-1} related to Si-C bonds.[113]
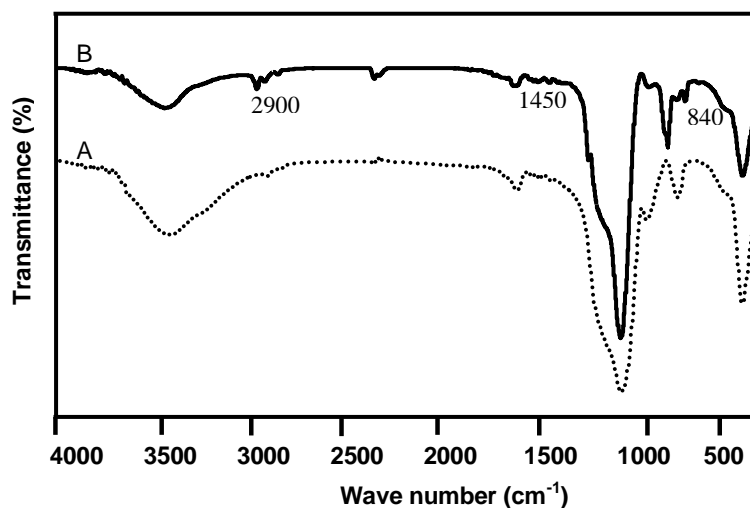

Fig. 2.1.8. FTIR spectra of silica aerogels A) Hydrophilic SiO$_2$ aerogel

B) Hydrophobic SiO$_2$ aerogel

DTA of hydrophilic and hydrophobic aerogels are given in Fig. 2.1.9. Hydrophilic silica aerogels show an endothermic peak at around 100 ^{o}C due to the

46

removal of adsorbed water. Such a peak is absent for hydrophobic silica aerogel which means that adsorbed water is absent in silica aerogels treated with trimethylchlorosilane. Exothermic peak at ~500 ^{o}C corresponds to the decomposition of methyl groups. Hence silica aerogels loose hydrophobicity at ~500 ^{o}C. TGA curve of hydrophobic and hydrophilic aerogels are provided as Fig. 2.1.10. Hydrophilic silica aerogels showed an initial weight loss of ~15% due to the removal of water. This weight loss is less than 2% in the case of hydrophobic silica aerogel.

BET surface area results of hydrophilic and hydrophobic silica aerogel are given in Table 2.1.4. Surface area, average pore size and total pore volume were increased from 621 m^{2}/g, 3.9 nm and 0.62 cc/g to 797 m^{2}/g, 6.4 nm and 1.28 cc/g respectively for hydrophobic silica aerogel. In the case of hydrophobic aerogel surface hydroxyls are replaced with methyl groups. Hence the condensation between hydroxyls at the internal surface of the aerogel is prevented. This will reduce the shrinkage during drying and an increase in average pore size and total pore volume is observed. Spring back effect also contributes to the retention of porosity of the aerogel structure.[109]
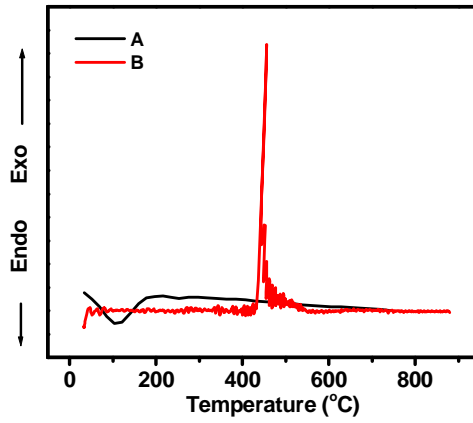
Fig. 2.1.9. DTA pattern A) Hydrophilic SiO$_2$ aerogel
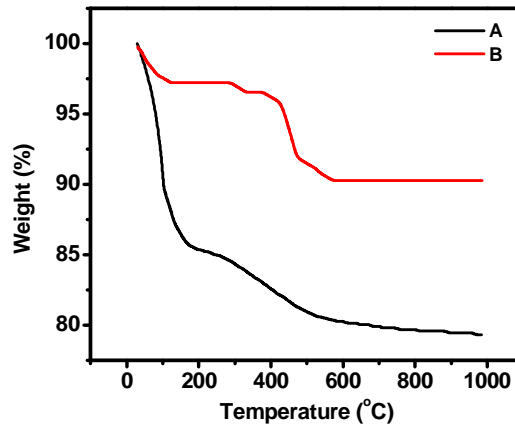
B) Hydrophobic SiO$_2$ aerogel

Fig. 2.1.10. TGA curve A) Hydrophilic SiO$_2$ aerogel

B) Hydrophobic SiO$_2$ aerogel

48

Table 2.1.4. BET surface area characteristics of silica aerogels

Sample	Surface area (m^2/g)	Average pore size (nm)	Total Pore volume (cc/g)	Contact angle
Hydrophilic silica aerogel	621	3.9	0.62	--
Hydrophobic silica aerogel	797	6.4	1.28	87°

Fig. 2.1.11 (A & B) shows the behaviour of hydrophilic and hydrophobic aerogels towards water. In the Fig. 2.1.11 A, hydophobic aerogel float on water where as hydrophilic aerogel sinks. Fig. B shows a single water drop on a hydrophobic silica aerogel surface. Water drop attains nearly spherical shape due to the hydrophobicity of the aerogel sample. Photographs of silica aerogel monoliths synthesized by subcritical technique are provided as Fig. C. The aerogels are either transparent or transluscent which are typical characteristics of silica aerogels. Scanning electron micrograph of silica aerogel (Fig. D.) shows the amorphous nature of the silica as well as uniform distribution of mesopores of size <10 nm.
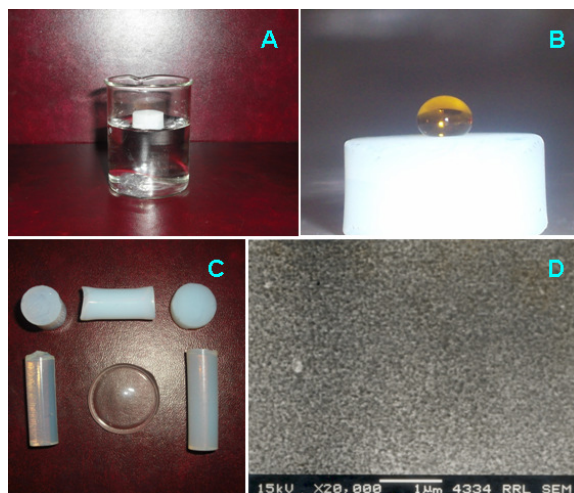
Fig. 2.1.11. A) Hydrophilic (sink) and Hydrophobic (float) aerogel in water B)
Water drop on a hydrophobic silica aerogel C) Photographs of silica aerogel D)
Microstructure of hydrophilic silica aerogel

2.1.4. Conclusions

1. Silica aerogels with tailored porosity were synthesized through subcritical
    drying technique. Tailoring of porosity was achieved by varying the
    experimental (hydrolysis temperature, gelation pH and surface
    modification) as well as aging parameters (aging pH and aging solvent).

2. Hydrolysis temperature and gelation pH influence the porosity of
    subcritically dried silica aerogels. This can be attributed to an enhancement
    in the dissolution-reprecipitation reactions of silica by an increase in
    temperature and pH. Pore size can be varied between 6.2 nm and 18 nm

50

where as pore volume can vary between 0.99 cc/g and 2.04 cc/g by changing the gelation pH.

3. Effect of water content in the aging solvent composition was investigated. Pore size, pore volume and surface area decrease as water content in the aging solvent is increased. The decrease in porosity is due to the high surface tension of solvent.

4. It was found that aging pH affect the porosity of subcritically dried silica aerogels. Surface area decreases from 607 m^2/g to 431 m^2/g where as pore size and pore volume increased from 5.8 nm and 0.88 cc/g to 13.5 nm and 1.45 cc/g respectively by changing the aging pH from 3 to 11. This can be attributed to the progress in dissolution-reprecipitation reactions of the silica with an increase in aging pH.

5. Hydrophobic silica aerogel was synthesized by TMCS/n-Hexane surface modification for long term application of aerogels and compared with the properties of hydrophilic silica aerogels synthesized through subcritical drying technique. It has been found that surface modification enhances the mesoporosity of silica aerogels. However oxidation of organic group responsible for hydrophobicity occurs at ~500 °C as evidenced by DTA and hence it loses hydrophobicity above that temperature.

2.2 Synthesis of Silica Aerogel Using Organic Templates

2.2.1 Introduction

Major problems during the synthesis of low-density, high-surface-area materials at ambient pressure primarily arise from the large capillary pressure that occurs during drying (a result of the small pore sizes) and low stiffness (a result of the low-density).[114] Supercritical drying reduces the capillary pressure to a minimum.[39] However this technique is not recommended for the commercial synthesis of aerogels because of its expensive and hazardous nature.[56,115,116] Several methods were attempted to avoid supercritical technique and synthesize aerogel at ambient conditions.[55,56,57,117] One approach is based on an aging technique in which wet gels are aged in mother liquor to promote dissolution-reprecipitation of silica monomer to improve the strength and stiffness of the network.[46,95,96,117,118] Another approach is the use of organic additives.[114,119,120] Organic additives either act as a template or as drying control chemical additive. In both the cases it increases the porosity of silica aerogels. DCCA will reduce the differential drying stresses by minimizing the differential rates of evaporation, and ensuring a gel structure with uniform pore and particle sizes.[121] DCCA can also control the rate of hydrolysis and condensation reaction, pore size distributions, pore liquid vapour pressure and drying stress. Uniform scale of structure achieved

during gelation results in uniform growth of the network during aging, which increase the strength of the gel and its ability to resist drying stress.[60]

Influence of various DCCAs in the sol-gel processing of xerogels have been investigated and discussed by many authors.[59,119] However, a few reports are available in the literature on the preparation of monolithic silica aerogels using DCCAs.[59,60,62,119,121] Haranath et al. investigated the influence of oxalic acid, glycerol, N, N dimethylformamide and formamide on the optical transmittance and porosity features of TMOS based aerogels.[121] They found that pore size distribution shifts towards smaller pore radii for acidic DCCA and larger pore radii for basic DCCAs. They also reported that DCCA/TMOS molar ratio of ~ 0.4 as the limiting value for almost all the modified aerogels, above which cracking probability of the aerogels increased drastically. Polyethyleneglycol was used by some researchers as a template for the synthesis of aerogels.[62,63] Their study revealed that high concentrations of PEG weaken the solid matrix whereas small concentration of PEG strengthen the matrix. Reetz et al.[64] used polyvinylalcohol and PEG as biocatalyst supports, because it was found that the lipase activity was significantly enhanced in the presence of these additives. Rao et al.[122] reported the influence of *N*, *N*-dimethylformamide and glycerol on the physical properties of TEOS silica aerogels. They got a narrow and uniform distribution of pores when DCCA was used. However use of organic templates to tailor the porosity of

subcritically dried silica aerogels still remains a great challenge and many factors need to be explored. We synthesized silica aerogels using different concentrations of Polyethyleneoxide (PEO), Cetyltrimethylammoniumbromide (CTAB), Polyethyleneglycol (PEG), Hexamethylenetetramine (HMTA) and investigated their effect on the porosity features of subcritically dried aerogels.

2.2.2 Experimental

Tetraethoxysilane (TEOS, Aldrich Chemicals) is mixed with isopropanol (SD Fine Chemicals) and kept for stirring. Acidified water (0.001M Hydrochloric acid) was added to this mixture very slowly. TEOS:isopropanol:water molar ratio was maintained as 1:4:16.[106] The stirring was continued until a homogeneous mixture was obtained. PEO (MW 80,000,00, Aldrich Chemicals) was added to the sol. Concentration of PEO was varied as 0, 0.1, 0.3, 0.5, 1 weight percentage (wt%) of silica. This sol was then transferred to cylindrical moulds for gelation. After gelation, the gels were transferred to a 1:1 mixture of isopropanol and water for 24 h. The solvent exchange was done by isopropanol. The gels were washed 5 times with isopropanol within 24 h. For aging, the gel was kept in a 80% silane in isopropanol solution for 48 h. The final step of solvent exchange of these gels was carried out with isopropanol. The gels were taken out and dried at 50 °C for one day and 70 °C for two days. Fig. 2.2.1 provides the process scheme used for the synthesis of silica aerogel. The experiment was repeated using CTAB (0.1, 0.3,

0.5, 1 wt%), HMTA (0.1, 0.3, 0.7, 1 wt%) and PEG (0.1, 1, 2, 3 wt%). CTAB,

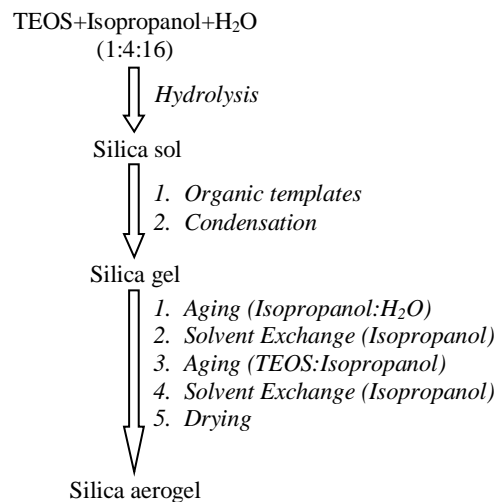HMTA and PEG (MW 285) was purchased from SD Fine Chemicals.

TEOS+Isopropanol+H$_2$O
(1:4:16)

Hydrolysis

Silica sol

1. *Organic templates*
2. *Condensation*

Silica gel

1. *Aging (Isopropanol:H$_2$O)*
2. *Solvent Exchange (Isopropanol)*
3. *Aging (TEOS:Isopropanol)*
4. *Solvent Exchange (Isopropanol)*
5. *Drying*

Silica aerogel

Fig. 2.2.1. Flow chart for the synthesis of silica aerogel

2.2.3. Results and Discussion

2.2.3.1 Silica-PEO Aerogel

Development of ordered mesoporous structures enhanced the significance

of surfactants as templates.[123-124] Surfactant templated synthesis of mesoporous

silica nanostructures is an area of great interest.[125-127] Matos et al. demonstrated the

effect of surfactants on the porosity of carbon xerogels.[128] They found that the

addition of cationic surfactant increased the pores size (2–25 nm) and the size of

carbon particles whereas anionic surfactants promote larger mesopore size (2–40

55

nm and larger than 80 nm) and a bimodal pore size distribution. Polyethyleneoxide block polymers as well as homo polymers have been used as an organic template for the synthesis of mesoporous silica by many researchers.[129] The present study deals with the synthesis of silica aerogels using polyethylene oxide as an organic template.

Fig. 2.2.2 provides DTA and TGA of silica and silica-PEO aerogels (Si-PEO). An endothermic peak corresponding to adsorbed water is observed in the DTA of silica and silica-PEO aerogel. An exothermic peak at around 250 ^{o}C in the case of Si-PEO is due to the thermal decomposition of polyethyleneoxide.[130] TGA shows a three step weight loss for both the aerogels. First step corresponds to the desoption of adsorbed water in both cases. Second step of weight loss is due to the chemically adsorbed water in the case of silica aerogels. Si-PEO aerogel showed a greater weight loss at this step since the weight loss due to decomposition of polyethylene oxide overlap with that of chemically adsorbed water.[130]

Fig. 2.2.3 provides adsorption isotherm of Si-PEO aerogels. All the isotherms show type IV behaviour which is the characteristics of mesoporous materials. Table 2.2.1 gives surface area results of silica aerogels synthesized with different concentration of PEO. Surface area, pore volume and pore size initially increases as the concentration of PEO increased from 0.1 to 0.3 wt%. Si-0.1 wt%

56

PEO has a surface area 731 m^2/g, pore size 5.8 nm and pore volume 1.07 cc/g. As the concentration increased to 0.3 wt% these values increased further to 907 m^2/g, 18.9 nm and 4.29 cc/g.
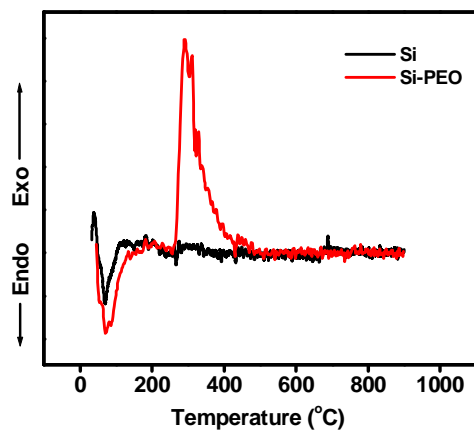

Fig. 2.2.2 A) DTA of Si and Si-PEO aerogel
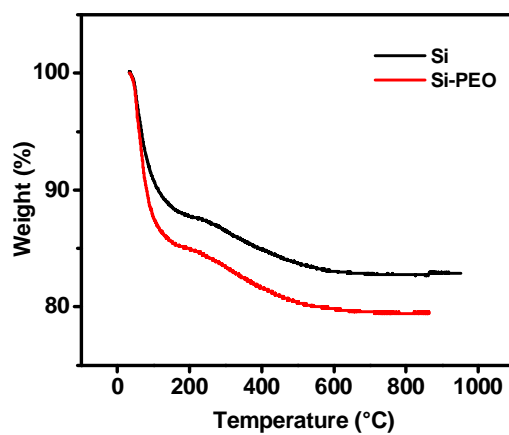

Fig. 2.2.2 B) TGA of Si and Si-PEO aerogel

57

Table 2.2.1. BET surface area results and dielectric constants of Si-PEO aerogels

PEO (wt%)	Surface area (m^2/g)	Average pore size (nm)	Total pore volume (cc/g)	Micro pore volume (cc/g)	Meso pore volume (cc/g)	Dielectric constant
0	635	6.2	0.99	0.03	0.96	2.52
0.1	731	5.8	1.07	0.048	1.022	2.33
0.3	907	18.9	4.29	0.057	4.233	2.29
0.5	492	20.8	2.49	0.036	2.454	2.34
1	672	9.6	1.62	0.047	1.573	2.38

The increase in surface area can be attributed to the corresponding increase in micro as well as mesoporosity. Christine et al. showed that a gradual transition occur from microporous to micro-mesoporous with increasing PEO content in the sol-gel mixture.[129] The present results also show similar effect. However surface area and pore volume decrease above 0.3 wt% of PEO. As the concentration of PEO is further increased to 0.5 wt% in the silica system the surface area and pore volume decreased to 492 m^2/g and 2.49 cc/g respectively. This means that above a

particular concentration, PEO does not increase the porosity of silica system. This is clear as even with 1 wt% PEO, pore volume shows a tendency to decrease.
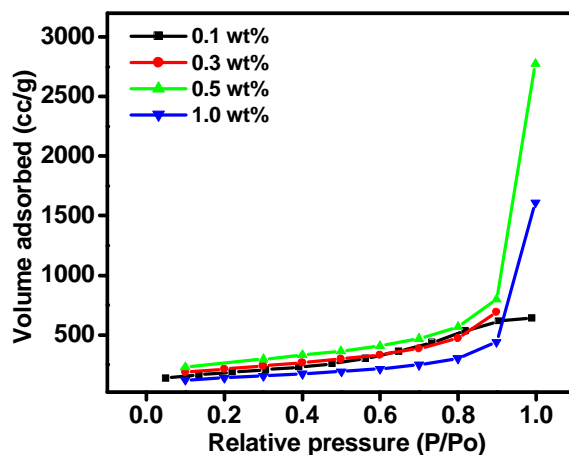

Fig. 2.2.3. Adsorption isotherms of Si-PEO aerogels with different concentration of PEO

The transition from a purely microporous to a micro-mesoporous material is attributed to the solubility limit of the hydrophilic PEO in the silica matrix.[129] Above a critical volume fraction of PEO in the sol-gel mixture, pores will increase in size until the mesopore regime is reached, which can be described by a process of unspecific nanoscale demixing.[129] In other words, the probability of a pore being formed by more than one individual PEO chain increases with the PEO volume fraction. The macroscopic properties of silica made in presence of large amounts of PEO in the sol-gel mixture confirm the unspecific demixing of Si-PEO hybrid by being opaque, the light scattering domains being crystalline PEO.

Samples made with lower PEO volume fractions are transparent and completely amorphous.

2.2.3.2 Silica-CTAB Aerogel

Cationic surtactants (Quarternary ammonium salts) are reported to be efficient templates for the synthesis of mesoporous materials.[124,127] In the present study CTAB is used as an organic template for the porosity control of mesoporous silica aerogels. Thermal analysis of the Si-CTAB aerogels were carried out using DTA and TGA. Fig. 2.2.4 provides DTA of the hybrid aerogels.
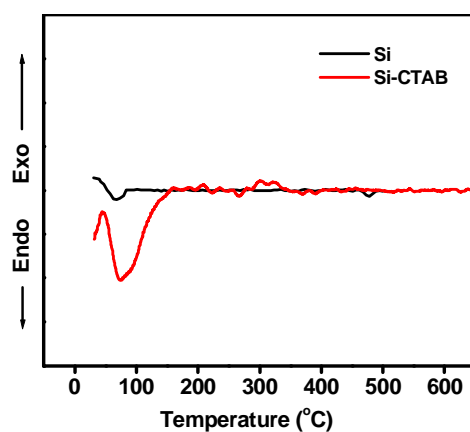

Fig. 2.2.4 DTA of Si and Si-CTAB aerogel

DTA of Si and Si-CTAB aerogel shows an endothermic peak at around 80 ^{o}C due to the removal of adsorbed water. Many exothermic peaks are observed in the temperature range 200-400 ^{o}C due to the decomposition of organic moieties. It has been reported that cetyltrimethylammonium surfactants undergo several

decomposition steps during the calcination. The majority of the surfactants first break down to form hexadecane and a trimethylamine species in the temperature range of 100 to 220 ^oC.[131] Upon heating at high temperatures the carbon chain fragments are eliminated and the available surface becomes hydrophilic. Fig. 2.2.5 shows the TGA of Si and Si-CTAB aerogel.
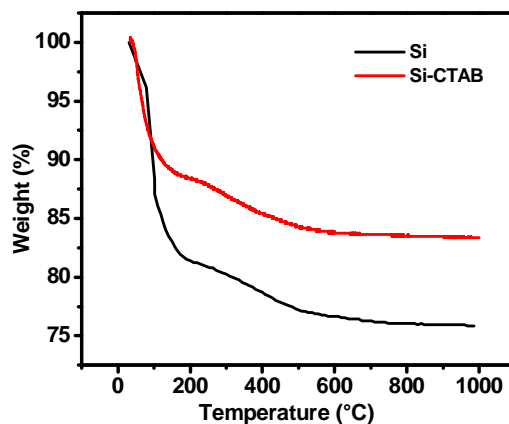

Fig. 2.2.5. TGA of Si and Si-CTAB aerogel

Both the curves show a three step decomposition pattern. First step is due to the loss of adsorbed water. Weight loss due to adsorbed water is lower in the case of Si-CTAB aerogel. Silica aerogels showed ~20% weight loss at this step where as Si-CTAB aerogels showed only 12%. This can be attributed to the partial hydrophobicity of Si-CTAB aerogels.[131] Second step of weight loss which starts from 200 ^oC is due to the removal of chemically bonded water in the case of silica aerogel. A similar weight loss is observed for Si-CTAB aerogel at this temperature

range corresponding to the decomposition of organic moieties in the DTA curve. Third step of weight loss corresponds to the dehydroxylation in both the cases.

Fig. 2.2.6 represents adsorption isotherms of Si-CTAB aerogels with different concentration of CTAB. All the isotherms are of type IV which show the mesoporous nature of the resultant aerogels. Table 2.2.2 provides the BET surface area results of Si-CTAB aerogels. Silica aerogel has a surface area of 635 m^2/g, pore size 6.2 nm and pore volume 0.99 cc/g. As the concentration of CTAB is increased surface area decreases and pore size and pore volume increases. Si-0.1 wt% CTAB has a surface area 545 m^2/g, pore size 8.1 nm and pore volume 1.04 cc/g. As the concentration of CTAB is increased to 1 wt% surface area decreases to 501 m^2/g, and pore size and pore volume increase to 19.5 nm and 2.45 cc/g respectively. Intermediate concentrations also showed similar trend. Matos et al. has reported that addition of cationic surfactant increases the pores size (2–25 nm) and the size of particles in the case of carbon xerogels.[128] The decrease in surface area is due to the increase in pore size. Smaller pores have a greater surface area compared to the larger pores.[107] The increase in pore size with respect to the concentration of surfactant is related to the elimination of surfactant upon calcination. Combustion of larger number of organic molecules enhances the porosity of the inorganic matrix.
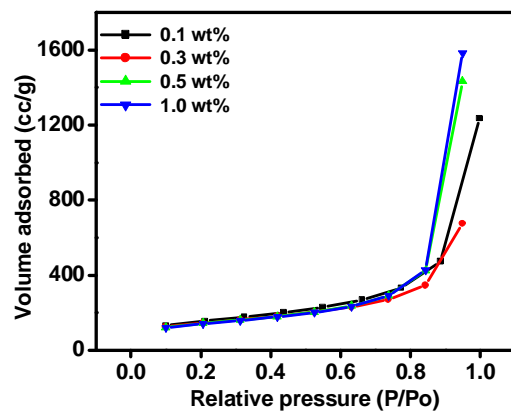
Fig. 2.2.6. Adsorption isotherms of Si-CTAB aerogels with
different concentration of CTAB

Table 2.2.2. BET surface area characteristics of Si-CTAB aerogels

CTAB (wt%)	Surface area (m^2/g)	Total pore volume (cc/g)	Average pore size (nm)
0	635	0.99	6.2
0.1	545	1.04	8.1
0.3	511	1.91	14
0.5	508	2.21	17.4
1	501	2.45	19.5

2.2.3.3 Silica-HMTA Aerogel

HMTA is reported as an organic template and cross linking agent for the synthesis of mesoporous materials. Wu et al. has used HMTA as a crosslinking agent for the synthesis of carbon aerogel.[132] They reported that HMTA works not only as a catalyst but also as a cross-linking reagent, which will affect the size and stacking of the organic particles and thus improve the strength of the alcogel network. In the present study we used HMTA as a template for the synthesis of silica aerogels at ambient conditions. Fig. 2.2.7 is the DTA pattern of Si and Si-HMTA aerogel where as Fig. 2.2.8 is the TGA curve of the same.
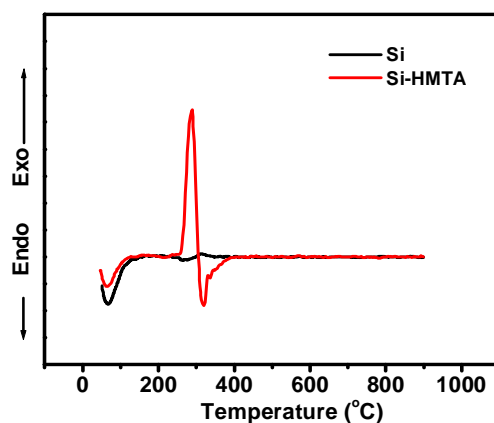

Fig. 2.2.7. DTA of Si and Si-HMTA aerogel

An endothermic peak at around 90 ^{o}C in the DTA is due to the removal of adsorbed water and is present in Si and Si-HMTA aerogel. This corresponds to ~12.5 wt% loss in the TGA curve. However Si-HMTA aerogel showed a slight

64

decrease in weight loss (~11 wt%) at this range. The phenomena may be due to the presence of organic groups on the surface of the silica which inhibits the adsorption of water. An exothermic peak at around 250 ^{o}C is due to the decomposition of methylene group in Si-HMTA aerogel. This weight loss is observed in the range 200-300 ^{o}C in the TGA and it is ~2.5 wt%. The rest of the weight loss in this temperature range corresponds to the removal of chemically bonded water and is observed in the silica aerogel also. Third step of weight loss at above 500 ^{o}C corresponds to dehydroxylation.
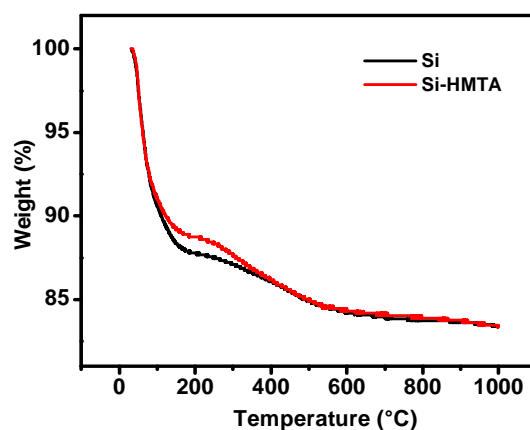

Fig. 2.2.8 TGA of Si and Si-HMTA aerogel

Table 2.2.3 provides BET surface area results of Si and Si-HMTA aerogels. Surface area, pore size and pore volume increase initially with increase of HMTA concentration and then it decreases. Silica aerogel has a surface area 635 m^2/g,

65

pore size 6.2 nm and pore volume 0.99 cc/g which increased to 884 m^2/g, 10.4 nm and 2.3 cc/g with an addition of 0.7 wt% HMTA. The increase is steady up to 0.7 wt%, but it decreases on further addition of HMTA. It has been reported that cross-linking with HMTA enhances the strength of the gel network.[132] Hence a drecrease in shrinkage during drying and an increase in porosity of the resultant aerogels. Fig. 2.2.9 provides adsorption isotherms of Si-HMTA aerogel. Isotherms exhibit type IV behaviour indicating the mesoporous nature of the aerogels.

Table 2.2.3. BET surface area results of Si-HMTA aerogels

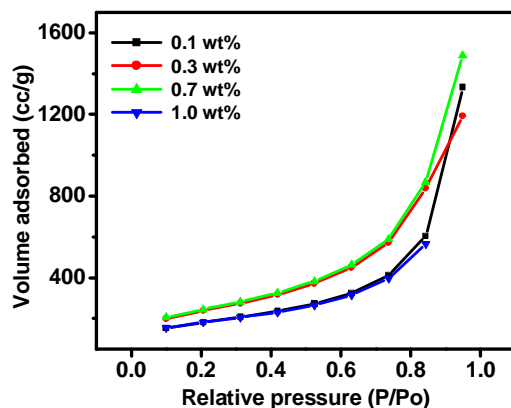| HMTA (wt%)	Surface area (m^2/g)	Total pore volume (cc/g)	Average pore size (nm)
0	635	0.99	6.2
0.1	648	2.06	12.7
0.3	884	2.3	10.4
0.7	860	1.84	8.5
1	648	0.87	5.4

66

Fig. 2.2.9. Adsorption isotherms of Si-HMTA aerogels with different concentration of HMTA

2.2.3.4 Si-PEG Aerogel

PEG has been widely used as a DCCA for the synthesis of mesoporous silica. PEG forms hydrogen bonds both with water and the silanol groups and helps to reduce the capillary pressure during drying.[133-134] We have adopted PEG as an organic template for the synthesis of silica aerogel at ambient conditions. DTA of Si and Si-PEG aerogel is provided as Fig. 2.2.10. An endothermic peak corresponding to the adsorption of water is observed at ~100 ^{o}C in both the case. The exothermic peak at ~300 ^{o}C is due to the oxidation of organic compounds.

Table 2.2.4 demonstrates surface area results of Si-PEG aerogels. Surface area increases with increase in concentration of PEG. Si-1 wt% PEG has a surface area of 697 m^2/g, pore volume 0.827 cc/g and 4.7 nm which increased to 762 m^2/g, 0.982 cc/g and 5.1 nm respectively as the concentration of PEG increased to 3

67

wt%. The increase in surface area and porosity can be attributed to the removal of organic template upon calcination. Fig. 2.2.11 provides adsorption isotherms of Si-PEG aerogels. All the isotherms are of type IV (mesoporous characteristics).
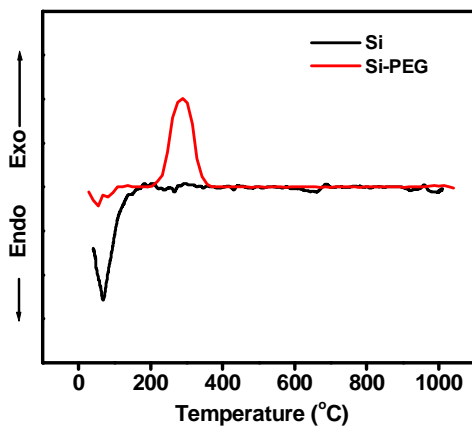

Fig. 2.2.10. DTA of Si and Si-PEG aerogel

Table 2.2.4. BET surface area results of Si-PEG aerogels

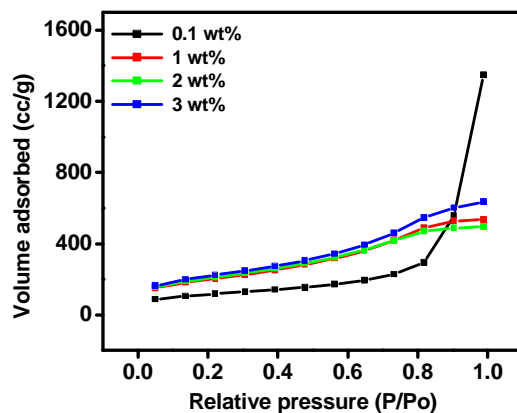| PEG (wt%)	Surface area (m^2/g)	Total pore volume (cc/g)	Average pore size (nm)
0	635	0.99	6.2
1	697	0.827	4.7
2	718	0.767	4.2
3	762	0.982	5.1

68

Fig. 2.2.11. Adsorption isotherms of Si-PEG aerogels with different concentration of PEG

2.2.4 Conclusions

1. Silica aerogels were synthesized at ambient conditions using different organic templates such as PEO, CTAB, HMTA and PEG, and investigated the effect of its concentration on the porosity features of resultant aerogels.

2. The pore size could be tailored well and so also pore volume and surface area, by varying the concentration of organic additives. All the aerogels showed type IV adsorption isotherms which are the characteristic of mesoporous materials.

3. Thermal analysis of silica aerogels with organic additives showed that decomposition of organics starts at ~200 ^{o}C and completes at ~400 ^{o}C. Hence 400 ^{o}C was selected as the calcination temperature to eliminate organic templates and attain porosity.

69

4. Use of PEO (0.3 wt%) as template resulted in a surface area as high as 907 m^2/g, pore size 18.9 nm and pore volume 4.29 cc/g. The dielectric constant of the aerogel is found to be 2.29 at 13 MHz.

5. Si-CTAB aerogels showed relatively lower surface area (501-545 m^2/g) compared to other organic additives. However we could get a total pore volume of 2.45 cc/g and 19.5 nm for Si-1 wt% CTAB.

6. Si-HMTA aerogels possessed a maximum surface area of 884 m^2/g, pore volume 2.3 cc/g and average pore size 10.4 nm for 0.3 wt% HMTA.

7. Si-PEG aerogels possess a lower pore size (4.2 nm-5.1 nm) compared to other silica aerogels. Maximum surface area obtained was for Si-3 wt% PEG and is 762 m^2/g. It had a total pore volume of 0.982 cc/g and an average pore size of 5.1 nm.

8. Correlation of the molecular weights of the polymers (PEO and PEG) with the surface area results we could say that molecular weight of the polymers affect the porosity of resultant aerogels. Low molecular weight polymer (PEG, Mw ~ 285) resulted in a lower pore size, pore volume and surface area whereas high molecular weight of the polymer (PEO, Mw ~80,000,00) resulted in a greater pore size, pore volume and surface area.

2.3 Synthesis of Silica Microspheres through Sol-Emulsion-Gel Technique

2.3.1 Introduction

Synthesis of mesoporous materials having regular geometries has been of considerable interest in recent years owing to their great potential in catalysis, adsorption, separation, sensing, medical use, ecology and nanotechnology.[135-140] Microspheres are widely employed as a feed material for plasma sprayed coatings, as thermal insulators, light weight filler in composites, internal confinement fusion of nuclear material, substrates for controlled drug release and gas storage materials.[141-144] Microspheres are generally synthesized by the dual nozzle hollow drop generation[145], spray pyrolysis[146], emulsion–evaporation[147], melting in dc plasma[148], or sol–emulsion–gel techniques.[149–152] The sol–emulsion–gel method is widely practiced for the preparation of ceramic microspheres. Mesoporous silica microspheres find application in diverse fields including clinical, pharmaceutical, electronic packaging, selective adsorption, chemical sensing, controlled drug delivery and also in the preparation of silica glass, structural ceramics and chromatographic columns.[153-154] Artificial opals are SiO_2 microspheres synthesized by self assembly methods to form a close packed structure.[155] Silica microspheres have been used as an immobilization matrix for several molecules.[143,144,156] Spherical silica particles with modified surface properties are important in composite materials, adsorbents, pigments, detergents, cosmetics and

71

pharmaceuticals.[157–159] Functionalization of the silica particle surface can be used to enhance or control the overall properties.[160–162] In the present work, a modified sol–emulsion–gel process was developed for the synthesis of hydrophobic silica microspheres. Hydrophobicity was induced by surface modification using trimethylchlorosilane. The sol–emulsion–gel process involves silica sol generated from TEOS as aqueous phase, n-Hexane as the oil phase and sorbitanmonooleate (Span 80) as the surfactant to enhance the emulsion formation. Effect of surfactant concentration, aging time and viscosity of the silica sol on microsphere formation is investigated.

2.3.2 Experimental

The water in oil emulsion was prepared using silica sol as the aqueous phase and n-Hexane (SD Fine Chemicals) as the oil phase. Silica sol was obtained by hydrolyzing tetraethylorthosilicate (Sigma Aldrich Chemie) with 10^{-3} M hydrochloric acid (SD Fine Chemicals) using isopropanol (SD Fine Chemicals,) as the homogenizing solvent. The tetraethylorthosilicate:isopropanol:water ratio was kept as 1:4:16.[50] In a typical synthesis of silica microspheres, 20 ml hexane was mixed with 5 ml silica sol and Span 80 (SD Fine Chemicals) was added under stirring (500 rpm). The effect of surfactant concentration on microsphere properties was studied by varying the concentration of surfactant as 0.5, 1, 1.4, 1.8, and 2 volume percentage. Constant stirring for 20 minutes resulted in silica

microspheres. The spheres were decanted, then solvent exchanged (five times) with hexane and the product divided into two parts. One part was made hydrophobic by treating with trimethylchlorosilane (TMCS) (Sigma Aldrich Chemie) for a period of 24 h and the other part was dried at 70 ^{o}C. The hydrophobic spheres were solvent exchanged with hexane (five times) after functionalization and dried at 70 ^{o}C. The flow chart for microsphere synthesis is provided in Fig. 2.3.1. In order to study the effect of viscosity, silica sols aged for different time periods (2, 5, 8, 11, and 17 h) were used for the preparation of the microspheres.
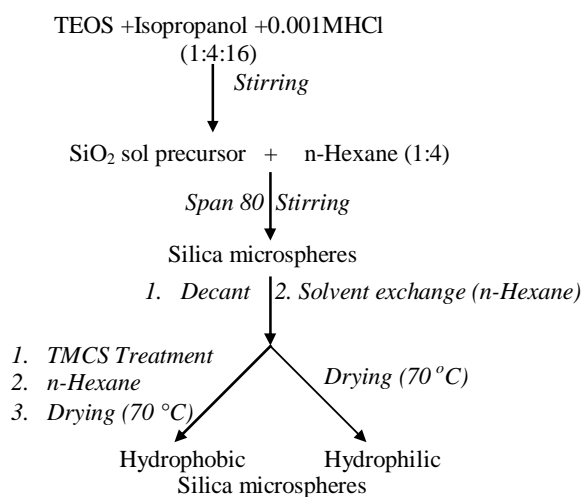
TEOS +Isopropanol +0.001MHCl
(1:4:16)
Stirring

SiO$_2$ sol precursor + n-Hexane (1:4)

Span 80 *Stirring*

Silica microspheres

1. Decant *2. Solvent exchange (n-Hexane)*

1. TMCS Treatment
2. n-Hexane
3. Drying (70 °C)

Drying (70 ^{o}C)

Hydrophobic   Hydrophilic
Silica microspheres

Fig. 2.3.1. Flow chart for the synthesis of silica microspheres

73

Rheological behaviour of the precursor sol was monitored using a rheo viscometer (Anton Paar GmbH) employing the cylinder and bob method. Structural characteristics of the microspheres were investigated by a Fourier Transform Infrared spectrophotometer (Magna 560, Nicolet) in the range 400–4,000 cm^{-1} by the KBr pellet method and thermal decomposition curves of the dried microspheres were obtained using a Differential Thermal Analyzer (DTA 50, Shimadzu) in air at a heating rate of 10 ^{o}C min^{-1}. Specific surface area and adsorption isotherm of the samples were obtained using a BET surface area analyzer (Gemini 2360, Micromeritics). Contact angles were measured using a Tensiometer (DCAT11, Data Physics) under dynamic mode. The increase in square of sample weight, when in contact with water was calculated using the same instrument. Microsphere morphology was observed using an Optical Microscope (MZ16 A, Leica) in transmission mode and by Scanning Electron Microscopy (JSM 5600LV, JEOL) in the secondary electron image (SEI) mode.

2.3.3 Results and Discussion

2.3.3.1 Effect of Surfactant Concentration

In a sol–emulsion–gel process, an aqueous sol phase is dispersed in a non polar oil phase to form the emulsion. The high interfacial tension between the aqueous phase and the oil phase is reduced by the addition of an amphiphilic surfactant making the emulsion kinetically stable.[163-164] Mechanical agitation

provides the energy to overcome the interfacial tension and disperse the aqueous phase to form the emulsion. Surfactant concentration and viscosity of the sol droplets control sphere formation in a sol–emulsion–gel process,[149-150] and although these influences have been observed in alumina and other systems there are few reports on their effect for silica.[164] Hence in the present study the effect of surfactant concentration (Span 80), effect of aging time, and sol viscosity on the synthesis outcome have been investigated.

Altering the concentration of Span 80 modified the morphology, diameter, and uniformity of the resultant silica microspheres (Fig. 2.3.2). For this study, silica sol as prepared (with out aging) was used. When 1 vol% surfactant was used, mostly irregular particles were obtained, as sphere formation was incomplete. Probably the concentration of surfactant was inadequate to form a monodispersed emulsion. On increasing the Span 80 concentration to 1.4 vol% smaller and more uniform particles (50 µm) resulted (Fig. 2.3.3). For a surfactant concentration of 1.8 vol% clustering and aggregation was observed while a further increase to 2 vol% yielded larger spheres and many spheres collapsed. The critical micelle concentration (CMC) of the surfactant in the continuous liquid phase controls emulsion stability and hence sphere formation.
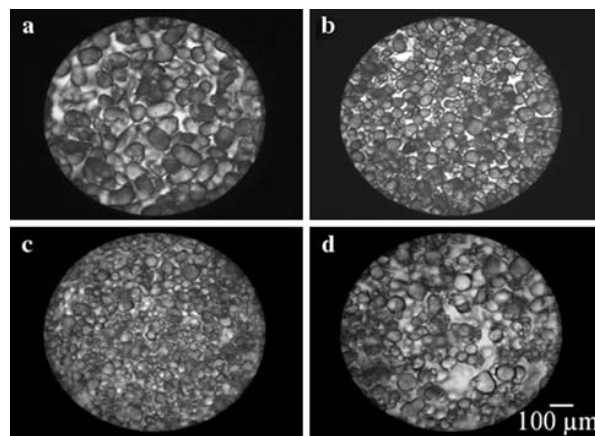
Fig. 2.3.2. Optical micrographs of silica microspheres synthesized by varying concentration of Span 80 a) 1 vol% b) 1.4 vol% c) 1.8 vol% d) 2 vol%
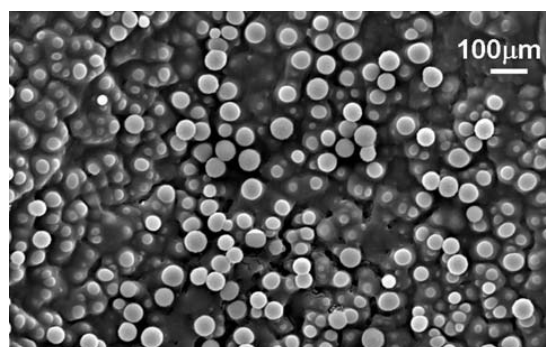

Fig. 2.3.3. Scanning electron micrograph of silica microspheres synthesized using 1.4 vol% Span 80

Fig. 2.3.4 shows the variation of surface tension of n-hexane with Span 80, where the discontinuity gives the CMC as between 1 and 1.5 vol%.[163-164] In a surfactant-hydrophobic solvent system, the surfactant molecules tend to reduce

unfavorable interactions by minimizing exposure of the hydrophilic end to the hydrophobic solvent molecules by locating at the interface at low concentrations and forming assembled structures at higher concentrations. The minimum concentration required to form assembled structures coincides with the CMC. In an emulsion, when the surfactant concentration is above CMC destabilization of the emulsion, flocculation will ultimately occur, a phenomenon exploited in the fractionation technique of Bibette.[165] Aggregated and deformed structures result when flocculated emulsion droplets undergo gelation.
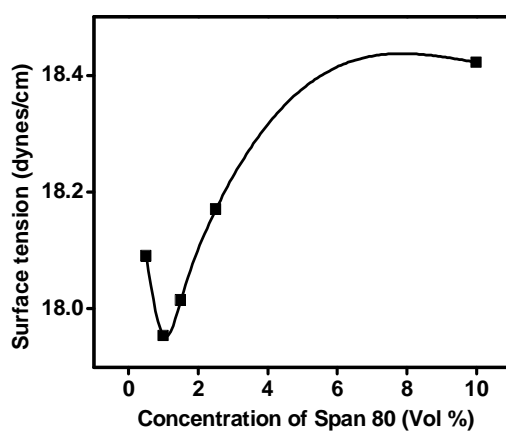

Fig. 2.3.4. Surface tension of n-Hexane with different concentration of Span 80

The surface area of the microspheres decreases when the concentration of Span 80 increases (Table 2.3.1). For 1 vol% Span 80 a surface area of 363 m^2/g was obtained and it decreases to 296 m^2/g for 1.8 vol%. Sol–gel condensation of

77

silica results in a highly porous gel network which collapse partially during drying, due to stress. The high surface area values are a clear indication of the porous nature of the spheres. The slight increase in average pore diameter with surfactant concentration arises from agglomeration observed for high surfactant concentrations. In the adsorption isotherms (Fig. 2.3.5) spheres prepared at lower surfactant concentrations (1–1.4 vol% Span 80) show a plateau at high pressures that is absent at higher concentrations. This indicates a greater contribution from larger pores (>50 nm) in latter material due to agglomeration.[107] When the contribution to the pore volume from larger pores increases the surface area decreases.

Table 2.3.1. BET surface area results of silica microspheres

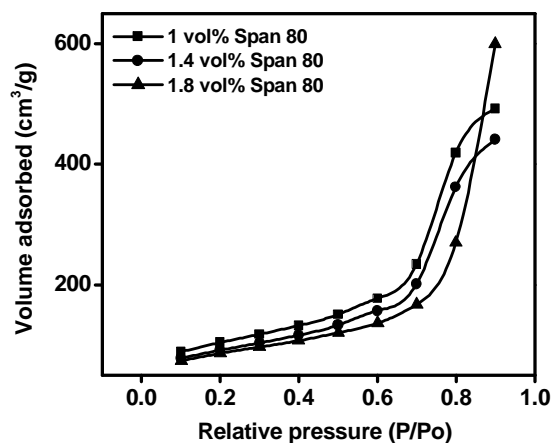| Span 80 (vol%)	Surface area (m^2/g)	Average pore size (nm)	Total pore volume (cc/g)
1	363	8.3	0.76
1.4	319	8.5	0.78
1.8	296	9.4	0.93

78

Fig. 2.3.5. Adsorption isotherms of silica microspheres
synthesized by varying the concentration of Span 80

2.3.3.2 Effect of Viscosity of Silica Sol

Viscosity of polymeric silica sol varies with time.[26] Kim et al. observed the influence of viscosity of silica sol on sphere formation in a hollow drop generation method for preparing hollow silica spheres.[145] Silica sol aged for different times of 5–17 h were used at a surfactant concentration of 1.4 vol%. Optical microscopy showed that 8 h aging gives more uniform spheres of size ~50 μ m (Fig. 2.3.6), with longer times (11 and 17 h) resulting in aggregated and deformed spheres. During aging, condensation reactions proceed in the silica sol and networked clusters start to form. After gelation has proceeded considerably, it will be difficult to form spherical droplets of uniform size and shape from the sol. The optimum

79

viscosity to obtain uniform spheres represents the balance between the extent of gelation and the droplet sizes achievable for the particular surfactant concentration, volume ratio (discontinuous phase/continuous phase), and shear rate. The viscosity of silica sol aged for different times shows the direct correlation between increasing viscosity and the degree of polymerization between silica particles (Fig. 2.3.7). Under mechanical agitation this polymer network breaks down at higher viscosities.
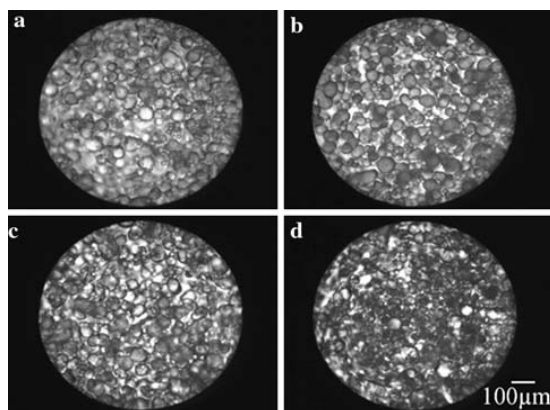

Fig. 2.3.6. Optical micrographs of silica microspheres synthesized after aging the sol for different time intervals (1.4 vol% Span 80) a) 5 h b) 8 h c) 11 h d) 17 h
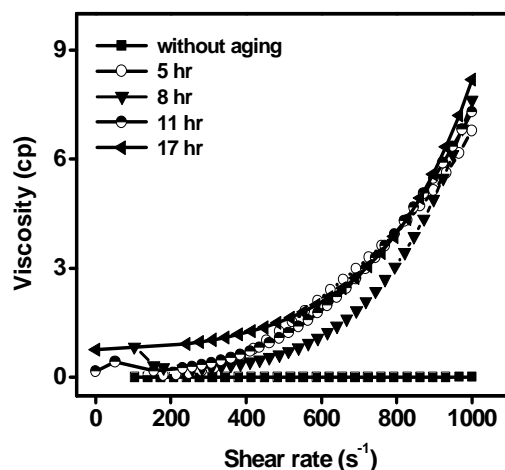
Fig. 2.3.7. Viscosities of silica sol aged at different time intervals

2.3.3.3 Hydrophobic Silica Microspheres

Fig. 2.3.8 shows the FTIR spectra of silica microspheres with and without surface modification using trimethylchlorosilane. A broad peak at 3449 cm^{-1} observed for the unmodified and modified microspheres can be ascribed to isolated hydrogen bonded Si–OH groups.[6] Peak intensity is lower in the latter case due to the replacement of Si–OH groups by the organic group leading to reduced hydrophilicity. Silanol hydroxyls undergo silanization with chlorosilane thereby replacing the hydroxyl groups by methyl groups. The peak at 1639 cm^{-1} corresponds to the deformation mode of adsorbed water molecules in the unmodified sample, and is very weak in the modified sample. The features at 840 and 1275 cm^{-1} correspond to the Si–C bond present in the hydrophobic silica

81

microspheres, while the CH_2 stretching vibration is located at 2959 cm^{-1} in the hydrophobic silica microspheres.[166] A schematic representation of the formation of hydrophobic silica microspheres is provided as Fig. 2.3.9.
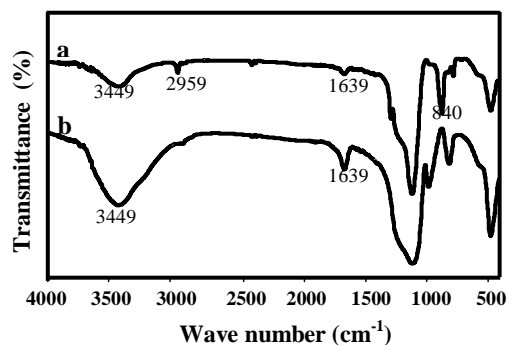

Fig. 2.3.8. FTIR spectra of silica microspheres
a) With surface modification b) Without surface modification

Contact angles of different silica microspheres heated at 70 and 350 ^{o}C are provided in Table 2.3.2. The increase in weight of the sample when in contact with water is also given. Surface modification with trimethylchlorosilane resulted in contact angle of 90° and in very low weight gain (0.00003 g^2/s). Spheres without modification showed a contact angle of 84° with an increase in weight per second of 0.00256 g^2/s and shows that surface modification with trimethylchlorosilane is effective in making the microspheres hydrophobic. Contact angle of unmodified silica decreases to 37° after heating at 350 ^{o}C where as contact angle of hydrophobic silica microspheres remains the same. The decrease in contact angle

82

can be attributed to the removal of some Span 80 that were not washed off by the
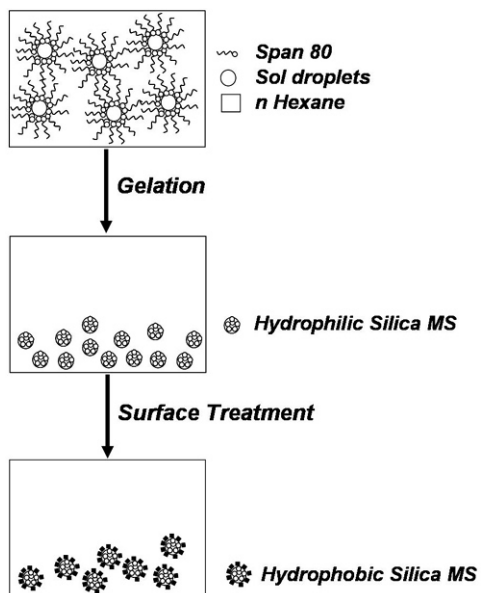
solvent exchange.

Fig. 2.3.9. A schematic representation of formation of

hydrophobic silica microspheres

Table 2.3.2. Contact angle measurements of silica microspheres

Sample details	Contact angle (°)	Increase in weight per second (g^2/s)
Spheres (TMCS modified)	90	0.00003
Spheres (Unmodified)	84	0.00256

83

Hydrophilic microspheres show strong endothermic peak at ~120 ^{o}C due to the removal of adsorbed water, while an exothermic peak is due to removal of residual surfactant at 345 ^{o}C (Fig. 2.3.10).[163] The endothermic peak at 120 ^{o}C is absent in the case of hydrophobic microspheres as expected. A sharp exothermic peak at 442 ^{o}C reflects the decomposition of the methyl groups and so hydrophobicity is retained up to that temperature.
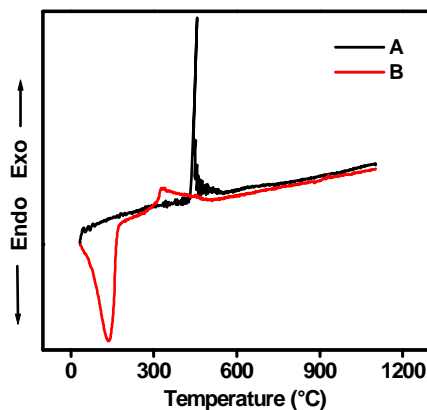

Fig. 2.3.10 DTA spectra of silica microspheres A) With modification
B) Without modification

2.4.4 Conclusions

1. Silica microspheres (~50 µm) were synthesized through a sol–emulsion–gel technique using Span 80 as the surfactant in silica sol/n-Hexane water in oil emulsion system.

2. Concentration of surfactant and viscosity of silica sol are found to be important factors in the synthesis of SiO_2 microspheres. It can be concluded that there is an optimum surfactant concentration and aging time for the silica sol to obtain uniform spheres, below which clustering, aggregation, and structural collapse occur. A surfactant concentration of 1.4 vol% yielded highly regular spheres with a surface area of 319 m^2/g and a pore size of 8.5 nm. Silica sol aged for 8 h gave the most uniform spheres when the aging time was varied in the preparation of microspheres.

3. Surface modification by trimethylchlorosilane resulted in hydrophobic microspheres with a contact angle of ~90°. Differential thermal analysis shows that the decomposition of organic moieties responsible for hydrophobicity occur around 440 ^{o}C and hence it can be concluded that hydrophobicity is retained up to that temperature.

Chapter III

Synthesis of Silica-Gelatin Hybrids and Further Functionalization

for Antiwetting Coatings

3.1 Synthesis of Silica-Gelatin Hybrids and Coatings

3.1.1 Introduction

A combination of unique properties of nano objects (such as nano particles and nano rods) and biomaterials provides a unique opportunity for physicists, chemists, biologists and material scientists to mould the new area of nano biotechnology. Nanoparticles and nano rods functionalised with biomolecules are used for various applications in biomolecular electronics[167], biosensors[168-169], bioactuators[170-171] and medicines, namely in photodynamic anticancer therapy[172], targeted delivery of radio isotopes, drug delivery, electronic DNA sequencing, nanotechnology of gene delivery system[173-175] and gene therapy.[176] Biopolymer-inorganic hybrid materials, particularly ceramic hybrids are interesting areas of research because of their importance in the field of biocompatible materials, bone substituents and cements for bone repair and reconstruction[177]. Typical advantages of biopolymers are flexibility, low density, toughness and formability where as ceramics have excellent mechanical and optical properties such as hardness, modulus, strength, transparency and high refractive index.[69] By framing

86

appropriate combinations of these materials with suitable inorganic substrates, new class of high performance, highly functional organic-inorganic hybrid materials can be achieved.[69]

Recently, there is an increasing interest in gelatin as an organic additive in such composites mainly because of its biodegradable and bioadhesive properties.[178] Gelatin is a protein derived from collagen which is the major structural protein in the connective tissue of animal, skin and bone, and has gained its popularity due to its multifunctional properties for the synthesis of biopolymer-inorganic composite matrix. Ohtsuki et al. developed a bioactive organic-inorganic hybrid for bone substitutes using gelatin.[177] Porous gelatin-siloxane hybrids have found possible application as biodegradable scaffolds that act as biocompatible materials for bone repair or generation.[72] Novel silica-gelatin composites for enzyme and cell immobilization have also been reported.[73,77,78,] Sol-gel processing is an effective technique for the synthesis of biopolymer-silica hybrid materials. Ren et al. synthesized porous gelatin-siloxane hybrids for bone tissue engineering through the sol-gel procedure.[74] Biocomposite layers of silica and various bone-relevant proteins such as collagen, gelatin and chitosan can be obtained from coatings of silica sol, modified with proteins, in water or dioxane. Such coatings are highly biocompatible with excellent mechanical properties.[73] Investigation into the gelatin-silica interactions, porosity features of the hybrid and optical

transmittance of the biopolymer-silica coating is seldom found in literature.[70,71,178] In the present study we have attempted to immobilize gelatin molecule in the mesoporous silica gel network through hydrolysis of tetraethoxysilane in presence of gelatin at controlled pH conditions. The resulting silica-gelatin sol is used to develop thin films on glass surfaces, by dip coating technique. The nature of chemical interactions, gelation characteristics, thermal decomposition, porosity features, optical transmittance and the thickness of silica-gelatin hybrid coatings were analysed.

3.1.2 Experimental

The starting materials were tetraethoxysilane (Fluka Chemicals) isopropanol (SD Fine Chemicals), hydrochloric acid (SD Fine Chemicals) and gelatin (SD Fine Chemicals). TEOS was hydrolysed by a method reported elsewhere[106] in presence of gelatin. In a typical experiment silica-gelatin sol was prepared by mixing 6.9 g TEOS with 7.9 g isopropanol and 9.5 g 0.001 M HCl (1:4:16 molar ratio) to which gelatin solution with different concentration was added under constant stirring. The concentration of gelatin in the silica sol was varied as 1, 2, 4, 6 and 8 wt%. The stirring was continued for one and half hour under room temperature and the resultant sol was used as the coating precursor. Coatings were made on glass slides by dip coating technique (KSV instruments Ltd.) at a withdrawal speed of 50 mm/minute. Rheological behaviour of the

precursor sol was monitored by Anton Paar Rheo Viscometer using the cylinder and bob method. Optical transmittance of coated glass slides was measured using a UV spectrophotometer (UV-2401 Pc Shimadzu). Structural characteristics of the hybrid were investigated by a Nicolet Impact 4000 FTIR Spectrometer in the range 400-4000 cm^{-1} by KBr pellet method and thermal decomposition pattern of the dried silica-gelatin hybrid materials were obtained using thermal analyzer (Shimadzu 50 H) in air at a heating rate of 10 °C/minute. Specific surface area of the hybrid gel was measured using BET surface area analyzer (Micromeritics, Gemini Model 2360). The sample was degassed at 100 °C before making the measurement.

3.1.3   Results and Discussion

Fig. 3.1.1 demonstrates the effect of concentration of gelatin on the gelation time of silica sol. Gelation time decreases with increase in gelatin content and in presence of 5 wt% of gelatin the gelation took place within about 5 minutes. In the case of hydrogel formation of gelatin, it has been observed that the gelation time decreases to the order of minutes on increasing the concentration.[179] The gelation characteristics were followed by viscosity measurements. Fig. 3.1.2 shows the viscosities of sols with different concentration of gelatin plotted against shear rate. The viscosity behaviour of silica-gelatin sol with different concentration of gelatin is nearly same. A Newtonian behaviour is evident at low shear rates where as a

shear thickening behaviour is observed at higher shear rates. There is also an increase in viscosity with an increase in concentration of gelatin. This is in accordance with the variation in gelation time.
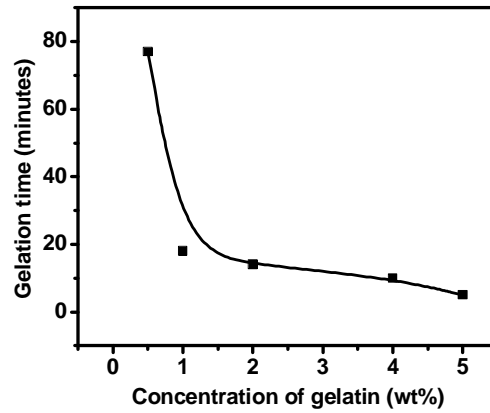

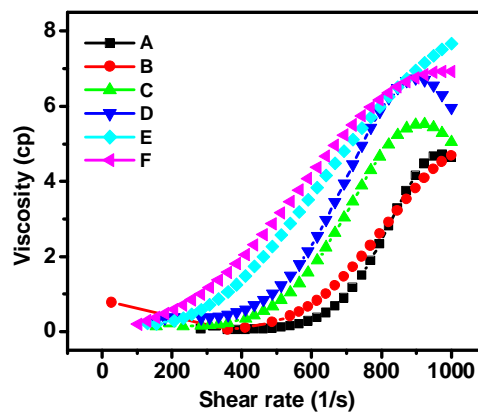**Fig. 3.1.1.** Gelation time of silica sol with respect to concentration of gelatin

Fig. 3.1.2. Viscosity curves of silica-gelatin hybrids by varying the concentration of gelatin A) 0 B) 1 wt% C) 2 wt% D) 4 wt% E) 6 wt% F) 8 wt%

90

Fig. 3.1.3. shows the viscosity of silica-gelatin sol with varying concentration of gelatin at a constant shear rate of 600. Coradin et al. reported that the interactions arising between sodium silicate solution, containing a mixture of oligomeric silicate anions $Si_xO_y(OH)_z^{n-}$ with x ranging from 2 to 8 and positively charged peptides or proteins activate silicate condensation.[71] This may be the reason for the faster gelation of silica in presence of gelatin. Bon et al. reported that the gelation of protein molecules increases steeply with increasing concentration and temperature.[180] The present observation is in agreement with Bon's. The connectivity between silica and gelatin should allow good compatibility between the two components in the hybrid composite.[70] However as the concentration of gelatin increases above 4 wt% a white precipitate was obtained indicating saturation concentration of gelatin, under the present experimental conditions to form a homogeneous sol. The pH of the resultant sol influences considerably the interactions between gelatin and silica particles.[71,73,181] As the concentration of gelatin increases from 0 to 8 wt% of silica, the pH of the mixture increased from 3 to 5.7. Above pH 5, the negative charge on silica increases rapidly.[26] This leads to an electrostatic interaction with positively charged gelatin leading to salting out. Therefore the pH was controlled in between 3-4.5 during the whole experiment to obtain a stable sol and coating precursor. A homogenous coating precursor sol could be obtained till 2 wt% gelatin. As the

91

concentration of gelatin increases further, the gelation becomes faster and viscosity increases considerably. Krishnamurthy et al. reported that adsorption of gelatin on the surface of silica colloids greatly increases the viscosity of dispersion.[181]
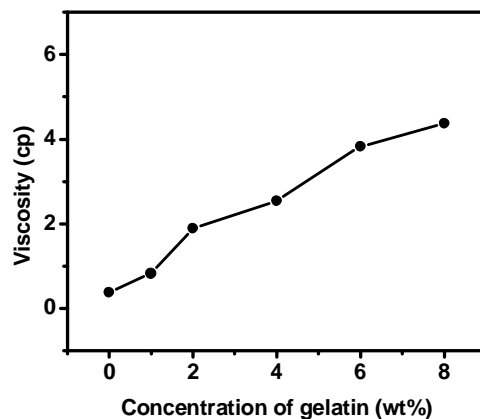

Fig. 3.1.3. Viscosity of silica-gelatin sol with different concentration of gelatin (Shear rate 600 s^{-1})

FTIR spectra of pure silica, gelatin and silica-gelatin hybrid are presented in Fig. 3.1.4. The spectrum of gelatin is characterized by a large band around 3450 cm^{-1} corresponding to NH stretching vibrations, narrow band at 2920 cm^{-1} attributed to CH stretching vibrations, two bands at 1643 cm^{-1} and 1546 cm^{-1} corresponding to the amide I and II bands (C=O stretching and NH in plane bend).[178] The presence of carboxylate groups at 1400 cm^{-1} and amino groups through several weak bands between 1200 cm^{-1} and 1000 cm^{-1} are also seen.[182] The

peak at 3400 cm^{-1} corresponds to the hydrogen bonded –OH groups in the hydrolysed silica.[183]
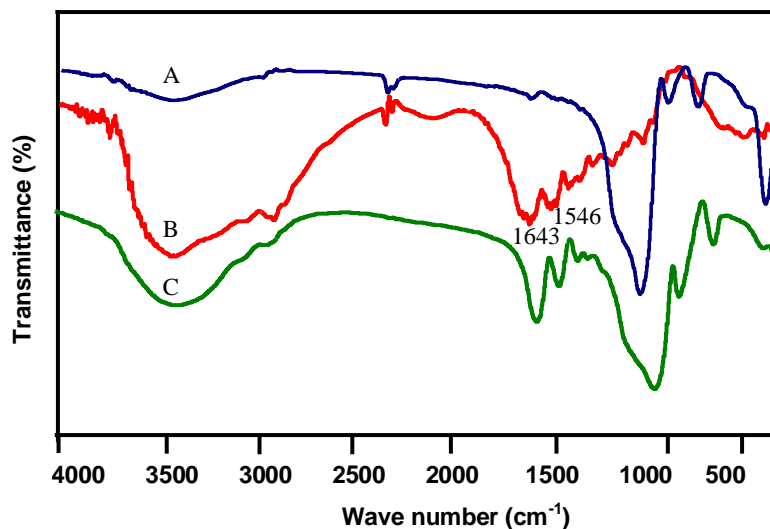

Fig. 3.1.4. FTIR spectra of A) Silica B) Gelatin C) Silica-2 wt% Gelatin

FTIR analysis shows a shift in amide I band to a lower region and amide II band to a higher wave number and this is due to the hydrogen bonding of the C=O and N-H groups of gelatin molecule to the silanol hydrogen.[178] The presence of silica leads to a better resolution of the amide vibration showing that the protein chain is in a folded conformation.[182] For the amide I band, a shift to lower wave number is anticipated as a result of the combined effects of the decrease in the force constant, and an increase in the reduced mass of the C-O vibrator in view of the coupling with H-O. In contrast, the amide II is expected to shift to higher wave

93

numbers as the force constant of the C-N bond is enhanced both by an increased "stiffness" of the H-N-CO angle due to the "immobilization" of H through hydrogen bonding and the increased strength of the C=N bond.[70,178]

Figs. 3.1.5 and 3.1.6 show the thermal decomposition patterns of silica and silica-2 wt% gelatin systems, respectively. For the silica and silica-gelatin hybrids, total weight loss is ~22%. Pure silica system shows an endothermic peak at ~100 °C due to the expulsion of physically adsorbed water corresponding to 18 wt% weight loss in thermo gravimetric analysis (Fig. 3.1.5 A). There is a decrease in this weight loss to ~13 wt% in the silica-gelatin system. As the silica is hydrogen bonded to gelatin, less silanol sites are available for adsorption of water.[26]
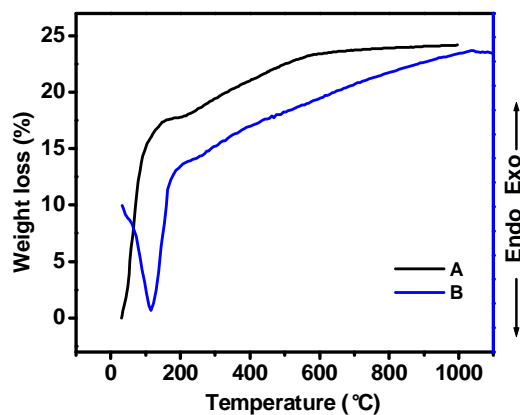

Fig. 3.1.5. A) TGA pattern of silica gel B) DTA curve of silica gel

The weight loss in silica is essentially from physically and chemically adsorbed solvents and water molecules which are partly replaced by the gelatin molecules in silica-gelatin hybrid. The peak at 313 °C in Fig. 3.1.6 B corresponds to the combustion of organic phase, which is absent in pure silica system. A corresponding weight loss of ~9 wt% is observed in the TGA pattern.
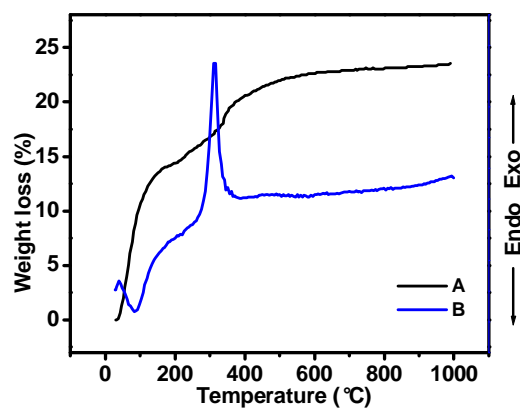

Fig. 3.1.6. A) TGA pattern of silica-2 wt% gelatin
B) DTA of silica-2 wt% gelatin

Table 3.1.1 gives the surface area analysis results of silica and silica-gelatin hybrid. A surface area of 458 m^2/g with an average pore size of 4.3 nm is obtained for pure silica. With an incorporation of 2 wt% gelatin surface area decreased to 341 m^2/g with an average pore size of 9.5 nm. There is no appreciable change in the values by increasing the gelatin content beyond 2 wt%. The pore size increases

95

considerably due to the immobilization of polymeric gelatin molecules in the silica structure.

Table 3.1.1. BET surface area analysis of silica hybrids

Sample	Surface area (m^2/g)	Average pore size (nm)
Silica	458	4.3
Silica-2 wt% gelatin	341	9.5
Silica-5 wt% gelatin	350	8.5

Silica shows a type I (Fig. 3.1.7 A) isotherm where as the silica-gelatin system shows a type IV isotherm corresponding to a mesoporous structure[107]. Usually silica gel is characterized by micropores under low pH conditions, adopted in the present investigation. Retuert et al. has prepared porous silica-gelatin hybrids with a surface area of 452 m^2/g.[70] But they extracted the gelatin molecules with water before making the measurements. A certain portion of the micropores undergoes coarsening as a result of interaction with gelatin and this will result in the reduction of specific surface area. Adsorption isotherm provides evidence to this phenomenon. Usually in silica gels, during drying, internal silanol groups in the pores condense, leading to shrinkage of the gel structure and hence a decrease in pore size is observed.[6] With addition of gelatin to the silica precursor,

96

the gel strength is improved[73] and there is a reduction in silanol sites available for internal condensation and this results in low drying shrinkage.
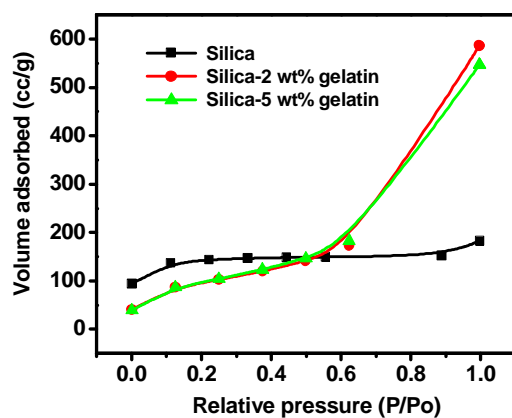

Fig. 3.1.7. Adsorption isotherms of silica hybrids

Fig. 3.1.8 presents the UV transmittance spectra of silica and silica-gelatin coated glass slides. All the samples show a maximum absorption at around 300 nm with more than 90% transmittance in the visible region. Transmittance is reduced with the increase in the number of coatings. The decrease in optical transmittance with an increase in number of coatings is may be due to the increase in the thickness of the coatings.
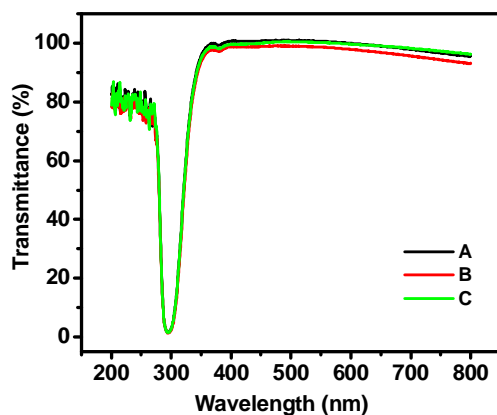
Fig. 3.1.8. Optical transmittance of A) Silica
B) Silica-2 wt% gelatin (1 coating) C) Silica-2 wt% gelatin (2 coating)

3.1.4 Conclusions

Silica-biopolymer hybrid was synthesized through sol-gel process using gelatin as the biopolymer. Coatings of silica-gelatin hybrid developed on glass surface has a thickness of 300 nm and were found to possess >90% transmittance The optical transparency will enable applications of the hybrid as coatings on various substrates, where no compromise of texture is possible; for example leather and textiles.

FTIR spectra was used for the structural investigation of the hybrid and it was found that the interaction of silica and gelatin is through the hydrogen bonding of C=O and N-H groups of gelatin to the silanol hydrogen. Thermal analysis data showed that the physically adsorbed water is replaced by gelatin molecule and the decomposition of gelatin took place above 350 °C. A surface

area as large as 350 m^2/g for silica-gelatin hybrid was obtained for the hybrid composite.

3.2 Development of Functionalized Silica-Gelatin Hybrids and Antiwetting Coatings on Glass and Leather

3.2.1 Introduction

Biopolymer–silica hybrid nanocomposites have drawn attention of many researchers recently because of their compatibility with living matter. Hence, such nanohybrids have already found promising applications in medical fields.[78,79,80] A few potential applications are chemical and biomedical sensors, semipermeable membranes for artificial organs, controlled drug release systems and enzyme and cell immobilization.[73,78,184,185,186] These hybrid materials also find application in the field of biocompatible materials, bone substituents and cements for bone repair and reconstruction.[78,79,80] Organic–inorganic nanocomposite, films and coatings containing gelatin or other polymers have found applications in optical coating, high refractive index films, contact lenses, thin film transistors, light emitting diodes, solar cells, optical wave guide materials and photo chromic materials, adsorption, catalysis and high energy fields.[187–191] Biocomposite layers of silica and various bone-relevant proteins such as collagen, gelatin and chitosan can be obtained from coatings of silica sols mixed with proteins in water/dioxane.[73] In addition to the intrinsic protein related properties of gelatin, gels can be further

modified by cross-linking agents, which improves the thermal stability and mechanical properties.[73] Chemical cross-linking relies on gelatin chain bridging via covalent bonding between the cross-linker and the amino groups of the protein.[192-194] In this context, silicate species can be considered as interesting cross-linking agents since they interact through both electrostatic interactions and hydrogen bonding with a few polyaminoacids and proteins.[195-198]

Protein containing hydrophobic coatings and films are known biologically active materials for biocatalysis, antifouling surfaces, bioseparation and biorecognition.[199] Biocompatible hydrophobic surfaces are used as implants or scaffolds for the purpose of tissue engineering.[192] Geckeler et al. developed a biocompatible hydrophobic coating using epoxy resins and silica.[192] Chen et al. developed new silica–chitosan hybrid biomaterials.[200] However, no attempts are reported on synthesis of hydrophobic biocompatible inorganic–organic hybrids using gelatin as the organic counter part. The main difficulty in the synthesis of such hybrids is the poor solubility of the precursors, especially tetramethoxysilane and tetraethoxysilane, and the presence of alcohol that may denature the biopolymers.[201]

The purpose of the present study is to synthesize silica–gelatin hybrids from colloidal silica in aqueous media and to functionalize the hybrid with methyltrimethoxysilane (MTMS) and vinyltrimethoxysilane (VTMS) so as to

introduce hydrophobicity to the resultant hybrid. MTMS and VTMS are known to be effective surface modifiers for the synthesis of hydrophobic silica hybrids.[202-203] In the present work, we have synthesized silica–gelatin hybrids starting from colloidal silica and functionalizing the hybrid by using MTMS or VTMS as intermediate precursors. The rheology of the hybrid precursor sol was monitored and the coating was done on glass substrates. This will extend transparent, functional coatings on biological subtrates such as leather and textiles. The hybrid gel was further characterized for chemical interaction, thermal degradation, hydrophobicity, particle size, optical properties and morphology.

3.2.2 Experimental

Silica–gelatin hybrid precursor sol was prepared by adding 2 wt% gelatin to a 5 g of colloidal silica (50 wt%, Aldrich Chemicals) in 100 ml water under constant stirring. Gelatin was purchased from SD Fine Chemicals available under the name Gelatin powder (Bacto). MTMS (98%, Aldrich Chemicals) was added to this mixture under stirring at a temperature of 30 ^{o}C to prepare silica–gelatin-MTMS (SGM) hybrid. Concentration of MTMS was varied as 5, 10, 30, 50, 70 and 90 wt% of the total silica content. SGM hybrid sol was kept at 70 ^{o}C to obtain the gel. The precursor sol was also coated on glass slides by the dip coating technique (KSV Instruments) at a coating rate of 50 mm/minute which was subsequently dried at 70 ^{o}C. Rheological behaviour of the precursor sol was

monitored by Anton Paar Rheo Viscometer using cylinder and bob method. The hybrid gels were powdered and redispersed in water under ultrasonication and the particle size of the dispersed powder was measured by Malvern Zetasizer 3000 HSA. Optical transmittance of the coated glass slides were measured by UV-2401 PC (Shimadzu) spectrophotometer. Structural characteristics of the hybrid were investigated by Nicolet Magna 560 FTIR spectrometer. Thermal decomposition pattern of the dried silica–gelatin hybrid materials were obtained using Shimadzu 50 H series thermal analyzer. Contact angle was measured using Data Physics DCAT11 tensiometer by Wilhelmy plate method. Stereomicrographs of water drops on coated glass slides were taken using a Leica MZ 16A stereomicroscope. Water drops were stained with methyl orange to enhance the clarity. The morphological features of the samples were investigated using a scanning electron microscope [JEOL, SEM].

3.2.3 Results and Discussion

3.2.3.1 Silica-Gelatin-MTMS Hybrids

Gelation of silica is influenced by several parameters such as sol concentration, pH, additives, etc. As the pH of the sol increases above isoelectric point of silica (~2) the negative charge on silica particle surface increases. Hence, at pH ~9 silica surface can be considered as highly negatively charged. This will lead to electrostatic interaction with positively charged gelatin molecules. Coradin

et al. have studied the electrostatic interactions arising between silicate anions and positively charged peptides or proteins.[71] This interaction leads to the formation of the silica–gelatin hybrid.

Fig. 3.2.1 shows the rheological behaviour of hybrid sol with varying concentration of MTMS. All the samples show non-Newtonian behaviour. For 30 wt% MTMS there is a sudden increase in viscosity up to a shear rate of 400 s^{-1} and thereafter it shows a shear thinning behaviour. The increase in viscosity corresponds to the faster condensation of silica–gelatin particles.[204] The shear thinning behaviour can be attributed to the collapse of the gel structure by further application of shear. Monomers generated from MTMS condense on to the silica–gelatin particles and above 30 wt% of MTMS, condensation is retarded, as less number of silanol groups are available per unit volume.[187]
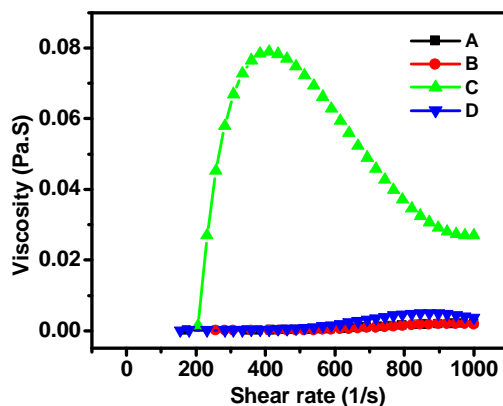

Fig. 3.2.1. Viscosity curves of Silica-gelatin(2 wt%) hybrids by varying the concentration of MTMS A) 0 B) 10 wt% C) 30 wt% D) 70 wt% MTMS

The lower viscosities of the samples with high concentration of MTMS can be attributed to the lower hydrolysis–condensation rates. Since MTMS possess a non-hydrolysable methyl group, the silica monomers generated from the precursor have functionality of three, compared to a functionality of four in the case of silica monomers from TEOS. Hence, these cannot interconnect to form a three-dimensional gel network, i.e. the monomers generated from MTMS can not condense among themselves to form a three-dimensional gel network.

Fig. 3.2.2 shows the particle size distribution of silica, silica–2 wt% gelatin and SGM hybrids containing varying concentration of MTMS. Silica–2 wt% gelatin hybrid gel dispersed in water shows a monomodal particle size distribution centered at ~550 nm. Increase of MTMS concentration to 10 wt% resulted in a bimodal particle size distribution, one peak around 600 nm and an other at ~200 nm. Jesionowski et al. studied the size distribution of primary particles, aggregates and agglomerate structures in silica particles modified with different silanes.[205] Accordingly the particle size at ~200 nm is due to the primary aggregates of silica particles and particles at ~600 nm corresponds to agglomerates. Silica particles from MTMS condense on to the silica–gelatin particles as evidenced by the DTA and contact angle measurements. This may be the reason for the increased particle size of the 10 wt% MTMS hybrid. Particle size of silica–gelatin hybrid prepared from 30 wt% MTMS, shows a unimodal particle size distribution with size around

750 nm, which is larger than that of 10 wt% MTMS. This increased particle size may be due to the condensation of MTMS monomers at the basic pH (~9) over silica surface. At this concentration of MTMS, the monomodal distribution indicates that sufficient amount of silica monomers are generated from MTMS to condense over the silica–gelatin particles.
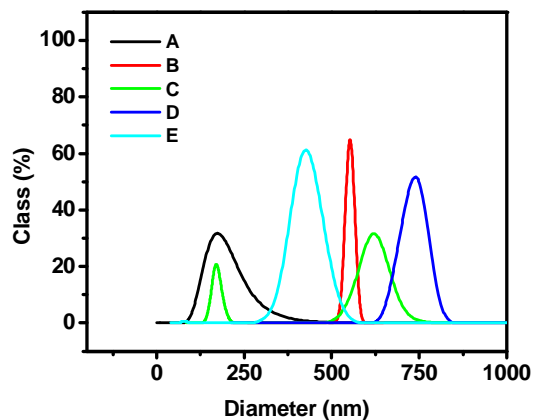

Fig. 3.2.2. Particle size distribution of A) Silica B) Silica-2 wt% gelatin C) Silica-2 wt% gelatin-10 wt% MTMS D) Silica-2 wt% gelatin-30 wt% MTMS E) Silica-2 wt% gelatin-70 wt% MTMS

At 70 wt% MTMS, particle size distribution is again unimodal, but size decreases to about 450 nm. The reduction in particle size may be due to the fact that silica particles from MTMS condense or aggregate among themselves forming bigger particles but smaller than the particles formed by the mutual condensation of silica and MTMS monomers. Once networking is disfavoured, at larger MTMS

105

concentrations the average aggregate size decreases. A schematic representation of the formation of silica–gelatin–MTMS hybrid is provided as Fig. 3.2.3.
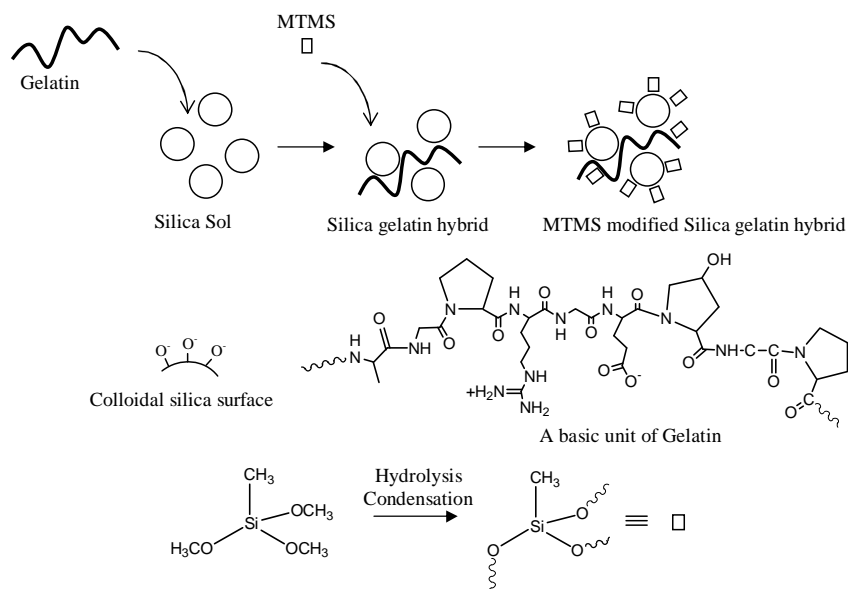

Fig. 3.2.3. Schematic representation of the formation of silica-gelatin-MTMS hybrid

DTA and TGA of silica-gelatin hybrids are provided as Figs. 3.2.4 and 3.2.5. The endothermic peak in Fig. 3.2.4A at 90 ^{o}C corresponds to removal of water. But in Fig. 3.2.5A the endothermic peak is absent at that particular temperature which clearly indicates the effective surface modification by MTMS.
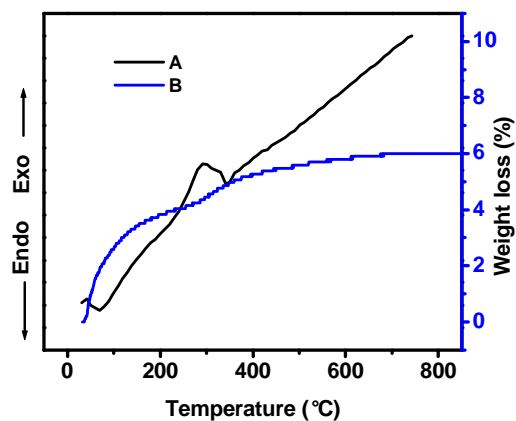
106

Fig. 3.2.4. A) DTA of silica-2 wt% gelatin B) TGA of silica-2 wt% gelatin
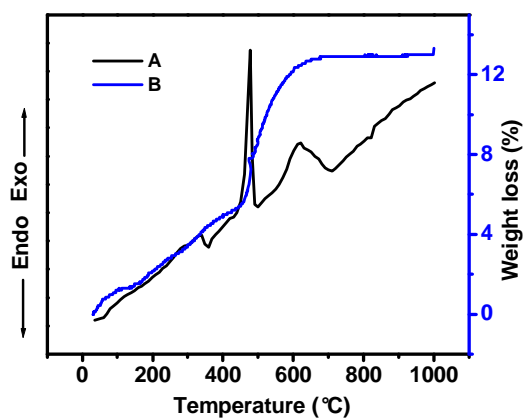

Fig. 3.2.5. A) DTA and TGA of silica-2 wt%gelatin-10 wt% MTMS

The broad peak at ~320 ^{o}C in Fig. 3.2.4A corresponds to the multi-step degradation and pyrolyzation of the complex helical structure of gelatin to tropocollagen macromolecules.[206] The sharp exothermic peak at ~520 ^{o}C in Fig. 3.2.5A corresponds to the oxidation of surface organic (CH_3) groups.[207] Rao et al.

107

have shown that oxidation of surface organic groups take place at around 480 $^{\circ}$C.[208] However, in the present case the exothermic peak at 530 $^{\circ}$C indicates that the hydrophobicity is retained at much higher temperatures. Differential thermal analysis also supports the formation of hydrophobic silica–gelatin hybrids. Figs. 3.2.4B and 3.2.5B show TGA pattern of silica-2 wt% gelatin and silica-2 wt% gelatin-10 wt% MTMS hybrid. Weight loss corresponding to water is approximately 4% in the case of silica-gelatin while the value is <2% for SGM.

FTIR spectroscopy was used to study the chemical interactions between the organic and inorganic structural units in SGM hybrid gels. Fig. 3.2.6 shows the FTIR spectra of silica–gelatin and silica–gelatin–MTMS hybrid. The most intensive band, at 1100 cm^{-1} is due to the stretching vibrations of the Si-O-Si bridges.[209] This peak is split into two separate bands at 1030 and 1130 cm^{-1} in the hybrid gel structures. This is due to the functionalization of silanols through siloxane bridged methyl groups. A sharp peak is observed at 1275 cm^{-1} which corresponds to Si-C bonds for the SGM hybrid.[209] The presence of CH$_3$ asymmetric stretching vibration is seen as a sharp peak at 2979 cm^{-1} and the peak due to CH$_3$ asymmetric bend is observed at around 1420 cm^{-1}. This confirms the functionalization of silica–gelatin hybrids by MTMS. MTMS undergoes in situ hydrolysis under basic conditions of silica and condenses with the surface

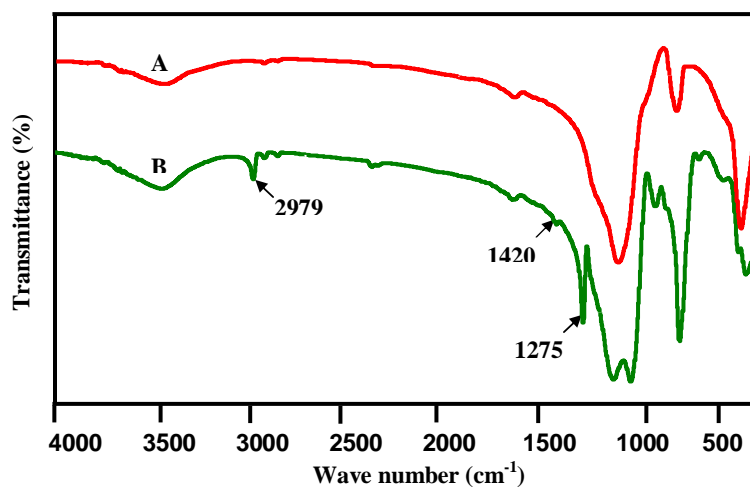hydroxyl groups of silica–gelatin particles imparting hydrophobic character to the resulting hybrid gels.

Fig. 3.2.6. FTIR spectra of A) Silica-2 wt% gelatin
B) Silica-2 wt% gelatin-10 wt% MTMS

SGM hybrid sols with varying concentrations of MTMS were coated on glass surfaces and were subjected to contact angle measurements. The contact angle values are plotted against the concentration of surface modifier and are represented in Fig. 3.2.7. The contact angle values show an increasing trend with increase in concentration of MTMS. A higher contact angle value shows the hydrophobic character and a lesser value indicates hydrophilic nature. Contact angle of silica is 47° and silica–gelatin hybrid is $\sim 45^{o}$, which indicating hydrophilic nature. Surface modification of silica–gelatin hybrid with 10 wt%

MTMS resulted in a high contact angle value ~100°. Conatct angle values of SGM hybrids calcined at 200 °C and 400 °C is also provided in the graph. Contact angle did not change with respect to calcination temperature upto 400 °C. This means that SGV hybrids retain their hydrophobicity even upto a temperature of 400 °C.
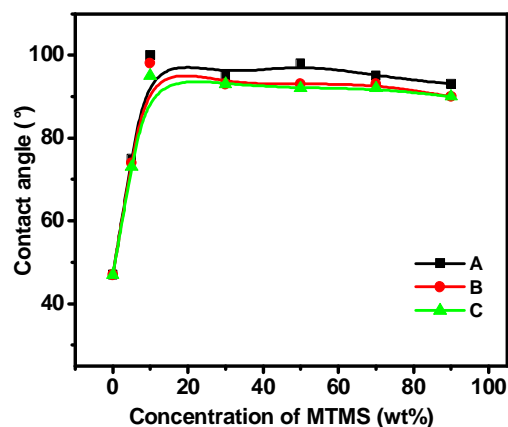

Fig. 3.2.7. Contact angle Vs concentration of MTMS of SGM hybrids calcined at different temperatures A) 70 °C B) 200 °C C) 400 °C

UV Spectra of silica–2 wt% gelatin hybrid sols, containing varying amounts of MTMS, coated on glass slides are represented in Fig. 3.2.8. The spectra indicate that the coated glass slides have 98% transmittance in the UV–visible region which may have applications in optical fields and also in transparent biocompatible hydrophobic coatings. The thickness of the coating was found to be ~135 nm as measured using ellipsometer. The percentage transmittance of silica-2 wt% gelatin-30 wt% MTMS and silica-2 wt% gelatin-70 wt% MTMS in the UV-

visible region are 92 and 96%, respectively. This is in accordance with their average particle sizes. Rheological studies also show the higher gelation rate of 30 wt% MTMS hybrid. Hence, the bigger particles retard transparency of the coatings at this concentration.
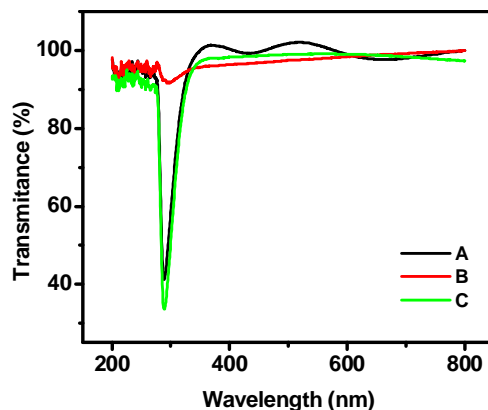

Fig. 3.2.8. UV spectra of A) Silica–2 wt% gelatin B) Silica–2 wt% gelatin–30 wt% MTMS C) Silica–2 wt% gelatin–70 wt% MTMS

Stereomicrographs of water drops on uncoated and coated glass slides is presented in Fig. 3.2.9. The difference in the behaviour of the two glass surfaces is clear. Water drops spread on an uncoated glass surface where as a spherical morphology is seen on the glass slides coated with silica-2 wt% gelatin-70 wt% MTMS due to the hydrophobic nature.

Scanning electron micrograph of silica–2 wt% gelatin–10 wt% MTMS is provided in Fig. 3.2.10. The SEM indicates more or less uniform coating in length

scales of 1µm. Imperfections due to the presence of higher agglomerates are also seen. Reagglomeration of hydrolysed silica-gelatin-MTMS precursor may have occurred under the coating conditions. This coated surface possesses high contact angles and therefore more hydrophobic property.
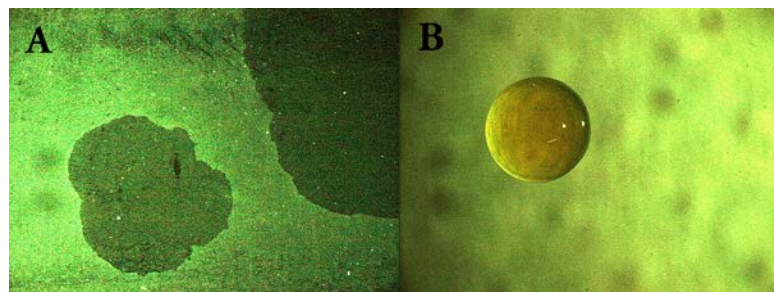

Fig. 3.2.9. Stereomicrographs of water drop on glass slides
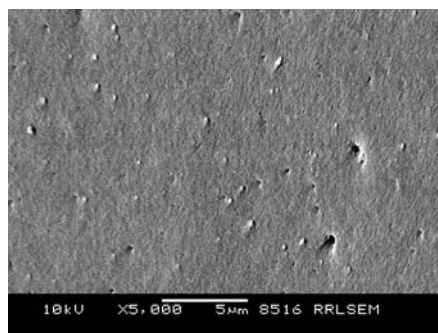A) Uncoated glass B) Silica-2 wt% gelatin -70 wt% MTMS

Fig. 3.2.10. Scanning electron micrograph of silica-2 wt% gelatin-10 wt% MTMS

Fig. 3.2.11 provides contact angle and surface energy values of leather samples coated with SGM hydrids. Uncoated leather has a contact angle of 30°

112

which increases with the concentration of MTMS in the coating composition. Even with a concentration of 10 wt% of MTMS, contact angle shows an increase of 75°. As the concentration of MTMS was further increased to 30 wt% contact angle reaches a maximum of 120°. However a further increase in MTMS does not have an increasing effect, instead it shows a tendency to decrease. This means that 30 wt% MTMS is sufficient to make the leather hydrophobic.
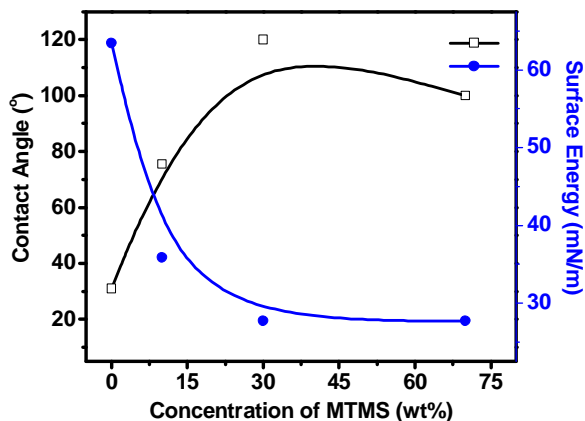
Fig. 3.2.11. Contact angle and surface energy of coated leather samples

Surface energy of the coatings is also provided in the graph. Surface energy decreases with concentration of MTMS. Introduction of methyl groups on the surface reduces the surface energy of the coating. The decrease in surface energy is the reason for the water repellant property of the coatings.[166] Surface energy of a material is related to its contact angle by Young's equation,

$$\text{Cos}(\theta) = \gamma_{SV} - \gamma_{SL} / \gamma_{VL}$$

113

where, γ_{SV}, γ_{SL} and γ_{LV} are the solid–vapor, solid–liquid and liquid–vapor interfacial energies per unit surface area, respectively. From this equation it is clear that surface energy of the solid should be minimum to obtain water repellant property.

Fig. 3.2.12 provides scanning electron micrographs of uncoated and coated leather samples. Uncoated leather samples show a highly porous and rough surface. It is clear from the picture than uncoated leather has a defective structure. Upon coating with silica hybrids, a surface with less defect and good finish is obtained. However coated surface still retain its porosity which is important for application of leather.
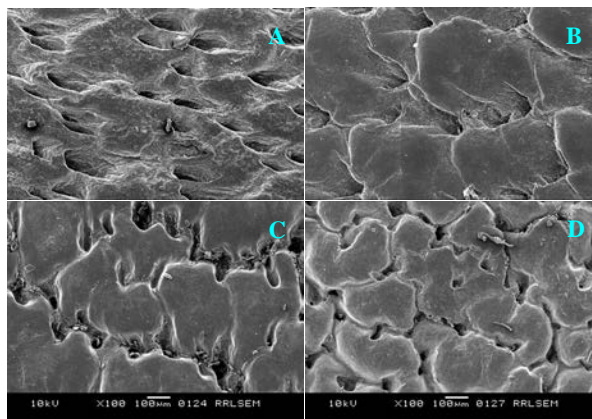

Fig. 3.2.12. Scanning electron micrographs of leater samples A) Uncoated B) Silica C) Silica-2 wt% gelatin D) Silica-2 wt% gelatin-30 wt% MTMS

114

3.2.3.2. Silica-Gelatin-VTMS Hybrids

Several parameters such as pH, temperature of the medium and particle size of the sol influence the gelation of colloidal silica.[26,210] Gelation is accompanied with a change in viscosity. In the present work silica–biopolymer hybrid precursor sol was synthesized and functionalized the sol to obtain hydrophobic transparent nanocoatings. Prior to coating on glass slides, we investigated the rheological characteristics of the resultant hybrid sol with respect to the concentration of VTMS. Rheological behaviour of hybrid sol with varying concentration of VTMS is presented in Fig. 3.3.1. All the samples show non-Newtonian behaviour, meaning that the viscosity varies with different shear rates. The increase in viscosity corresponds to the faster condensation and gelation of silica particles.[204] For 10 wt% vinyltrimethoxysilane, viscosity increases from 300 s^{-1} shear rate, reaches a maximum and then decreases. The increase in viscosity with shear rate in a sol with networked particles is due to the fact that an amount of energy supplied as shear is expended in breaking the networked structure rather than increasing the flow rate. The shear thinning behaviour at higher shear rate is due to the collapse of the gel structure by further increase in shear rate. Upon addition of VTMS, hydrolysis–condensation reactions of VTMS along with partial condensation on to the silica–gelatin particles take place. VTMS networking between the silica particles can also occur. At higher percentages of VTMS, the

ability for networking is reduced due to the fact that one of the valency of silicon is the nonhydrolysable vinyl group and condensable silica surface gets completely covered with nonhydrolysable vinyl groups. The viscosity of silica-2 wt% gelatin and with 30 and 70 wt% VTMS is presented as inset of Fig. 3.3.1.
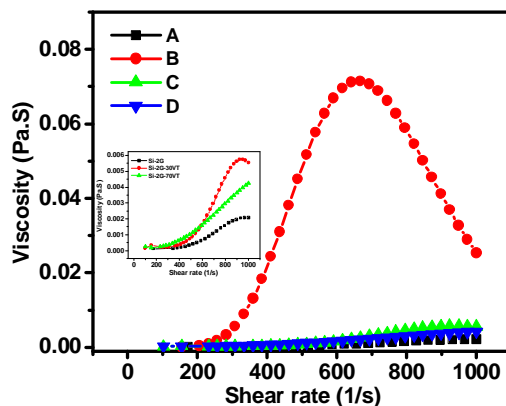
Fig. 3.3.1. Viscosity curves of silica-gelatin hybrids with varying concentration of VTMS A) 0 B) 10 wt% C) 30 wt% D) 70 wt%

All the samples show a similar trend in rheology with respect to shear rate. The basic reaction taking place during the silylation of different surfaces is the hydrolysis of trialkoxysilanes into silanols and condensation of these silanols on to the surface.[211] In the present case, VTMS undergoes in situ hydrolysis in the acidic pH conditions[212] and monomers generated from the VTMS precursor condense on to the silica–gelatin particles. Since VTMS has a non-hydrolysable vinyl group, at high concentrations this will inhibit the formation of a three-dimensional gel network as in the case for 30 and 70 wt% VTMS. The lower viscosities of the

116

samples in the presence of higher concentration VTMS can be attributed to the same reason.

Particle size analysis of silica–gelatin hybrid gels dispersed in water containing varying amounts of VTMS is given in Fig. 3.3.2. The particle sizes obtained indicate the aggregate nature of the gels. Pure silica gel showed a mean aggregate size of ~150 nm. Unmodified silica–gelatin hybrid gel shows a narrow distribution with a mean aggregate size of ~550 nm. Since gelatin favours gelation of the colloidal silica sol, the average aggregate size increases from that obtained for the dried colloidal sol. Silica–gelatin hybrid containing 10 wt% VTMS shows a bimodal distribution, in which one peak is around 800 nm and the other is at ~160 nm. The particle size at ~160 nm is due to the primary aggegates of silica particles and particles at ~800 nm correspond to agglomerates of silica particles. Jesionowski et al. studied the size distribution of primary particles, aggregates and agglomerate structures in the silica particles modified with different silanes.[205] The increase in mean aggregate size with the concentration of VTMS is due to the condensation of vinylsilsesquioxane particles over the silica–gelatin particles in the medium. At the present acidic pH conditions (pH~2.5), VTMS undergoes in situ hydrolysis and condense over the silica–gelatin particles.[212] Particle size distribution of silica–gelatin hybrid prepared from 30 wt% VTMS also shows a bimodal distribution as that of 10 wt% VTMS. However, percentage distribution

of secondary particles becomes wide with the concentration of VTMS. In the figure, we can see a broader distribution of aggregates ranging from 500 to 1000 nm. Since the silica–gelatin particles in the medium are quite larger in number than the silica particles generated from the VTMS, the concentration of VTMS is not sufficient to functionalize all the silica–gelatin particles. This is the reason for the bimodal distribution with 10 and 30 wt% VTMS.
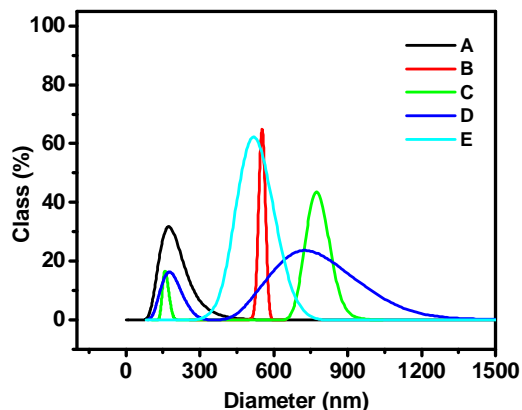
Fig. 3.3.2. Particle size distribution of A) Silica B) Silica-2 wt% gelatin C) Silica-2 wt% gelatin-10 wt% VTMS D) Silica-2 wt% gelatin -30 wt% VTMS E) Silica-2 wt% gelatin-70 wt% VTMS

As observed from the viscosity measurements, the addition of VTMS in small amounts favours networking of the gel and upon increasing the concentration of VTMS networking is disfavoured due to the complete coverage of silica–gelatin particles by VTMS. The networking of silica–gelatin colloidal particles at lower VTMS concentrations results in a broader distribution with

118

larger average aggregate size. But for 50 wt% VTMS, a unimodal distribution with a mean aggregate size of ~500 nm is obtained. At this concentration of VTMS, the monomodal distribution indicates that sufficient amount of monomers are generated from VTMS to condense over the colloidal silica–gelatin particles. Once networking is disfavoured, the average aggregate size declines.

Contact angle measurements were done on glass slides coated with colloidal SGV hybrid sols of varying VTMS concentrations. Fig. 3.3.3 plots the contact angle against the concentration of VTMS. The values show a trend of increase in contact angle with increase in concentration of VTMS. Silica–gelatin hybrid without functionalisation show a contact angle of 45°, that increases to ~114° for silica–gelatin modified with 30 wt% VTMS. This means that VTMS imparts anti-wetting property to the resultant hybrids. VTMS undergoes hydrolysis under acidic conditions of colloidal silica and condenses on to the already existing silica particle surface, as mentioned earlier. However, above 50 wt% of VTMS, the contact angle decreases. This means that above a particular concentration, there is not much enhancement of the hydrophobicity with respect to the modifier. 50 wt% can be considered as an optimum concentration in terms of hydrophobisation. SGV hybrids calcined at 400 ^{o}C showed a contact angle of ~45° which is approximately same as that of the silica-gelatin hybrid. The graph reveals that the hydrids lose its hydrophobicity above 200 ^{o}C.
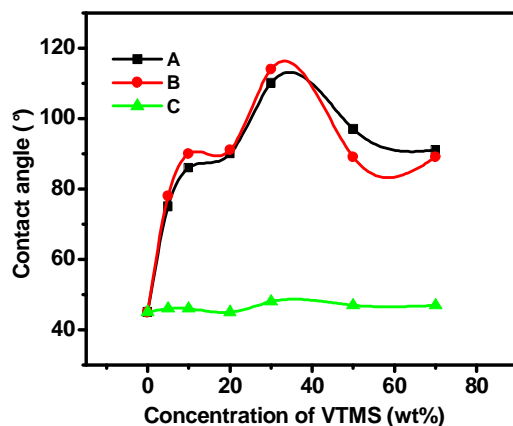
Fig. 3.3.3. Contact angle versus concentration of VTMS of SGV hybrids calcined at different temperatures A) 70 ^{o}C B) 200 ^{o}C C) 400 ^{o}C

Fig. 3.3.4 shows DTA of modified and unmodified samples. In the case of silica-2 wt% gelatin hybrid, there is an endothermic peak at ~72 ^{o}C, which corresponds to the removal of adsorbed water. This shows that silica-2 wt% gelatin hybrid is hydrophilic in nature. The broad peak at ~320 ^{o}C in the figure (silica-2 wt% gelatin) corresponds to the multi-step degradation and calcinations of the complex helical structure of gelatin to tropocollagen macromolecules.[206]

Weight loss with respect to the temperature is given in Fig. 3.3.5. The first step of the weight loss corresponding to removal of adsorbed water (below 100 ^{o}C) decreases with increase in concentration of VTMS. The unmodified silica–gelatin hybrid showed a weight loss of ~4 wt% up to 100 ^{o}C. The weight loss decreases to less than 1 wt% upon a surface modification with 50 wt% VTMS.

120

There is a drastic decrease in weight above 300 ^{o}C for 50 wt% modified samples due to the decomposition of vinyl groups.
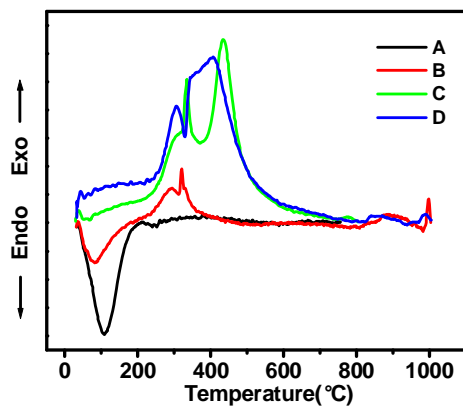

Fig. 3.3.4. DTA curve of A) Silica B) Silica-2 wt% gelatin C) Silica-2 wt% gelatin-10 wt% VTMS D) Silica-2 wt% gelatin-50 wt% VTMS
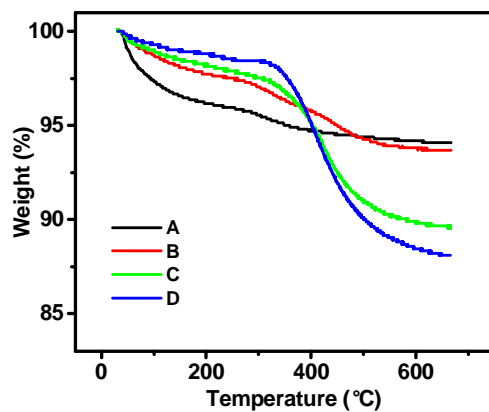

Fig. 3.3.5. TGA of A) Silica-2 wt% gelatin
(B) Silica-2 wt% gelatin-10 wt% VTMS C) Silica-2 wt% gelatin-30 wt% VTMS
D) Silica-2 wt% gelatin-50 wt% VTMS

121

Organic surface modifications were qualitatively confirmed using FTIR spectroscopy (Fig. 3.3.6). The most intensive band, at 1100 cm^{-1} is due to the stretching vibrations of the Si–O–Si bridges.[6] This peak splits into two separate bands at 1030 and 1130cm^{-1} in the hybrid gel structures. Olejniczak et al. have shown that in the hybrid gel structure, asymmetric stretching vibration of Si–O–Si splits into two separate bands.[209] The splitting of the peak is due to the functionalization of silanols linked through siloxane bridges to vinyl groups. VTMS-modified hybrids showed a peak at 545 cm^{-1} due to CH=CH$_2$ bonds that are not present in the unmodified gel structure.
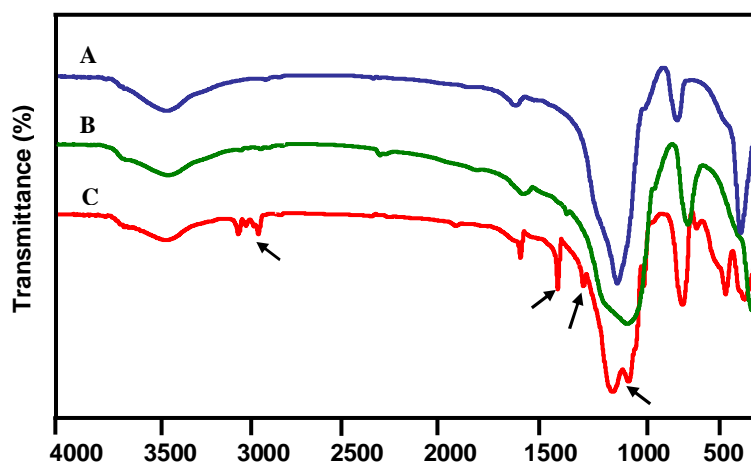

Fig. 3.3.6. FTIR spectra of A) Silica-2 wt% gelatin
B) Silica-2 wt% gelatin-10 wt% VTMS C) Silica-2 wt% gelatin-50 wt% VTMS

The peak at 1420 cm^{-1} is due to the CH$_2$ vibrations that are present in the vinyl group. A weak band between 1400–1415 cm^{-1} was used to confirm the

presence of vinyl group by Gellermann.[213] A sharp peak is observed at 1275 cm^{-1} corresponding to Si–C bonds.[213] The presence of C–H stretching vibration is supported by three peaks at 2979, 3050 and 3072 cm^{-1}. VTMS undergoes in situ hydrolysis under acidic conditions of colloidal silica and condenses with the surface hydroxyl groups of silica–gelatin particles. This will impart hydrophobic character to the resulting hybrid gels.

UV spectra of silica–gelatin hybrid and silica-2 wt% gelatin-50 wt% VTMS hybrid are given in Fig. 3.3.7. Both the coatings show >95% transparency in the visible region. The coatings have an average thickness of ~130 nm.
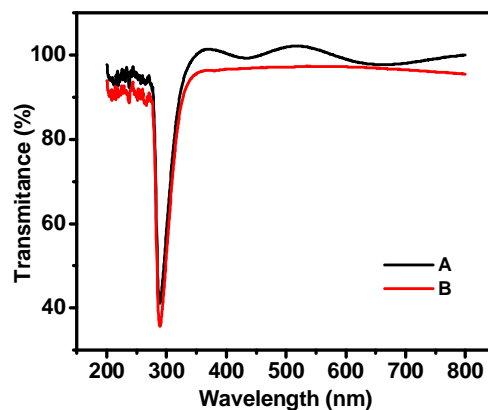

Fig. 3.3.7. UV spectra of A) Silica-2 wt% gelatin
B) Silica-2 wt% gelatin-50 wt% VTMS

Stereomicrographs of water drops on glass slides coated with various concentrations of vinyltrimethoxysilane are presented in Fig. 3.3.8. The difference

in the behaviour of various coated surfaces is clearly seen in the figures. Water drops spread on a glass surface coated with silica-2 wt% gelatin, which is hydrophilic whereas a spherical morphology is seen on the glass slides coated with silica-2 wt% gelatin-50 wt% VTMS. There is a change in the morphology of water drops with change in concentration of VTMS and this is in accordance with the contact angle values of the coatings. Hence, we can tailor the hydrophobicity of the coatings by changing the concentration of the functionalizing agent.
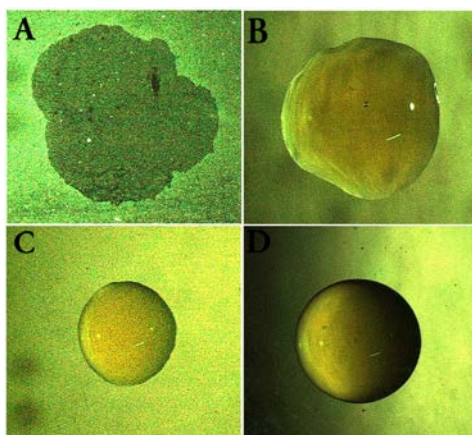
Fig. 3.3.8. Water drops on coated glass slides (10x) A) Silica-2 wt% gelatin B) Silica-2 wt% gelatin-10 wt%VTMS C) Silica-2 wt% gelatin-30 wt% VTMS D) Silica-2 wt%gelatin-50 wt% VTMS

Fig. 3.3.9 provides contact angle and surface energy values of leather samples coated with SGV hydrids. Uncoated leather has a contact angle of 30° and increases with the concentration of VTMS in the coating composition. Even with a

concentration of 10 wt% of VTMS, contact angle of 110° was obtained. As the concentration of VTMS was further increased to 30 wt%, contact angle reaches a maximum of 125°. However a further increase in VTMS does not have an increasing effect, instead it shows a tendency to decrease. Surface energy of the coatings is also provided in the graph. Surface energy decreases with increase in concentration of vinyl groups on the coating surface.
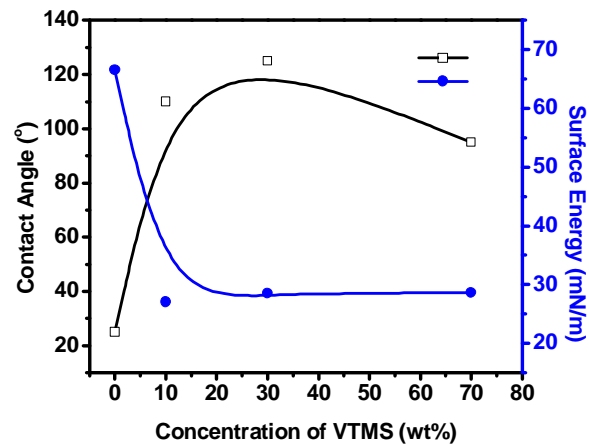
Fig. 3.3.9. Contact angle and surface energy values of coated leather samples

Fig. 3.3.10 provides stereomicrographs of uncoated and coated leather samples. Uncoated leather samples show a highly porous and rough surface. The finish of the leather substrate improves with the coating along with the preservation of porosity.

125
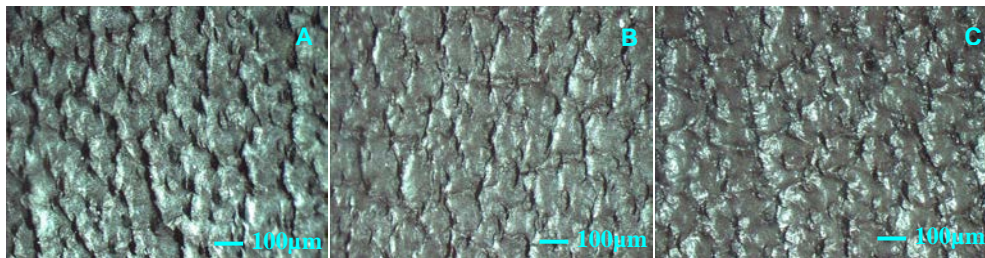
Fig. 3.3.10. Stereo micrographs of leather samples A) Uncoated B) Silica
C) Silica-2 wt% gelatin D) Silica-2 wt% gelatin-30 wt%VTMS

3.2.4 Conclusions

1. Silica–gelatin biohybrid was synthesized using colloidal silica as the precursor for silica. Surface functionalization of the hybrid with MTMS and VTMS was successfully achieved and is reported for the first time as a possible biocompatible hydrophobic silica–gelatin hybrid.

2. FTIR showed the presence of methyl and vinyl groups and Si-C bonds which are responsible for the hydrophobicity of the SGM and SGV hybrids respectively.

3. By varying the concentration of MTMS/VTMS, the hydrophobic properties can be tailored and a maximum contact angle of 95° was obtained for coatings on glass. The optimum concentration for the effective surface modification of silica–gelatin hybrid was found to be 50 wt%. SEM micrograph provides evidence to the uniformity of the coatings.

126

4. Thermal analysis confirms the absence of endothermic peak corresponding to the removal of H_2O in the SGM hybrids. The exothermic peak occurring at 530 ^{o}C is due to the oxidation of the organic groups. This confirms that the hydrophobic feature is retained up to 530 ^{o}C.

5. Optical transmittance of SGM/SGV hybrid coatings on glass substrates was found to be nearly 100% which will enable the use of such coatings in optical applications and also for transparent biocompatible coatings.

6. SGM/SGV hybrid coatings were applied on leather substrates. We could achieve a contact angle of 120° for 30 wt% MTMS still retaining the porosity of the leather. A contact angle of 125° could be achieved by using 30wt% VTMS modified hybrid coatings for leather. The hybrid coatings on leather substrates, improves the finish of leather without compromising the porosity and induce the added hydrophobic property.

Chapter IV

Synthesis of Silica-Chitosan Hybrids and Further Functionalization for Antiwetting Coatings

4.1 Synthesis of Silica-Chitosan Hybrids and Coatings

4.1.1. Introduction

Biopolymers such as gelatin, chitosan, cellulose, and alginates are suitable candidates for the organic counterpart in inorganic-organic hybrid materials because of their low cost, non toxicity, biocompatibility, and multifunctional properties.[71,77] These hybrid materials are biocompatible and have been used as bone substituents, cements for bone repair and reconstruction, and also for immobilization of cells and enzymes.[77,78] Silica is the most widely investigated inorganic component in these hybrids, and the compatibility of silica with various bone relevant proteins such as collagen, gelatin, and chitosan has already been demonstrated.[73,214]

A number of articles and reviews are available in the literature on the promising properties of silica-chitosan composites.[81-83] Silica–chitosan composites are also known to act as immobilization matrices for several molecules and complexes.[83-87] However synthesis of silica-chitosan hybrids and its functionalization for coating application is a potential field which is little exploited. Hence for the present study silica-chitosan hybrids and coatings were

synthesized through sol-gel process by varying the concentration of chitosan. The hybrids were characterized for the chemical interactions, gelation characteristics, thermal decomposition, porosity features, optical transmittance and thickness of silica-chitosan hybrid coatings.

4.1.2 Experimental

Chitosan (1 g) was dissolved in 2% acetic acid (aqueous) under stirring. Chitosan [MW = 1.7×10^5, Degree of deacetylation (DD) = 90%] was purchased from Sea Foods Pvt. Ltd., Cochin. Silica–chitosan hybrid precursor sol was prepared by adding chitosan solution to a 5 g of colloidal silica (50 wt%, Aldrich Chemicals) in 100 ml water under constant stirring. The concentration of chitosan in the silica sol was varied as 1, 2, 4, 6 and 8 wt%. The stirring was continued for 1 h under 30 ^{o}C and the resultant sol was used as the coating precursor. Silica-chitosan sol was coated on glass slides by dip coating technique (KSV Instruments Ltd. Dip Coater) at a rate of 50 mm/min.. Rheological behaviour of the precursor sol was monitored by Anton Paar Rheo Viscometer through a cylinder and bob method. Optical transmittance of coated glass slide was measured by UV-2401 Shimadzu Spectrophotometer. Structural characteristics of the hybrid were investigated using a Nicolet Impact 4000 FTIR Spectrometer and thermal decomposition pattern of the dried silica-gelatin hybrid materials were obtained using Shimadzu 50 H Thermal Analyzer in air at a heating rate of 10 °C/min..

4.1.3 Results and Discussion

The sol-gel method has been effectively used for the synthesis of homogenous and flexible films containing chitosan and silica/titania.[74] However at high concentration of chitosan will increase the sol viscosity to a greater extent and may interfere with the uniformity of coating. Hence rheological behaviour of silica-chitosan sol with respect to the concentration of chitosan was investigated initially. Fig. 4.1.1 presents the viscosity of different silica-chitosan hybrid sols plotted against shear rate.
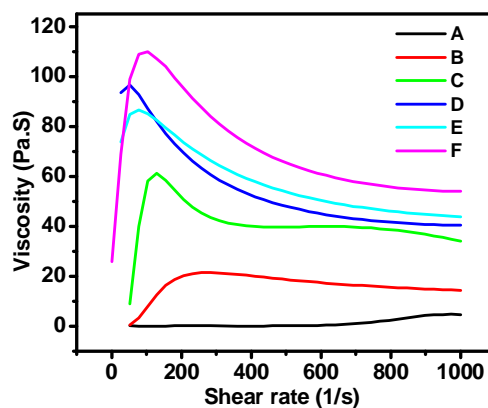

Fig. 4.1.1. Viscosity of silica-chitosan sols of varying concentration of chitosan
A) 0 B) 1 wt% C) 2 wt% D) 5 wt% E) 10 wt% F) 15 wt%

Viscosity increases with increase in concentration of chitosan in the silica sol. At lower shear rates a shear thickening behaviour was observed for silica-chitosan sol irrespective of the concentration of chitosan. However a Newtonian character was

observed at a shear rate above 400 s^{-1}. The chitosan is reported to adsorb on silica particles via electrostatic attraction and hydrogen bonds. The electrostatic attraction is between negative charge on silica particles and positive charge on chitosan molecule, whereas the hydrogen bonding is between hydroxyl, amino, or carbonyl groups of chitosan and silanol groups of silica.[215-216] The cross linking and network formation between silica and chitosan increases viscosity of silica-chitosan sols compared to the silica sol.

In Fig. 4.1.2, A, B, and C represent FTIR spectra of chitosan, silica and silica-2wt% chitosan respectively. The characteristic peaks of chitosan corresponding to amide I (=C=O) is at 1653 cm^{-1} and NH$_2$ bending is at 1540 cm^{-1}. Antisymmetric stretching vibration of C-O-C bridge is present at 1155 cm^{-1} and skeletal vibrations involving C-O stretching are observed at 1082 and 1023 cm^{-1}.[217] The peak at 1085 cm^{-1} due to Si-O-Si symmetric stretching vibration has been widened in the case of silica-chitosan hybrid. This is due to the overlapping of Si-O-Si, Si-O-C and C-O stretching peaks.[218] Si-O stretching of silanol is observed at 940 cm^{-1} in the case of pure silica, and is shifted to 963 cm^{-1} in the case of silica-chitosan. The amide I peak at 1653 cm^{-1} has been shifted to a lower wave number of 1640 cm^{-1} for silica-chitosan hybrid. This is due to the hydrogen bonding of silanol hydrogen with the carbonyl group.[218]

131
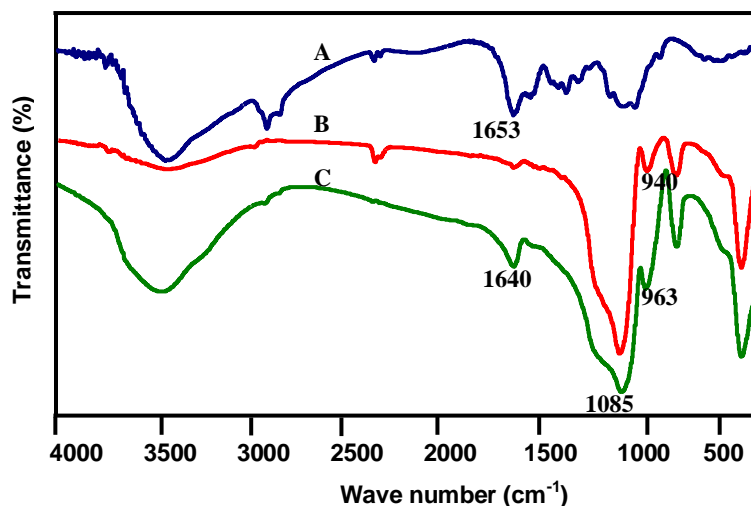
Fig. 4.1.2. FTIR spectra of A) Chitosan B) Silica C) Silica-2 wt% chitosan

Fig. 4.1.3. provides the DTA curve of silica and silica-chitosan hybrid. The endothermic peak at ~100 ^oC corresponds to the removal of adsorbed water. The exothermic peak at ~350 ^oC in the case of silica-chitosan, is due to the oxidative degradation of chitosan. Ding et al. have shown that degradation of chitosan takes place at 322 °C.[219] Shift of the peak to higher temperature in the present case can be attributed to the higher thermal stability of chitosan on cross linking with silica. TGA patterns of silica and silica-chitosan hybrid is given in Fig. 4.1.4. A three step weight loss is observed in both the cases. The first step of weight loss is due to the removal of adsorbed water. This weight loss is greater in the case of silica-chitosan hybrid compared to silica. This is due to the fact that in addition to the surface hydroxyls of silica, chitosan also adsorbs water. Second step of weight loss

132

in the case of silica is due to the removal of chemically adsorbed water. This weight loss overlaps with the degradation of chitosan in the case of silica-chitosan hybrid. Third step of weight loss is due to the dehydroxylation in both cases.
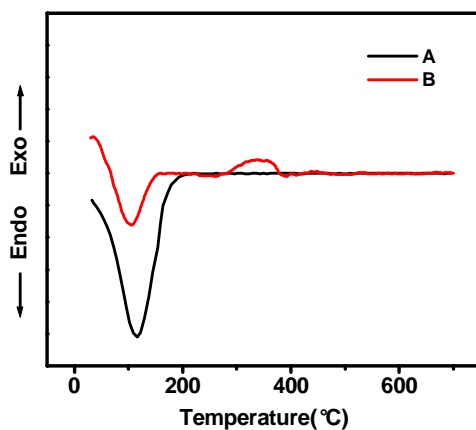
Fig. 4.1.3. DTA pattern of A) Silica B) Silica-2wt% chitosan

Fig. 4.1.5 presents UV transmittance spectra of silica and silica-chitosan coated glass slides. All the samples show a maximum absorption at around 300 nm with more than 90% transmittance in the visible region. Transmittance is reduced with concentration of chitosan. This can be correlated with the viscosity of silica-chitosan hybrid sol. Sol viscosity increases with the concentration of chitosan (Fig. 4.1.1). This may result in an increase in thickness of the coating which may be areason for the decrease in transparency.
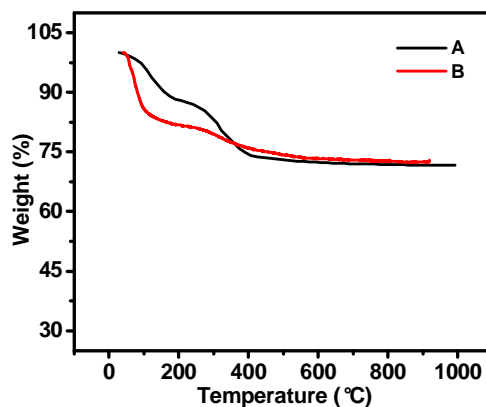
Fig. 4.1.4. TGA curve of A) Silica B) Silica-2 wt% chitosan

Fig. 4.1.5. Optical transmittance of silica-chitosan hybrid coatings on glass slides synthesised by varying the concentration of chitosan A) 0 B) 2 wt% C) 5 wt% D) 10 wt% E) 15 wt%

4.1.4 Conclusions

Sol-gel process was used as an effective technique for the synthesis of silica-chitosan hybrid. Transparent coatings of these hybrids were developed on

134

glass surface which will enable the hybrid for possible application in other substrates without affecting the texture of the substrates. Structural investigation of the hybrid using FTIR spectra revealed that the interaction o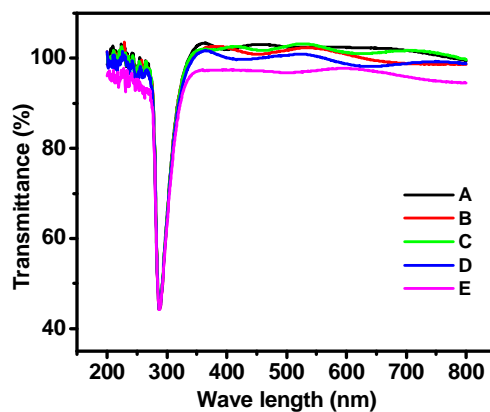f silica and chitosan is through the hydrogen bonding of C=O groups of chitosan and the silanol hydrogen. Thermal analysis showed that the degradation of chitosan took place at ~ 350 °C.

4.2. Synthesis of Functionalized Silica-Chitosan Hybrids and Antiwetting Coatings on Glass, Leather and Textiles

4.2.1. Introduction

The use of organically modified silane precursors for the silica component in the hybrids is rare but can impart enhanced properties to the hybrid. Fuentes et al. had synthesized oriented silica–chitosan hybrid films using 3-aminopropyltrimethoxysilane precursor by a sol-gel process.[88] Protein-containing hydrophobic coatings and films are known biologically active materials for biocatalysis, antifouling surfaces, bioseparation, and biorecognition.[199] A major problem with the synthesis of such hybrids is the precipitation of biopolymers at certain pH's, and hence a compromise is required on the transparency of the hybrid. Therefore in the present investigation a new organic–inorganic hybrid was synthesized with alkylalkoxysilanes and chitosan. Functionalization of hybrid was carried out with methyltrimethoxysilane (MTMS) and vinyltrimethoxysilane

(VTMS), and the hybrid precursor sol was coated on glass substrates, which resulted in water-repellant surfaces without affecting the transparency. Chemical interactions between silica, chitosan, and functionalizing agents; thermal decomposition; transparency under the ultraviolet (UV)-visible region; and hydrophobicity were investigated.

4.1.2 Experimental

Chitosan (1 g) was dissolved in 2% acetic acid (aqueous) under stirring. Chitosan [MW = 1.7×10^5, Degree of deacetylation (DD) = 90%] was purchased from Sea Foods Pvt. Ltd. Cochin. Silica–chitosan hybrid precursor sol was prepared by adding chitosan solution to a 5 g of colloidal silica (50 wt%, Aldrich Chemicals) in 100 ml water under constant stirring. The concentration of chitosan in the silica sol was fixed as 2 wt%. Stirring was continued for 10 min., and MTMS (95% MTMS, Aldrich Chemicals) was added to this mixture, drop by drop to prepare hydrophobic silica–chitosan-MTMS (SCM) hybrids. MTMS/Si molar ratio was varied as 0.05, 0.5, 1, 2.5 and 9. Silica-chitosan-VTMS (SCV) hybrids were also synthesized using VTMS instead of MTMS in the above procedure. Silica-chitosan hybrid sol were coated on glass slides by dip coating technique (KSV Instruments Ltd. Dip coater) at a rate of 50 mm/min.. Rheological behaviour of the precursor sol was monitored by Anton Paar Rheo Viscometer through a cylinder and bob method. Optical transmittance of coated glass slides were

136

measured by UV-2401 Pc Shimadzu Spectrophotometer. Thickness of the coating was measured by HORIBA Jobin Yvon Uvsel Spectroscopic Ellipsometer. Structural characteristics of the hybrid were investigated by a Nicolet Impact 4000 FTIR Spectrometer in the range 400-4000 cm^{-1} by KBr pellet method and thermal decomposition pattern of the dried silica-gelatin hybrid materials were obtained using Shimadzu 50 H Thermal Analyzer in air at a heating rate of 10 °C/min.

4.2.3 Results and Discussion

4.2.3.1 Silica-Chitosan-MTMS Hybrids

Fig. 4.2.1 corresponds to FTIR spectra of MTMS modified silica–chitosan hybrid. The peak at 1100 cm^{-1} corresponds to the stretching vibrations of Si–O–Si bridges. The transmittance peak splits into two separate bands at 1030 and 1130 cm^{-1} in the hybrid gel structures due to the functionalization of silanols by methyl groups through siloxane bridges. Asymmetric stretching vibration of Si–O–Si is reported to split into two separate bands in the hybrid gel structures.[227-228] The same phenomenon is observed in the present system, confirming the formation of hybrid structures. The peaks at 1275 cm^{-1} correspond to Si–C symmetric bending vibrations in SCM hybrids.[213] The presence of C–H stretching vibration is supported by three peaks at 2979, 3050, and 3072 cm^{-1}. A peak due to CH$_3$ asymmetric bending is observed at around 1420 cm^{-1} for the SCM hybrid.

137
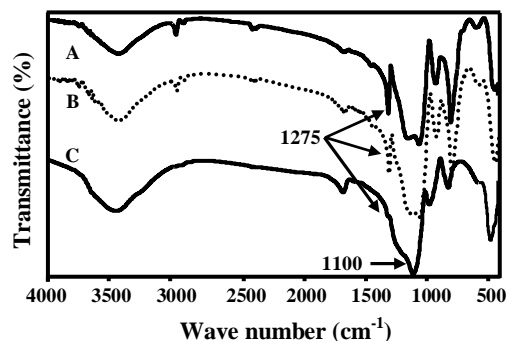
Fig. 4.2.1. FTIR spectra of Silica–chitosan–MTMS hybrids with change in MTMS/Colloidal SiO_2 molar ratio A) 0.05 B) 1 C) 9

MTMS undergoes in situ hydrolysis under acidic conditions of silica–chitosan sol and condense with the surface hydroxyl groups of silica–chitosan particles, which subsequently impart hydrophobic character to the resulting hybrid gels.[217-218] However, with a minimum molar ratio (0.05) of MTMS, there is no significant functionalization on the surface of silica–chitosan particles. Hence the peaks present in silica–chitosan hybrids having a high molar ratio of MTMS are relatively small or absent in the case of silica-chitosan hybrids with a lower molar ratio of MTMS. Schematic representation of formation of SCM hybrids is provided in Fig. 4.2.2.

138
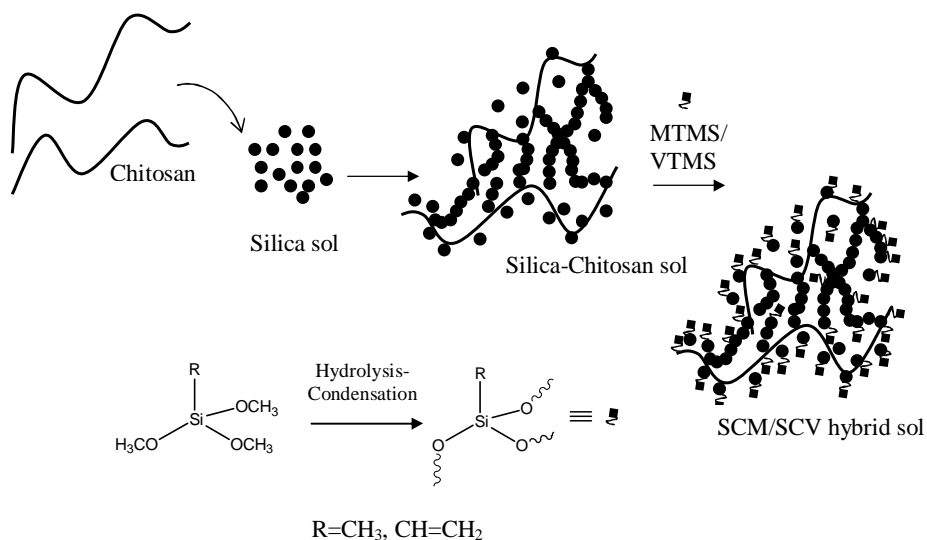
Fig. 4.2.2. Schematic representation of formation of silica–chitosan hybrids

Thermo gravimetric analysis and differential thermal analysis were used to investigate the thermal stability of the hybrid. Fig. 4.2.3 shows the thermo gravimetric pattern of the SCM hybrid with different concentration of MTMS. First step of weight loss corresponding to removal of adsorbed water (at ~100 °C) decreases with respect to the concentration of MTMS. Weight loss corresponding to water is approximately 18% in the case of silica–chitosan hybrid, while the value is <2% for SCM hybrid. As the concentration of MTMS is increased, functionalization of surface silanol takes place to a greater extent, and this imparts hydrophobic character to the resultant hybrid, and hence there is decrease in weight loss with respect to the concentration of functionalizing agent.

139
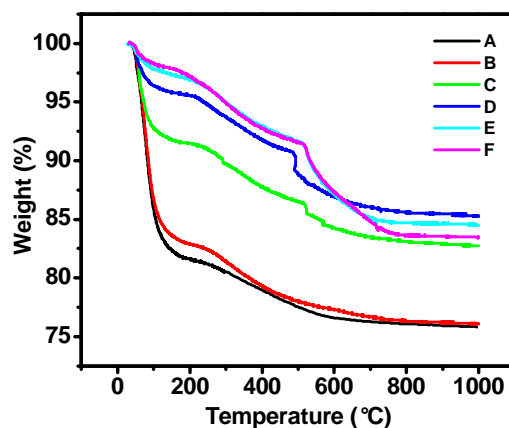
Fig. 4.2.3. TGA thermograms of silica–chitosan–MTMS hybrid with different molar ratio of MTMS/Si A) 0 B) 0.05 C) 0.5 D) 1 E) 2.5 F) 9

The endothermic peak in the DTA pattern (Fig. 4.2.4) of silica–chitosan at ~100 °C corresponds to desorption of water. As the concentration of MTMS increases, the peak area decreases. In the case of hybrids functionalized with MTMS:Si molar ratio 2.5, the endothermic peak is absent at 100 °C due to the effective surface functionalization by MTMS. Since the surface hydroxyl groups are functionalized with methyl groups, the surface does not have any adsorbed water. Hence, a molar ratio of 2.5 of functionalizing agent to TEOS is optimum for effective functionalization. In the differential thermal analysis curve an exothermic peak occurs at around 350 °C, which shows the higher thermal stability of chitosan on cross linking with silica. In the case of MTMS modified sample the peak is absent, which may have overlapped with the corresponding

140

oxidation peaks of other organic groups. The broad peak starting from 470 °C in the case of SCM corresponds to the oxidation of surface organic (CH$_3$) groups.[220] Since the organic groups responsible for hydrophobic property of the hybrid decompose at 470 °C, the hydrophobicity is retained up to 400 °C for SCM hybrids.
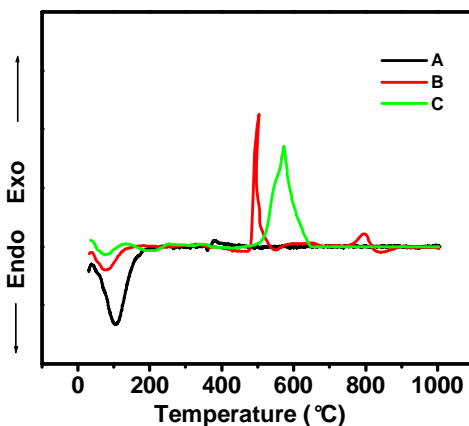
Fig. 4.2.4. DTA of Silica-chitosan–MTMS hybrid with different concentration of MTMS A) 0 B) 1 C) 2.5

Contact angle measurements were performed on coatings of SCM hybrid sols of different MTMS concentration. Fig. 4.2.5 shows contact angle values versus the concentration of surface modifier. The silica–chitosan hybrid without functionalization showed a contact angle of 55°, which increased up to ~95° as modifier to TEOS concentration increased to 9. The contact angle values increased with an increase in concentration of MTMS since MTMS impart an antiwetting

141

property to the resultant hybrid.[217-218] This can be attributed to the condensation of silanols generated from the MTMS precursor with the surface hydroxyl groups of silica–chitosan particles. The increase in contact angle was sharp up to a molar ratio of 2.5 and then proceeded slowly. This clearly compliments the observation of thermoravimetric analysis. Heat treatment of the hybrid coatings up to a temperature of 400 ^{o}C does not vary the contact angle. This means that coatings are stable up to 400 ^{o}C in terms of hydrophobicity.
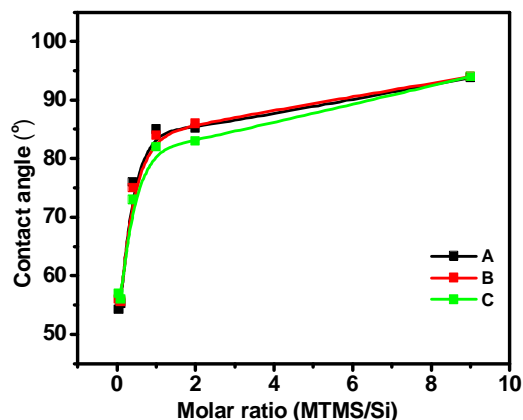
Fig. 4.2.6. Contact angle versus concentration of functionalizing agent
of glass slides heat treated at different temperatures A) 70 ^{o}C B) 200 ^{o}C C) 400 ^{o}C

Stereomicrographs of water drops on uncoated glass slides as well as coated with SCM hybrids are presented in Fig. 4.2.7. The difference in the behaviour of various coated surfaces is clear in these figures. Water drop spreads on an uncoated glass surface, whereas it attains a spherical morphology on the

142

glass slides coated with SCM hybrid. As the concentration of the modifier increases, the hydrophobicity increases, and hence the water drop appears spherical.
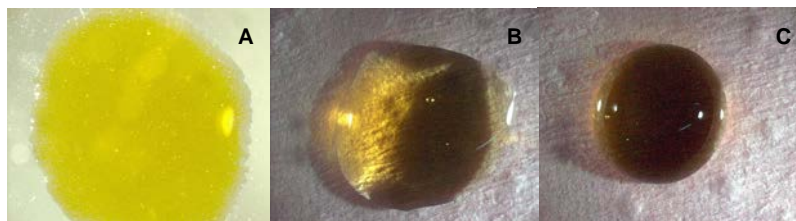
Fig. 4.2.7. Stereomicrographs of water drops on glass slides coated with different MTMS/Si molar ratio A) Uncoated B) 1 C) 2.5

UV transmittance of hydrophobic silica–chitosan hybrid coatings on glass substrates is provided in Fig. 4.2.8. The hybrid coatings showed 98% transmittance in the visible region which is required for applications in optics and transparent biocompatible hydrophobic coatings. Fig. 4.2.9 provides photographs of coatings on glass slides. The figure clearly indicates the transparency of coatings. There is no difference between coated and uncoated glass slides. Stereomicrograph of a single glass slide is provided at the inset. At higher magnification, the boundary between coated and uncoated surface is very clear.
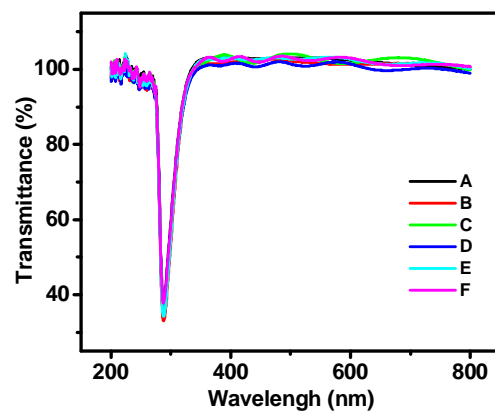
Fig. 4.2.8. UV spectra of glass slides coated with SCM hybrid sols with different MTMS/Si molar ratio A) 0 B) 0.05 C) 0.5 D) 1 E) 2.5 F) 9
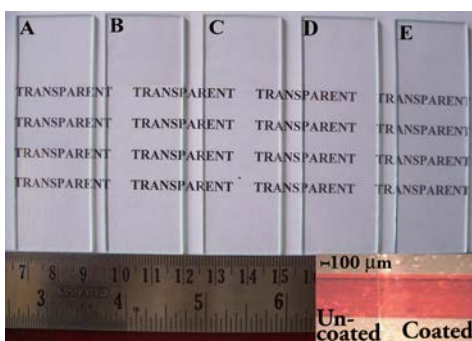
Fig. 4.2.9. Photographs of glass slides coated with SCM hybrid sols with different MTMS/Si molar ratio A) 0 B) 0.5 C) 1 D 2.5 E) 9

{Inset: Stereomicrograph of a single glass slide}

Table 4.2.1 gives contact angle and wetted length of cotton fabric coated with SCM hybrids of varying MTMS/Si molar ratio. Wetted length is measured when a piece of coated textile is dipped in water. In the case of hydrophilic fabric

water level increases due to the capillary rise of water through the fibre where as hydrophobic fabric repel the water as it penetrates through water. Contact angle of uncoated textile can not be determined since it is completely wetting. MTMS/Si molar ratio of 0.5 resulted in a contact angle of 124° and a wetted length of -6.6 mm. Further increase of MTMS concentration does not vary the contact angle considerably. However wetted length dereases up to -20.1 mm which means that increasing MTMS concentration enhances the water repellency of coatings

Table 4.2.1. Contact angle and wetted length of textiles coated by varying the concentration of MTMS

MTMS/Si (molar ratio)	Contact Angle (^{o})	Wetted Length (mm)
0	0	--
0.05	0	33.8
0.5	124	-6.6
1	123	-15.6
2.5	123	-17.5
9	125	-20.1

Fig. 4.2.10 gives contact angle hysteresis of textiles coated with SCM hybrid sols by varying the concentration of MTMS in the coating solution. Uncoated textile (A) showed a sudden gain of weight on exposure to water. In the case of 0.05 moles of MTMS, the increase of weight of the fabric is gradual which

145

means that slight modification of the surface was taken place. But figure C and D indicate the hydrophobic characteristics of coated textiles. The fabric has tendency to push the water downward as it penetrates through the surface which in turn results in a negative increase in weight on the graph.
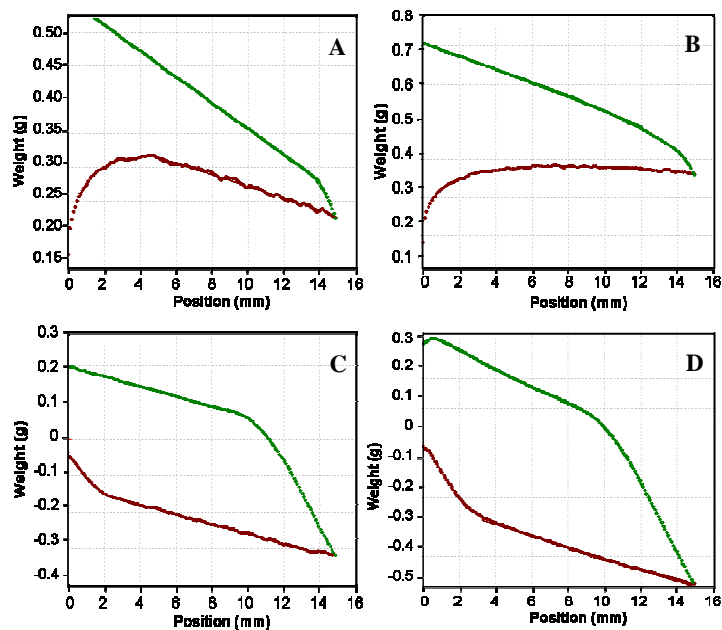
Fig. 4.2.10. Increase in weight of the textile on dipping in water
A) 0 B) 0.05 C) 2.5 D) 9 (● = Advancing ● = Receding)

Photographs of water drops on coated textiles prepared by changing the concentration of MTMS in the coating solution is given as Fig. 4.2.11. Fig. A presents the cotton fabric modified with 0.05 molar MTMS. Water drops spread

on the textile since it is hydrophilic. Figs. B, C, D and E correspond to the fabric modified with 0.5, 1, 2.5 and 9 molar MTMS. Water drop attains a spherical shape on all of these coated fabrics indicating the hydrophobicity of the coated surface. Even with a 0.5 molar MTMS in the coating precursor sol water repellant property is obtained.

Fig. 4.2.11. Photographs of water drops on coated textiles prepared by changing the concentration of MTMS in the coating solution A) 0.05 B) 0.5 C) 1 D) 2.5 E) 9

Table 2 gives contact angle values of cotton fabric coated with MTMS/Si molar ratio 2.5 but varying the coating time of the fabric in the sol. Contact angle is ~120° which does not vary much with the coating time. Even with a coating time of 2 min. we could attain a contact angle of 123°. Contact angle hysteresis of coated fabric is given as Fig. 4.2.12. All the graphs show a decrease in weight (negative). Antiwetting property of the coated fabric inhibits the weight gain of the fabric due to the adsorption of water.

147

Table 4.2.2. Contact angle of textile coated with SCM hybrid sols by

changing coating time

MTMS/Si (Molar ratio)	Coating time (Minute)	Contact angle (^{o})
2.5	2	123
2.5	5	120
2.5	10	120
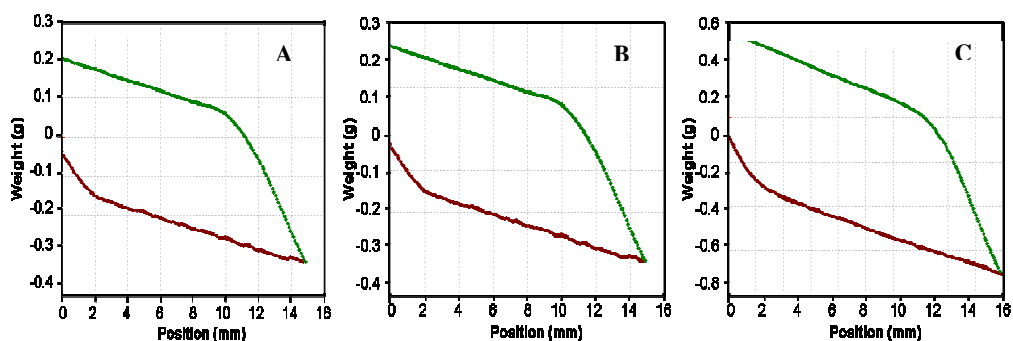
Fig. 4.2.12. Increase in weight of the textile on treatment with water

(• = Advancing • = Receding) by changing coating time (minutes) A) 2 B) 5 C) 10

4.2.3.2 Silica-Chitosan-VTMS Hybrids

Fig. 4.2.13 corresponds to FTIR spectra of VTMS modified silica–chitosan

hybrid. The peak at 1100 cm^{-1} corresponds to the stretching vibrations of Si–O–Si

bridges. The transmittance peak splits into two separate bands at 1030 and 1130

cm^{-1} in the hybrid gel structures due to the functionalization of silanols by vinyl

148

groups through siloxane bridges. It has been shown that in the hybrid gel structure, asymmetric stretching vibration of Si–O–Si splits into two separate bands.[217-218] The same phenomenon is observed in the present system also, confirming the formation of hybrid structures. The SCV hybrid showed a peak at 1613 cm^{-1} due to C=C stretching vibration. The peak is not present in the unmodified gel structure. The peak at 1420 cm^{-1} is due to the deformation mode of CH$_2$ vibrations, which are present in the vinyl group. A weak band between 1400 and 1415 cm^{-1} was reported by Gellermann to confirm the presence of vinyl group.[213] The peak at 1281 cm^{-1} correspond to Si–C symmetric bending vibrations in SCV hybrid.[213] The presence of C–H stretching vibration is supported by three peaks at 2979, 3050, and 3072 cm^{-1}. The peak is not present in the unmodified gel structure. The peaks at 1275 and 1281 cm^{-1} correspond to Si–C symmetric bending vibrations in the SCV hybrid.[213] VTMS undergo in situ hydrolysis under the acidic conditions of the silica–chitosan sol and condense with the surface hydroxyl groups of silica–chitosan particles, subsequently imparting hydrophobic character to the resultant gels.[217-218] However, for a molar ratio (0.05) of VTMS, there is no significant functionalization of the surface of the silica–chitosan particles. Hence the peaks present in silica–chitosan hybrids having a high molar ratio of VTMS are relatively small or absent in the case of silica-chitosan hybrids

149

with a lower molar ratio of VTMS. Schematic representation of formation of SCV hybrids is provided in Fig. 4.2.2.
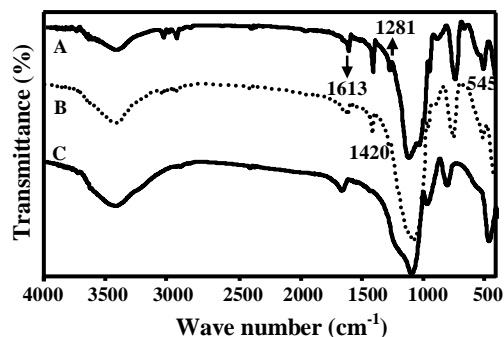
Fig. 4.2.13. FTIR spectra of Silica-chitosan–VTMS hybrid A) VTMS:Si =9
B) VTMS:Si = 1 C) VTMS:Si = 0.05.

Thermo gravimetric analysis and differential thermal analysis were used to investigate the thermal stability of the hybrids. Fig. 4.2.14 shows the TGA pattern of SCV hybrids synthesized by varying the concentration of VTMS. First step of weight loss corresponding to desorption of adsorbed water (at ~100 °C) decreases with respect to the concentration of VTMS. Weight loss corresponding to water is approximately 18% in the case of silica–chitosan, while the value is <2% for SCV hybrid. As the concentration of VTMS is increased, functionalization of surface silanol takes place to a greater extent, and this imparts hydrophobic character to the resultant hybrid, and hence there is a decrease in weight loss with respect to the concentration of functionalizing agent. As the VTMS-to-Si ratio increased to one, there is a drastic increase in weight loss above 200 °C due to the

150

decomposition of vinyl groups. The endothermic peak in the DTA pattern (Fig. 4.2.15.) of silica–chitosan at ~100 °C corresponds to removal of water.
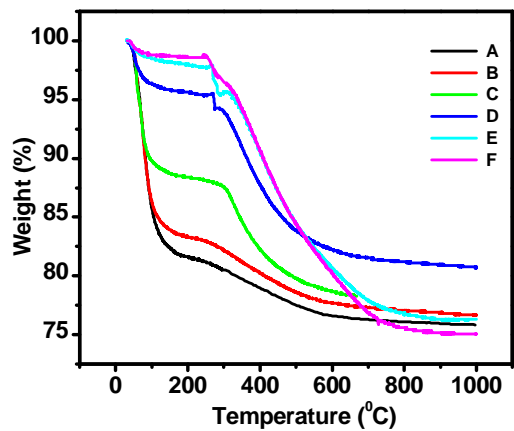
Fig. 4.2.14. TGA thermograms of silica–chitosan–VTMS hybrid with different molar ratio of VTMS/Si A) 0 B) 0.05 C) 0.5 D) 1 E) 2.5 F) 9
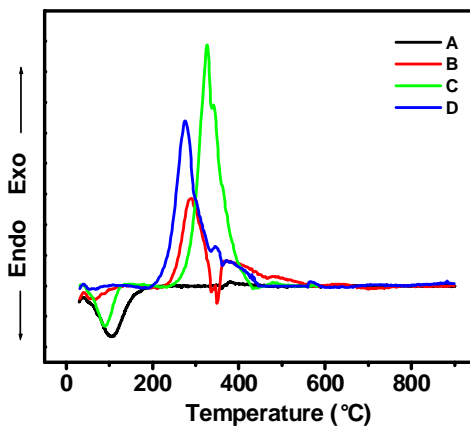
Fig. 4.2.15. DTA of silica-chitosan–MTMS hybrid with different concentration of MTMS A) 0 B) 1 C) 2.5

151

As the concentration of VTMS increases, the peak area decreases. In the case of hybrids functionalized with VTMS:Si molar ratio 2.5, the endothermic peak is absent at 100 °C due to the effective surface functionalization by VTMS. Because the surface hydroxyl groups are functionalized with vinyl groups, the surface does not have any adsorbed water. Hence, a molar ratio of 2.5 of functionalizing agent to silica is optimum for effective functionalization. Ding et al. have shown that the oxidative degradation of chitosan takes place at 322 °C.[219] In the DTA curve an exothermic peak occurs at around 350 °C indicating the higher thermal stability of chitosan on crosslinking with silica. In the case of VTMS-modified sample, such a peak is absent, which may have overlapped with the corresponding oxidation peaks of other organic groups. The broad exothermic peak from 180 °C for SCV is due to the oxidative decomposition of vinyl groups.[221] Since the organic groups, responsible for hydrophobic property of the hybrid decompose at 180° the hydrophobicity is retained up to 150 °C for silica–chitosan–VTMS hybrid.

Contact-angle measurements were performed on coatings of SCV hybrid sols of different VTMS concentration on glass slides. Fig. 4.2.16 shows contact angle values versus the concentration of surface modifier. The silica–chitosan hybrid without functionalization showed a contact angle of 55°, which increased to ~93° as modifier to Si concentration was increased to 9. The contact angle values

increased with an increase in concentration of VTMS. This means that VTMS imparts an antiwetting property to the resultant hybrid.[217-218] This can be attributed to the condensation of silanols generated from the VTMS precursors with the surface hydroxyl groups of silica–chitosan particles. The increase in contact angle was sharp up to a molar ratio of 2.5 and then proceeded slowly. Contact angle decreased with increasing temperature. SCV hybrids lost its hydrophobicity at 200 °C.
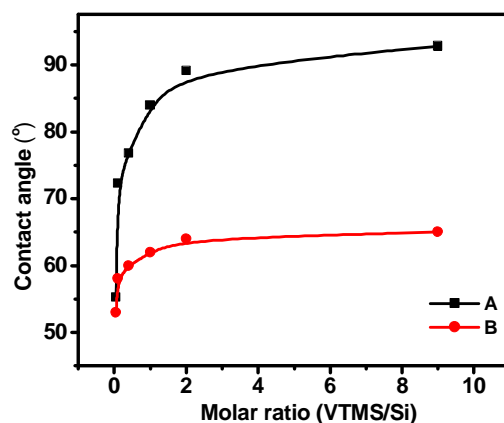
Fig. 4.2.16. Contact angle versus concentration of functionalizing agent of glass slides heated at different temperatures A) 70°C B) 200°C

Stereomicrographs of water drops on uncoated and coated glass slides with SCM/SCV hybrids are presented in Fig. 4.2.17. The difference in the behaviour of various coated surfaces is clearly seen in these figures. Water drops spread on an uncoated glass surface, whereas it attains a spherical morphology on the glass

153

slides coated with SCM/SCV hybrid. As the concentration of the modifier increases, the hydrophobicity increases, and hence the water drop appears spherical. This is due to the hydrophobic nature of the coating on the glass slide. UV transmittance of hydrophobic silica–chitosan hybrid coatings on glass substrates is provided in Fig. 4.2.18. The hybrid coatings showed 98% transmittance in the visible region, ideal for applications in optics and transparent biocompatible hydrophobic coatings.
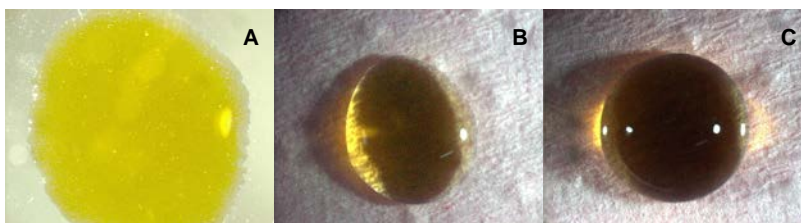
Fig. 4.2.17. Stereomicrographs of water drops on glass slides coated with different VTMS/Si molar ratio A) Uncoated B) 1 C) 2.5

Table 4.2.2. gives contact angle and wetted length of cotton fabric coated with SCV hybrids of varying VTMS/Si molar ratio in sol composition. VTMS/Si molar ratio of 0.5 resulted in a contact angle of 52° and a wetted length of 6.8mm which increase to a maximum of 130° with an increase in VTMS/Si ratio of 2.5. Further increase of VTMS concentration does not significantly influence the contact angle. However wetted length decreased up to -20.1 mm which means that

increasing MTMS in the coating solution enhances the water repellency of coatings
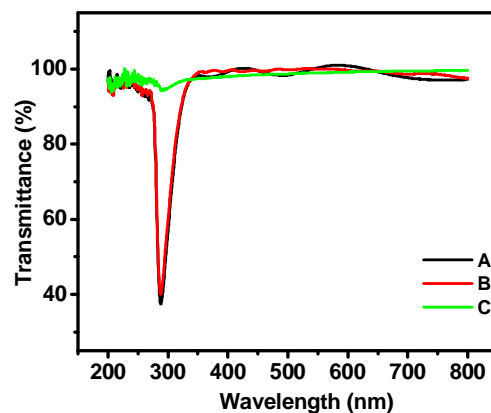
Fig. 4.2.18. UV spectra of glass slides coated with SCM hybrid sols with different VTMS/Si molar ratio A) 0 B) 1 C) 9

Table 4.2.2. Contact angle and wetted length of textiles coated by varying the concentration of VTMS

VTMS/Si (Molar ratio)	Contact angle (^{o})	Wetted length (mm)
0	0	--
0.05	0	33.02
0.5	52	6.87
1	74	6.356
2.5	130	2.09
9	128	-2.62

155

Fig. 4.2.19 gives contact angle hysteresis of textiles coated with SCV hybrid sols by varying the concentration of VTMS in the coating solution. A minimum concentration of VTMS (0.05) shows a sudden gain of weight on exposure to water. For the 0.05 VTMS modified coating there is an initial increase in weight, where as the 1 VTMS modified coating does not gain weight. The coatings with higher concentration of VTMS show a decrease in weight indicating their hydrophobic nature.
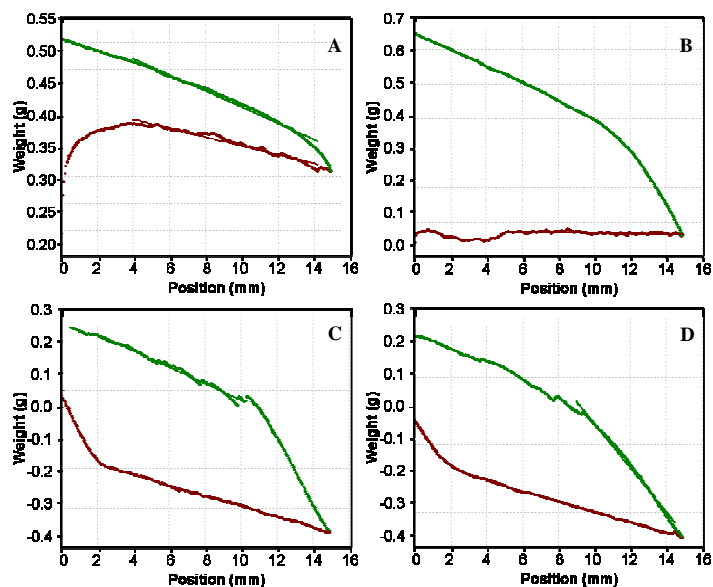
Fig. 4.2.19. Increase in weight of the textile on dipping in water A) 0.05 B) 1 C) 2.5 D) 9 (● = Advancing ● = Receding)

Photographs of water drops on textiles coated with various VTMS modified sol is given as Fig. 4.2.20. Fig. A is the cotton fabric modified with 0.05 molar VTMS. Water drops spread on the textile since it is hydrophilic. Figs. B, C, D and E correspond to the fabric modified with 0.5, 1, 2.5 and 9 molar VTMS in the coating sol. Water drop attains a spherical shape on all of these coated fabrics due to their hydrophobic nature. Even with 1 molar ratio of VTMS in the coating precursor sol we could get water repellant textile.
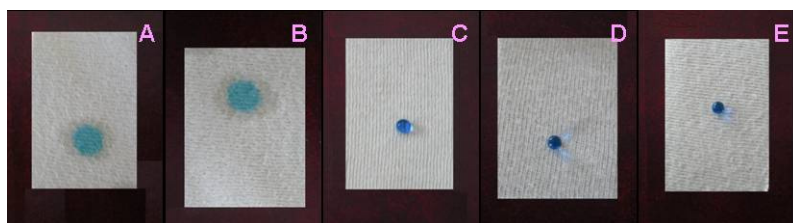
Fig. 4.2.20. Photographs of water drops on coated textiles prepared by changing the concentration of VTMS in the coating solution A) 0.05 B) 0.5 C) 1 D) 2.5 E) 9

4.2.4 Conclusions

A new organic–inorganic hybrid material with antiwetting property was synthesized through a sol-gel process using alkylalkoxysilanes (MTMS/VTMS) and chitosan. The process involved an in situ hydrolysis–condensation reaction of MTMS/VTMS in the reaction medium followed by gelation at room temperature. Structural investigation using FTIR revealed that the hydrophobicity arises due to the methyl/vinyl groups present in the hybrid. By varying the concentration of MTMS and VTMS, the hydrophobic property was tailored. A maximum contact

angle of 95° (modifier to colloidal silica ratio = 9) was obtained for transparent hydrophobic silica–chitosan coatings on glass substrates. An optimum molar ratio of 2.5 of functionalizing agent to Si is required for the effective functionalization in terms of hydrophobicity in the case of glass substrates. Optical transmittance of hybrid coatings on glass substrates was nearly 100%, which makes the hybrid suitable for optical applications. Water repellant textile was achieved by the application of functional coatings on cotton fabrics. The contact angle of these hydrophobic textiles was found to be as high as ~130° even with 2.5 moles VTMS in the coating solution. Effect of coating time on the hydrophobicity was investigated and was found that coating time does not have much effect on the hydrophobicity of the coated textile.

References

1. A. L. Porter, J. Youtie, P. Shapira, D. J. Schoeneck, *J. Nanopart. Res.* **2008**, 10, 715.

2. J. He, J. M. Schoenung, *Mat. Sci. Eng. A* **2002**, 336, 274.

3. N. Z. Logar, V. Kaučič, *Acta Chim. Slov.* **2006**, 53, 117.

4. A. Lu, F. Schüth, *Adv. Mater.* **2006**, 18, 1793.

5. K. Ishizaki, S. Komarneni, M. Nanko, Porous Materials: Process Technology and Applications, Springer, New York, **1998**.

6. C. J. Brinker, G. W. Scherer, Sol-Gel Science:The Physics and Chemistry of Sol-Gel Processing, Academic Press, New York, **1990**.

7. M. M. Collinson, *Crit. Rev. Anal. Chem.* **1999**, 29, 289.

8. H. K. Schmidt, M. Mennig, R. Nonninger, P. W. Oliveira, H. Schirra, *Mater. Res. Soc. Symp. Proc.* **1999**, 576, 395.

9. H. K. Schmidt, E. Geiter, M. Mennig, H. Krug, C. Becker, R. P. Winkler, *J. Sol-Gel Sci. Technol.* **1998**, 13, 397.

10. T. Chung, T. Yeh, *J. Non-Cryst. Solids* **2001**, 279, 145.

11. S. P. Mukherjee, *J. Non-Cryst. Solids* **1980**, 42, 447.

12. S. Sakka, K. Kamiya, *J. Non-Cryst. Solids* **1982**, 48, 31.

13. M. Yamane, S. Inoue, Yasumori, *J. Non-Cryst. Solids* **1984**, 63, 13.

14. S. Ulku, D. Balkose, H. Baltacboglu, *Colloid Polym. Sci.* **1993**, 271, 709.

15. E. J. A. Pope, J. D. Mackenzie, *J. Non-Cryst. Solids* **1986**, 87, 185.

16. F. Kirkbir, H. Murata, S. D. Meyer, R. Chaudhuri, A. Sarkar, *J. Non-Cryst. Solids* **1994**, 178, 284.

17. J. C. Ro, I. J. Chung, *J. Non-Cryst. Solids* **1991**, 130, 8.

18. M. W. Colby, A. Osaka, J. D. Mackenzie, *J. Non-Cryst. Solids* **1986**, 82, 37.

19. K. T. Chou, B. I. Lee, *Ceram. Int.* **1993**, 19, 315.

20. A. Yasumori, H. Kawazoe, M. Yamane, *J. Non-Cryst. Solids* **1988**, 100, 215.

21. B. I. Lee, K. T. Chou, *J. Mater. Sci.* **1996**, 31, 1367.

22. F. Hayashi, K. Takei, Y. Machii, T. Shimazaki, *J. Ceram. Soc. Jpn* **1990**, 98, 670.

23. B. S. Shukla, G. P. Johari, *J. Non-Cryst. Solids* **1988**, 101, 263.

24. P. J. Davis, C. J. Brinker, D. M. Smith, R. A. Assink, *J. Non-Cryst. Solids* **1992**, 142, 197.

25. P. J. Davis, C. J. Brinker, D. M. Smith, *J. Non-Cryst. Solids* **1992**, 142, 189.

26. R. K. Iler, Chemistry of Silica, Wiley & Sons, New York, **1979.**

27. J. Fricke, A. Emmerling, *J. Am. Ceram. Soc.* **1992,** 75, 2027.

28. J. Fricke, in: J. Fricke (Ed.), Aerogels, Springer Proceedings in Physics, Vol. 6, Springer, Heidelberg, **1986**, p. 2.

29. S. J. Teichner, in: J. Fricke (Ed.), Aerogels, Springer Proceedings in Physics, Vol. 6, Springer, Heidelberg, **1986**, p. 22.

30. P. Tsou, *J. Non-Cryst. Solids* **1995**, 186, 415.

31. M. S. Ahmed, Y. A. Attia, *J. Non-Cryst. Solids* **1995**, 186, 402.

32. J. Alkemper, T. Bucholz, K. Murakami, L. Ratke, *J. Non-Cryst. Solids* **1995**, 186, 395.

33. R. W. Pekala, S. T. Mayer, J. L. Kaschmitter, F. M. Kong, *Phys. Rev. B* **1994**, 49,15027.

34. H. D. Gesser, P. C. Goswami, *Chem. Rev.* **1989**, 89, 765.

35. G. Hermann, R. Iden, M. Mielke, F. Teich, B. Ziegler, *J. Non-Cryst. Solids* **1995**, 186, 380.

36. B. C. Dave, B. Dunn, J. S. Valentine, J. I. Zink, *Mater. Res. Soc. Sympos. Proc.* **1996**, 431, 285.

37. S. J. Teichner, M. Khalfallah, D. Bianchi, J. L. Gass, in: Y. A. Attia (Ed.), Sol–Gel Processing and Applications, Plenum, New York, **1994**, p. 323.

160

38. L. W. Hrubesh, *Mater. Res. Soc. Sympos. Proc.* **1995**, 381, 267.

39. A. C. Pierre, G. M. Pajonk, *Chem. Rev.* **2002**, 102, 4243.

40. M. Schmidt, F. Schwertfeger, *J. Non-Cryst. Solids* **1998**, 225, 364.

41. A. Soleimani, M. Dorchehand, H. Abbasi, *J. Mater. Process. Tech.* **2008**, 199, 10.

42. Y. K. Akimov, *Instrum. Exp. Tech.* **2003**, 46, 287.

43. S. S. Kistler, *Nature* **1931**, 127, 741.

44. S. J. Teichner, G. A. Nicolaon, M. A. Vicarini, G. E. E. Gardes, *Adv. Coll. Interf. Sci.* **1976**, 5, 245.

45. Z. J. Prauas, J. Phalipou, *J. Mater. Sci.* **1982**, 17, 3371.

46. M. A. Einarsrud, E. Nilsen, *J. Non-Cryst. Solids* **1998**, 226, 122.

47. D. M. Smith, G. W. Scherer, J. M. Anderson, *J. Non-Cryst. Solids* **1995**, 188, 191.

48. S. Haereid, E. Nilsen, M. A. Einarsrud, *J. Non-Cryst. Solids* **1996**, 204, 228.

49. M. A. Einarsrud , M. B. Kirkedelen, E. Nilsen, K. Mortensen, J. Samseth, *J. Non- Cryst. Solids* **1998**, 231, 10.

50. S. Smitha, P. Shajesh, P. R. Aravind, S. Rajesh Kumar, P. Krishna Pillai, K. G. K. Warrier, *Micro. Meso. Mater.* **2006**, 91, 286.

51. S. Smitha, P. Shajesh, S. Rajesh Kumar, P. Krishna Pillai, K. G. K. Warrier, *J. Porous Mater.* **2007**, 14, 1.

52. S. Haereid, J. Anderson, M. A. Einarsrud, D. W. Hua, D. M. Smith, *J. Non-Cryst. Solids* **1995**, 185, 221.

53. R. Deshpande, D. M. Smith, C. J. Brinker, US patent No. 5, 565, 142, 1**996**.

54. A. P. Rao, G. M. Panjonk, A. V. Rao, *J. Mater. Sci.* **2005**, 40, 3481.

55. A. V. Rao, E. Nilsen, M. A. Einarsrud, *J. Non-Cryst. Solids* **2001**, 296, 165.

56. F. Schwertfeger, D. Frank, M. Schmidt, *J. Non-Cryst. Solids* **1998**, 225, 24.

57. G. S. Kim, S. H. Hyun, *J. Mater. Sci.* **2003**, 38, 1961.

58. C. J. Lee, G. S. Kim, S. H. Hyun, *J. Mater. Sci.* **2002**, 37, 2237.

59. L. L. Hench, in: L. L. Hench (Ed.), Science of Ceramic Chemical Processing, Wiley, New York, **1986**, p. 52.

60. S. H. Wang, in: C. J. Brinker (Ed.), Better Ceramics Through Chemistry, Materials Research Society, Pittsburg, **1984**, p. 71.

61. S. Wallace, L. L. Hench, in: C. J. Brinker (Ed.), Better Ceramics Through Chemistry, Materials Research Society, Pittsburg, **1984**, p. 4752.

62. K. Nikanishi, H. Minakuchi, N. Soga, N. Tanaka, *J. Sol-Gel Sci. Technol.* **1997**, 13, 163.

63. J. Martin, B. Hosticka, C. Lattimer, P. M. Norris, *J. Non-Cryst. Solids* **2001**, 288, 222.

64. M. T. Reetz, A. Zonta, J. Simpelkamp, *Biotechnol. Bioeng.* **1996**, 49, 527.

65. A. V. Rao, M. M. Kulkarni, *Mater. Chem. Phy.* **2003**, 77, 819.

66. L. Beaudct, K. Hossain, L. Mercier, *Chem. Mater.* **2003**, 15, 327.

67. F. Mammeria, E. L. Bourhis, L. Rozesa, C. Sancheza, *J. Eur. Ceram. Soc.* **2006**, 26, 259.

68. T. Kokabo, T. Nakamara, *Biomaterials* **1999**, 20, 1127.

69. S. Yano, K. Iwata, Kimiokurita, *Mater. Sci. Eng. C* **1998**, 6, 75.

70. J. Retuert, Y. Martinez, R. Quijada, M. Yazdani-Pedram, *J. Non-Cryst. Solids* **2004**, 347, 273.

71. T. Coradin, S. Bah, J. Livage, *Colloid Surface B* **2004**, 35, 53.

72. L. Ren, K. Tsuru, S. Hayakawa, A. Osaka, *Biomaterials* **2002**, 23, 4765.

73. I. Brasack, H. Bottcher, U. Hempel, *J. Sol–Gel Sci. Technol.* **2000**, 19, 479.

74. L. Ren, K. Tsuru, S. Hayakawa, A. Osaka, *J. Sol–Gel Sci. Technol.* **2001**, 21, 115.

75. L. Ren, K. Tsuru, S. Hayakawa, A. Osaka, *J. Non-Cryst. Solids* **2001**, 285, 116.

162

76. V. M. Gunko, I. V. Mikhailova, V. I. Zarko, I. I. Gerashchenko, N. V. Guzenko, W. Janusz, R. Leboda, S. Chibowski, *J. Colloid Interf. Sci.* **2003**, 260, 56.

77. H. J. Watzke, C. Dieschbourg, *Adv. Colloid Interf. Sci.* **1994**, 50, 1.

78. M. Schuleit, P. L. Luisi, *Biotechnol. Bioeng.* **2001**, 72, 249.

79. D. M. Liu, I. W. Chen, *Acta Mater.* **1999**, 47, 4535.

80. G. L. Yuan, M. Y. Yin, T. T. Jiang, M. Y. Huang, Y. Y. Jiang, *J. Mol. Catal. A: Chem.* **2000**,159, 45.

81. M. Corrado, A. Riccardo, *J. Inorg. Biochem.* **2002**, 92, 89.

82. Q. Shi, Y. Tian, X. Dong, Y. Sun, *Biochem. Eng. J.* **2003**, 16, 317.

83. S. Takahiro, M. Yasuyuki, *J. Ferment. Bioeng.* **1997**, 84, 128.

84. T. Xue-Cai, T. Yuan-Xin, C. Pei-Xiang, Z. Xiao-Yong, *Anal. Biochem.* **2005**, 381, 500.

85. J. Jing-Ji, C. Guo-Cheng, H. Mei-Yu, J. Ying-Yan, *React. Polym.* **1994**, 23, 95.

86. Z. Jun, X. Chun-Gu, *J. Mol. Catal. A: Chem.* **2003**, 206, 59.

87. Y. Miao, S. N. Tan, *Anal. Chim. Acta* **2001**, 437, 87.

88. S. Fuentes, P. Retuert, A. Ubilla, J. Fernandez, G. Gonzalez, *Biomacromolecules* **2000**, 1, 239.

89. M. Karine, Q. Francoise, B. Daniel, B. Michel, D. Jean-Marie, *Chem. Mater.* **2004**, 16, 3367.

90. R. Schephend, S. Reader, A. Falshaw, *Glycoconjugate J.* **1997**, 14, 535.

91. J. Fricke, A. Emmerling, *J. Am. Ceram. Soc.* **1992**, 75, 20.

92. N. Husing, U. Schubert, *Angew. Chem. Int. Ed.* **1998**, 37, 22.

93. M. M. Girona, E. Martinez, A. Roig, J. Esteve, E. Molins, *J. Non- Cryst. Solids* **2001**, 285, 244.

94. R. Deshpande, D. M. Smith, C. J. Brinker, *J. Non-Cryst. Solids* **1992**, 144, 32.

95. S. Haereid, M. Dahle, S. Lima, M. A. Einarsrud, *J. Non-Cryst. Solids* **1995**, 186, 96.

96. R. Takahashi, K. Nakanishi, N. Soga, *J. Non-Cryst. Solids* **1995**, 189, 66.

97. A. V. Rao, A. P. Rao, M. M. Kulkarni, *J. Non- Cryst. Solids* **2004**, 350, 224.

98. J. K. West, R. Nikles, G. Latorre, *Mater. Res. Soc. Sympos. Proc.* **1988**, 121, 219.

99. G. W. Scherer, S. A. Pardenek, R. M. Swiatek, *J. Non-Cryst. Solids* **1988**, 107, 14.

100. M. K. Titulaer, J. B. H. Jansen, J. W. Geus, *J. Non-Cryst. Solids* **1994**, 170, 11.

101. K. Chou, B. I. Lee, *J. Mater. Sci.* **1994**, 29, 3565.

102. H. Hdach, T. Woignier, J. Phalippou, G. W. Scherer, *J. Non-Cryst. Solids* **1990**, 121,202.

103. P. J. Davis, R. Deshpande, D. M. Smith, C. J. Brinker, R. A. Assink, *J. Non-Cryst. Solids* **1994**, 167, 295.

104. G. M. Pajonk, E. Elaloui, P. Achard, B. Chevalier, J. Chevalier, M. Durant, *J. Non-Cryst. Solids* **1995**, 186, 1.

105. S. Lee, Y. C. Cha, H. J. Hwang, J. Moon, I. S. Han, *Mater. Lett.* **2007**, 61, 3130.

106. S. Rajesh Kumar, P. Krishnapillai, K. G. K. Warrier, *Polyhedron* **1998**, 17, 1699.

107. S. J. Gregg, K. S. W. Sing, Adsorption, Surface Area and Porosity, Academic Press, London, **1995**.

108. A. V. Rao, D. Haranath, *Micro. Meso. Mater.* **1999**, 30, 267.

109. D. M. Smith, R. Deshpande, C. J. Brinker, *Mater. Res. Soc. Symp. Proc.* **1992**, 271, 567.

110. M. I. Liu, D. Yang, Y. Qu, *J. Non-Cryst. Solids* **2008**, 354, 4927.

111. K. Kanamori, M. Aizawa, K. Nakanishi, T. Hanada, *J. Sol-Gel Sci. Technol.* **2008**, 48, 172.

112. P. M. Shewale, A. V. Rao, A. P. Rao, *Appl. Surf. Sci.* **2008**, 254, 6902.

113. A. V. Rao, M. M. Kulkarni, D. P. Amalnerkar, T. Seth, *Appl. Surf. Sci.* **2003**, 206, 262.

114. J. Zarzycki, M. Prassas, J. Phalippou, *J. Mater. Sci.* **1982**, 17, 3371.

115. A. P. Rao, A. V. Rao, G. M. Pajonk, *J. Sol–Gel Sci. Technol.* **2005,** 36, 285.

116. S. S. Prakash, C. J. Brinker, A. J. Hurd, S. M. Rao, *Nature* **1995,** 374, 439.

117. M. A. Einarsrud, S. Haereid, *J. Sol–Gel Sci. Technol.* **1994**, 2, 903.

118. S. Hæreid, M. A. Einarsrud, G. W. Scherer, *J. Sol–Gel Sci. Technol.* **1994**, 3, 199.

119. J. B. Chan, J. Jonas, *J. Non-Cryst. Solids* **1990**, 126, 79.

120. M. R. Ayers, A. J. Hunt, *J. Non-Cryst. Solids* **2001***,* 285, 123.

121. D. Haranath, A. V. Rao, P. B. Wagh, *J. Porous. Mater.* **1999**, 6, 55.

122. A. V. Rao, H. M. Sakhare, A. K. Tamhankar, M. L. Shinde, D. B. Gadave, P. B. Wagh, *Mater. Chem. Phy.* **1999**, 60, 268.

123. B. G. Trewyn, I. I. Slowing, S. Giri, H. Chen, S.Y. Victor, *Acc. Chem. Res.* **2007**, 40, 846.

124. P. V. D. Voort, C. Vercaemst, D. Schaubroeck, F. Verpoort, *Phys. Chem. Chem. Phy.* **2008**, 10, 347.

125. W. Whitnall, L. Cademartiri, G. A. Ozin, *J. Am. Chem. Soc.* **2007**, 129, 15644.

126. F. Hoffmann, M. Cornelius, J. Morell, M. Fröba, *Angew. Chem. Int. Edit.* **2006**, 45, 3216.

127. N. Y. Yu, Y. J. Gong, D. Wu, Y. H. Sun, Q. Luo, W. Y. Liu, F. Deng, *Acta Phys.- Chim. Sin.* **2004**, 20, 81.

128. I. Matos, S. Fernandes, L. Guerreiro, S. Barata, A. M. Ramos, J. Vital, I. M. Fonseca, *Micro. Meso. Mater.* **2006**, 92, 38.

129. C. G. Spickermann, *Curr. Opin. Colloid. Inter. Sci.* **2002**, 7, 173.

130. K. Pielichowski, K. Flejtuch, *J. Anal. Appl. Pyrolysis* **2005**, 73, 131.

131. Y. Wan, D. Zhao, *Chem. Rev.* **2007**, 107, 2821.

132. D. Wu, R. Fu, S. Zhang, M. S. Dresselhaus, G. Dresselhaus, *Carbon,* **2004***, 42, 2033.

133. M. Stefanescu, M. Stoia, O. Stefanescu, A. Popa, M. Simonand C. Ionescu, *J. Therm. Anal. Calorim.* **2007**, 88, 19.

134. M. Stefanescu, M. Stoia, O. Stefanescu, *J. Sol-Gel Sci. Technol.* **2007**, 41, 71.

135. A. Vinu, T. Mori, K. Ariga, *Sci. Technol. Adv. Mater.* **2006**, 7, 753.

136. S. S. Park, C. S. Ha, *Chem. Rec.* **2006**, 6, 32.

137. A.Vinu, K. Z. Hossain, K. Ariga, *J. Nanosci. Nanotechnol.* **2005**, 5, 347.

138. A. Stein, *Micro. Meso. Mater.* **2001**, 44, 227.

139. K. Kosuge, P. S. Singh, *Micro. Meso. Mater.* **2001**, 44, 139.

140. V. G. Pol, A. Gedanken, J. Calderon-Moreno, *Chem. Mater.* **2003**, 15, 1111.

141. B. Duret, A. Saudin, *Int. J. Hydrogen Energy* **1994**, 19, 757.

142. Z. Zhanwen, T. Yongjian, W. Chaoyang, L. Bo, Q. Xiaobo, *J. Chem. Ind. Eng.* **2006**, 57, 1677.

143. X. M. Zeng, G. P. Martin, C. Marriott, *Eur. J. Pharm. Sci.* **1995**, 3, 87.

144. P. Kortesuo, M. Ahola, M. Kangas, I. Kangasniemi, A. Yli-Urpo, J. Kiesvaara, *Int. J. Pharm.* **2000**, 200, 223.

145. K. K. Kim, K. Y. Jang, R. S. Upadhye, *J. Am. Ceram. Soc.* **1991**, 74, 1987.

146. A. M. Gadalla, H. F. Yu, *J. Mater. Res.* **1990**, 5, 2923.

147. Y. Sarikaya, M. Akinc, *Ceram. Int.* **1988**, 14, 239.

148. G. Pravdic, M. S. J. Gani, *J. Mater. Sci.* **1996**, 31, 3487.

149. M. Chatterjee, M. K. Naskar, D. Ganguli, *J. Sol-Gel Sci. Technol.* **1999**, 16, 143.

150. M. Chatterjee, M. K. Naskar, D. Ganguli, *J. Sol-Gel Sci. Technol.* **2003**, 28, 217.

151. M. K. Naskar, M. Chatterjee, N. S. Lakshmi, *J. Mater. Sci.* **2002**, 37, 343.

152. C. R. Miller, R. Vogel, P. P. T. Surawski, K. S. Jack, S. R. Corrie, M. Trau, *Langmuir*, **2005**, 21, 9733.

153. Y. Ma, L. Qi, J. Ma, Y. Wu, O. Liu, H. Cheng, *Colloids Surf. A* **2003**, 229, 1.

154. R. Roque-Malherbe, F. Marquez, *Surf. Interface Anal.* **2005**, 37, 393.

155. R. Roque-Malherbe, F. Marquez, *Mater. Sci. Semicond. Process* **2004**, 7, 467.

156. S. Ramesh, H. Minti, R. Reisfeld, A. Gedanken, *Opt. Mater.* **1999**, 13, 67.

157. Z. Wu, H. Han, W. Han, B. Kim, K. H. Ahn, K. Lee, *Langmuir* **2007**, 23, 7799.

158. Z. Wu, H. Xiang, T. Kim, M. S. Chun, K. Lee, *J. Colloid Interface Sci.* **2006,** 304, 124.

159. M. Marquez, B. P. Grady, I. Robb, *Colloids Surf. A* **2005**, 266, 18.

160. K. Nozawa, H. Gailhanou, L. Raison, P. Panizza, H. Ushiki, E. Sellier, J. P. Delville, M. H. Delville, *Langmuir* **2005**, 21, 1516.

161. A. Matsumoto, K. Tsutsumi, K. Schumacher, K. K. Unger, *Langmuir* **2002**, 18, 4014

162. M. T. Guise, B. Hosticka, B. C. Earp, P. M. Norris, *J. Non-Cryst. Solids* **2001**, 285, 317.

163. M. Chatterjee, A. Patra, *J. Am. Ceram. Soc.* **2001**, 84, 1444.

167

164. B. Siladitya, M. Chatterjee, D. Ganguli, *J. Sol-Gel Sci. Technol.* **1999**, 15, 271.

165. J. Bibette, *J. Colloid Interface Sci.* **1991**, 147, 474.

166. S. D. Bhagat, Y. H. Kim, Y. S. Ahn, *Appl. Surf. Sci.* **2006**, 253, 2217.

167. M. Rawlett, T. J. Hopsan, I. Amlani, R. Zhang, J. Tresek, L. A. Nagahara, R. K. Tsui, H. Goronkin, *Nanotechnology* **2003**, 14, 377.

168. W. Fritzsche, T. A. Taton, *Nanotechnology* **2003**, 14, R63.

169. R. Moller, A. Csaki, W. Fritzsche, *Tech. Mess.* **2003**, 70, 582.

170. A. C. S. Samina, X. Chen, C. Burda, *J. Am. Chem. Soc.* **2003**, 125, 15736.

171. P. R. Lockman, M. O. Oyewumi, J. M. Koziara, K. E. Roder, R. J. Mumper, D. D. Allen, *J. Control. Release* **2003**, 93, 271.

172. T. M. Allen, P. R. Cullis, *Science* **2004**, 303, 1818.

173. K. Salem, P. C. Searson, K. W. Leong, *Nat. Mater.* **2003**, 2, 668.

174. Z. R. Cui, R. J. Mumper, *Crit. Rev. Ther. Drug Carr. Syst.* **2003**, 20, 103.

175. D. Luo, E. Han, N. Belcheva, W.M. Satlsman, *J. Control. Release* **2004**, 95, 333.

176. D. Miller, *Chem. Bio Chem.* **2004**, 5, 53.

177. C. Ohtsuki, T. Miyazaki, M. Tanihara, *Mater. Sci. Eng. C* **2002**, 22, 27.

178. I. A. Farhat., S. Orset, P. Moreau, J. M. V. Blanshard, *J. Colloid Interface Sci.* **1998**, 207, 200.

179. M. K. McDermott, T. Chen, C. M. Williams, K. M. Markley, G. F. Payne. *Biomacromolecules* **2004**, 5, 1270.

180. C. L. Bon, T. Nicolai, D. Durand, *Macomolecules* **1999**, 32, 6120.

181. N. Krishnamurthy, E. C. Weigert, N. J. Wagner, D. C. Boris, *J. Colloid Interface Sci.* **2004**, 280, 264.

182. T. Coradin, J. Livage, *Mater. Sci. Eng. C* **2005**, 25, 201.

183. B. Smith, Infra red spectral interpretation: A systematic approach, CRC Press, New York, **1999**.

184. A. Kros, M. Gerritsen, V. S. I Sprakel, N. Sommerdijk, J. A. Jansen, R. J. M Nolte, *Sens. Actuators B: Chem.* **2001**, 81, 68.

185. T. Coradin, N. Nassif, J. Livage, *Appl. Microbiol. Biotechnol.* **2003**, 61,429.

186. B. Malafaya, G. A. Silva, E. T. Baran, R. L. Reis, *Curr. Opin. Solid State Mater. Sci.* **2002**, 6, 283.

187. M. Mennig, K. Fries, M. Lindenstruth, H. Schmidt, *Thin Solid Films* **1999**, 351, 230.

188. Awazu, H. Onuki, *J. Non-Cryst. Solids* **1997**, 215, 176.

189. V. Matejec, K. Rose, M. Hayer, M. Pospisllova, M. Chomat, *Sens. Actuat. B: Chem.* **1997**, 39, 438.

190. S. Mimura, H. Naito,Y. Kanemitsu, K. Matsukawa, H. Inoue, *J. Organomet.Chem.* **2000**, 611, 40.

191. T. P. Chou, C. Chandrasekaran, S. J. Limmer, S. Seraji, Y. Wu, M. J. Forbess, C. Nguyen, G. Z. Cao, *J. Non-Cryst. Solids* **2001**, 290, 153.

192. K. E. Geckeler, R. Wacker, F. Martini, A. Hack, W. K. Aicher, *Cell. Physiol. Biochem.* **2003**, 13, 155.

193. I. Honda, K. Arai, H. Mitomo, *J. Appl. Polym. Sci.* **1998,** 64, 1879.

194. A. J. Kuijpers, G. H. Engbers, J. Feijen, S. C. De Smedt, J. Demeester, J. Krijgveld, S. A. J. Zaat, J. Dankert, *Macromolecules* **1999,** 32, 3325.

195. T. Coradin, J. Livage, *Colloid Surf. B* **2001**, 21, 329.

196. T. Coradin, O. Durupthy, J. Livage, *Langmuir* **2002**, 18, 2331.

197. T. Coradin, A. Coupe, J. Livage, *Colloid Surf. B* **2003**, 29, 189.

198. S. G. Clark, P. F. Holt, C. W. Went, *Trans. Faraday Soc.* **1957,** 53, 1500.

199. Q. Chen, F. Miyaji, T. Kokubo, T. Nakamura, *Biomaterials* **1999,** 20, 1127.

200. H. Chen, *Artif. Cells Blood Substit. Immobil. Biotechnol.* **1998**, 26, 431.

201. Y. A. Shchipunov, *J. Colloid Interface Sci*. **2003,** 268, 68.

202. J. Sharma, H. B. Bohidar, *Colloid Polym. Sci.* **2000**, 278, 15.

203. F. Schwertfeger, W. Glaubitt, U. Schubert, *J. Non-Cryst. Solids* **1992**, 145, 85.

204. S. J. Novick, J. S. Dordick, *Biomaterials* **2002**, 23, 441.

205. T. Jesionowski, A. Krysztafkiewicz, *Colloid Surf. A* **2002**, 207, 49.

206. M. C. Chang, C. C. Ko, W. H. Douglas, *Biomaterials* **2003,** 24, 2853.

207. S. K. Kang, S. Y. Choi, *J. Mater. Sci.* **2000**, 35, 4971.

208. A. V. Rao, M. M. Kulkarni, D. P. Amalnerkar, T. Seth, *J. Non-Cryst. Solids* **2003**, 330, 187.

209. Ł. Z. Olejniczaka, K. Cholewa-Kowalskab, K. Wojtachb, M. Rokitab, W. Mozgawab, *J. Mol. Struct.* **2005**, 744, 465.

210. L. Trompette, M. Meireles, *J. Colloid Interface Sci.* **2003**, 263, 522.

211. F. Bauer, H. J. Gl ̈asel, E. Hartmann, E. Bilz, R. Mehnert, *Nucl. Instrum. Methods Phys Res. Sect B: Beam Interact. Mater. Atoms* **2003**, 208, 267.

212. Y. Dubitsky, A. Zaopo, G. Zannoni, L. Zetta, *Mater. Chem. Phys.* **2000**, 64, 45.

213. C. Gellermann, W. Storch, H. Wolter, *J. Sol-Gel Sci. Technol.* **1997**, 8, 173.

214. S. Smitha, P. Mukundan, P. Krishna Pillai, K. G. K. Warrier, *Mater. Chem. Phys.* **2007**, 103, 318.

215. A. Thierry, L. Béatrice, M. Michel, *Langmuir* **1999,** 15, 2380.

216. M. Yadienka, R. Jaime, M. Yazdani-Pedram, C. Helmut, *Polymer* **2004,** 45, 3257

217. S. Smitha, P. Shajesh, P. Mukundan, K. G. K. Warrier, *J. Sol-Gel Sci. Technol.* **2007,** 42, 157.

218. S. Smitha, P. Shajesh, P. Mukundan, T. D. R. Nair, K. G. K. Warrier, *Colloids Surf., B* **2007,** 55, 38.

219. D. Ping, H. Ke-Long, L. Gui-Yin, L. Yan-Fei, *Int. J. Biol. Macromol.* **2007,** 41, 125.

220. Y. Mao-Ya, Y. Guo-Li, W. Yong-Qiang, H. Mei-Yu, J. Ying-Yan, *J. Mol. Catal. A: Chem.* **1999**, 147, 93.

221. T. Li-Ming, H. Mei-Yu, J. Ying-Yan, *Macromol. Rapid Commun.* **1994**, 15, 527.

Summary

Aerogels are a fascinating class of nano porous materials derived by sol-gel technique and have shown great potential for a range of applications. They possess unique properties such as ultra low density, high porosity, large inner surface area, small index of refraction, low sound velocity, low thermal conductivity and low dielectric constant. The thesis entitled **"Sol-Gel Mesoporous Silica Aerogels and Bio Hybrids for Functional Applications"** has emphasis on the influence of the experimental parameters which control the porous structure and morphology of aerogels and surface functionalization of silica using biopolymers.

Effect of hydrolysis temperature, gelation pH, aging pH and aging solvent on the porosity characteristics of subcritically dried silica aerogels was investigated. By changing the hydrolysis-condensation conditions, average pore size in the range 6.2-18 nm and total pore volume in the range 0.99-2.04 cc/g were achieved. Aging pH was also varied to tailor the porosity, and an average pore size in the range 5.8-13.5 nm and total pore volume in the range 0.88-1.45 cc/g were obtained by changing the pH from 3 to 11.

Silica aerogels were also synthesized using different organic templates/DCCAs such as PEO, CTAB, HMTA and PEG, and the effect of concentration of these on the porosity features of resultant aerogels were investigated. By controlled incorporation of these organic additives, it was possible

172

to obtain average pore size varying between 5-20 nm, total pore volume in the range 0.8- 4.5 cc/g and surface area 400-910 m^2/g. The dielectric constant of aerogel was measured and a value of 2.29 was obtained at 13 MHz for a typical composition of the precursor. Use of low molecular weight polymer (PEG, MW ~ 285) resulted in lower average pore size, total pore volume and surface area whereas high molecular weight polymer (PEO, MW ~80,000,00) resulted in a larger average pore size, total pore volume and surface area.

Mesoporous silica microspheres were synthesized through sol–emulsion–gel process using Span 80 as surfactant in silica sol/n-hexane water in oil emulsion system. Surfactant concentration and aging time for the silica sol to obtain uniform spheres were optimised to 1.4 volume percentage and 8 hours respectively. Various parameters related to the synthesis of microspheres, including concentration of surfactant and viscosities of sol were studied. Thermal stability, porosity, and morphological features of the microspheres were also investigated. Surface modification of the microspheres was done with trimethylchlorosilane to obtain hydrophobic silica microspheres. Hydrophobic microspheres with a contact angle of ~90° could be synthesized.

Inorganic-organic hybrid concept was used to obtain well defined pore structure, highly accessible functional groups and controlled surface reactivity. Sol–gel process was used to prepare inorganic or hybrid films with tunable

thickness. Sol-gel process was therefore explored as an effective technique for the synthesis of silica-biopolymer hybrids using gelatin and chitosan as biopolymer counter parts. Gelatin is immobilized in the mesoporous silica gel network through hydrolysis of tetraethoxysilane in presence of gelatin solution at controlled pH conditions. Silica–gelatin hybrid is also synthesised starting from colloidal silica and functionalising the hybrid by using methyltrimethoxysilane (MTMS) and vinyltrimethoxysilane (VTMS) as an intermediate precursor so as to introduce hydrophobicity and improve the mechanical properties. MTMS/VTMS undergoes in situ hydrolysis-condensation reaction in the reaction medium to obtain silica-gelatin-MTMS (SGM) and silica-gelatin-VTMS (SGV) hybrids which are novel materials. The hybrid precursor sol was coated on glass and leather substrates. The chemical interactions, gelation characteristics, thermal decomposition, porosity features, optical transmittance and thickness of silica-gelatin hybrid coatings were analyzed. Structural investigation using FTIR spectra revealed that silica and gelatin interact through the hydrogen bonding of C=O and N-H groups of gelatin with the silanol hydrogen. Optical transmittance of coatings on glass substrates is found to be nearly 100% which could lead such coatings for use in optical devices and also as transparent biocompatible coatings. Thermal analysis data show that the physically adsorbed water is replaced by gelatin molecule and the decomposition of gelatin takes place at ~320 °C. Oxidation of organic group

responsible for the hydrophobicity took place at ~200 ^{o}C and ~530 ^{o}C in the case of SGV and SGM hybrids respectively. Hence SGM hybrids possess a greater thermal stability compared to SGV hybrids in terms of hydrophobicity. By varying the concentration of MTMS/VTMS, the hydrophobic property was tailored. The optimum concentration for the effective surface modification of silica–gelatin hybrid is found to be 50 wt%. SEM micrograph indicates uniform distribution of silica–gelatin hybrid over the substrate. A maximum contact angle of 125° is achieved for SGV hybrids coated on leather still retaining the porosity features of leather.

Silica-chitosan hybrids were synthesised through sol-gel process and functionalization of hybrid was carried out using methyltrimethoxysilane (MTMS) and vinyltrimethoxysilane (VTMS). The process involved an in situ hydrolysis–condensation reaction of MTMS/VTMS in the reaction medium to obtain silica–chitosan–MTMS (SCM) and silica–chitosan–VTMS (SCV) hybrids which are novel materials. The hybrid precursor sol was coated on glass substrates, which resulted in water-repellant surfaces without affecting the transparency of substrates. The chemical interactions, gelation characteristics, thermal decomposition, porosity features, optical transmittance and thickness of silica-chitosan hybrids and coatings were analysed. Coatings of silica-chitosan hybrid developed on glass surface had a thickness of 130 nm through ellipsometric

175

measurements and were found to be >90% transparent as evidenced by optical transmittance measurements. FTIR spectra were used to study the interaction of silica and chitosan. The linkage as identified to be through hydrogen bonding of C=O groups of chitosan and the silanol hydrogen. Thermal degradation of chitosan took place at ~ 350 °C. Oxidation of organic group responsible for the hydrophobicity took place at ~180 °C and ~470 °C in the case of SCV and SCM hybrids respectively. In terms of hydrophobicity, SCM hybrids showed a higher thermal stability compared to SCV hybrids. By varying the concentration of MTMS and VTMS, the hydrophobic properties were tailored. A maximum contact angle of 95° (modifier to precursor ratio = 9) was obtained for transparent hydrophobic silica–chitosan coatings on glass substrates. An optimum molar ratio of 2.5 of functionalizing agent to precursor is required for the effective functionalization in terms of hydrophobicity in the case of glass substrates. Water repellant textile could be obtained by the application of these novel ternary hybrid coatings on cotton fabrics as an indicative investigation. The contact angle of the hydrophobic textiles was found to be as high as ~130° even with 2.5 moles VTMS in the coating solution.

The thesis therefore covers a systematic investigation on the synthesis of silica aerogels and microspheres with tailored porosity, at ambient conditions by varying the experimental parameters as well as using organic templates. Organically modified silica-gelatin and silica-chitosan hybrids were developed for the first time using alkylalkoxysilanes such as MTMS and VTMS. Application of novel silica-biopolymer antiwetting coatings on different substrates such as glass, leather and textile is also demonstrated in the thesis. The products developed as part of the investigation is shown below:
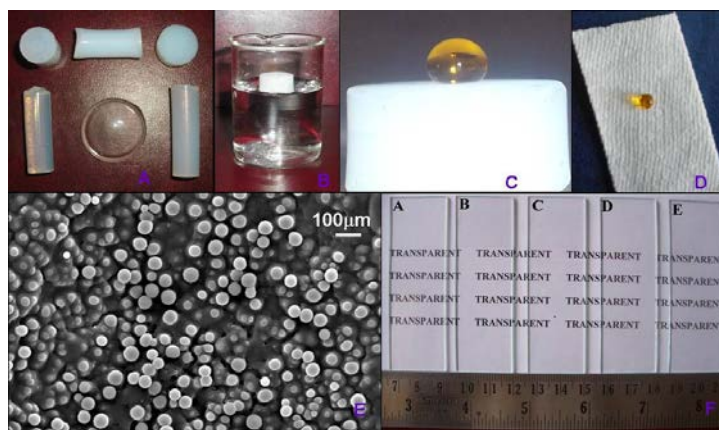
A) Silica aerogels synthesized by subcritical drying technique
B) Hydrophobic silica aerogel floats on water and hydrophilic silica aerogel sink C) Water drop on a hydrophobic silica aerogel D) Water drop on a hydrophobic textile E) Silica aerogel microspheres F) Transparent water repellant coatings on glass slides

List of Publications

1. **S. Smitha**, P. Shajesh, P. Mukundan, K. G. K. Warrier, *Synthesis of mesoporous hydrophobic silica microspheres through a modified sol–emulsion–gel process,* **Journal of Sol-Gel Science and Technology,** *48 (2008) 356.*

2. **S. Smitha**, P. Shajesh, P. Mukundan, K. G. K. Warrier, *Sol-gel synthesis of biocompatible silica-chitosan hybrids and hydrophobic coatings,* **Journal of Materials Research**, *23 (2008) 2053.*

3. **S. Smitha**, P. Mukundan, K. G. K. Warrier, *Synthesis of Biocompatible Hydrophobic Silica-Gelatin Nano Hybrid by Sol-Gel Process,* **Colloids and Surfaces B: Biointerface**, *55 (2007) 38.*

4. **S. Smitha**, P. Shajesh, P. Mukundan, K. G. K. Warrier, *Antiwetting Silica-Gelatin Nanohybrid And Transparent Nano Coatings Synthesised Through An Aqueous Sol-Gel Process,* **Journal of Sol-Gel Science and Technology,** *42 (2007) 157.*

5. **S. Smitha**, P. Mukundan, P. Krishna Pillai, K. G. K. Warrier, *Silica-Gelatin Bio-Hybrid and Transparent Nano Coatings through Sol-Gel Technique,* **Materials Chemistry and Physics**, *103 (2007) 318.*

6. **S. Smitha**, P. Shajesh, P. R. Aravind, S. Rajesh Kumar, P. Krishna Pillai, K. G. K. Warrier, *Effect of aging temperature on the porosity characteristics of subcritically dried silica aerogels,* **Journal of Porous Materials**, *14 (2007)1.*

7. **S. Smitha**, P. Shajesh, P. R. Aravind, S. Rajesh Kumar, P. Krishna Pillai, K. G. K. Warrier, *Effect of Aging Time and Concentration of Aging Solution on the Porosity Characteristics of Subcritically Dried Silica Aerogels*, **Microporous and Mesoporous Materials,** *91 (2006) 286*.

8. Parakkulam Ramaswamy Aravind, Palantavida Shajesh, **Sashidharan Smitha**, Poothayil Mukundan, Krishna Gopakumar Warrier, *Non-Supercritically Dried Silica-Alumina Aerogels-Effect of Gelation pH,* **Journal of the American Ceramic Society,** *91 (2008) 1326*.

9. P. Shajesh, **S. Smitha**, P. R. Aravind and K. G. K. Warrier, *Effect of 3-glycidoxypropyltrimethoxysilane Precursor on an Ambient Pressure Process*

for Silica Aerogels, **Journal of Sol-Gel Science and Technology,** *50 (2009)* 353.

10. P. Shajesh, **S. Smitha**, P. R. Aravind and K. G. K. Warrier, *Synthesis, structure and properties of cross linked $R(SiO_{1.5})/SiO_2$ (R=3-glycidoxypropyl) Porous Organic Inorganic Hybrid Networks dried at Ambient Pressure,* **Journal of Colloid and Interface Science,** *336 (2009) 691.*